**University of Dundee**

**MASTER OF SCIENCE**

# The effect of reinforcing soil inclusion on offshore pipeline ploughs

Tovey, Scott

*Award date:*
2012

MASTER OF SCIENCE

# The effect of reinforcing soil inclusion on offshore pipeline ploughs

Scott Tovey

2012

University of Dundee


College of Art, Science & Engineering
School of Engineering, Physics and Mathematics
Department of Civil Engineering

# The Effect of Reinforcing Soil Inclusions on Offshore Pipeline Ploughs

Scott Tovey

A dissertation submitted for the
degree of Master of Science
to the University of Dundee
May 2011

# Declaration

This is to certify that, the candidate is the author of the thesis; that, unless otherwise stated, all references cited have been consulted by the candidate; that the work of which the thesis is a record has been done by the candidate, and that it has not been previously accepted for a higher degree.

Scott Tovey (candidate), Dundee, 31/05/12

Dr Michael Brown (supervisor), Dundee, 31/05/12

# Abstract

The installation of pipelines on the seabed is a vital part of the oil and gas industry as they allow the safe transfer of oil and gas between oil and gas fields, rigs and countries. It is important to install pipelines as efficiently as possible as it costs hundreds of thousands of pounds per day when installing.

It is extremely important to clearly understand the soil on the proposed pipeline route to accurately design the trench being excavated for the use of a pipeline. There are many types of soil which a plough could encounter when being pulled along the seabed. Three of the most common soils encountered by a plough are sand, silt and clay in which numerous research projects have investigated how these effect plough performance. It is common for the plough to encounter some sort of fibrous or reinforced soils on the seabed. Not anticipating the plough encountering fibrous or reinforced soils on the sea bed could prove to be extremely costly as in some cases, numerous multi passes have been needed to achieve the targeted trench depth when a reinforced soil has been encountered. The full effect of fibrous or reinforced soil on an offshore pipeline ploughs performance is still unknown. It is important to improve and develop a knowledge and understanding of the effect

This research project has investigated the effect of one type of soil reinforcement on the performance of an offshore pipeline plough. The results found enabled the possibility of incorporating the effect of the reinforced soil into a tow force prediction model widely used in industrial practice.

# Acknowledgements

I would like to thank my supervisors, Dr. Michael Brown and Dr. Fraser Bransby for their continued support and guidance throughout this study. I would also like to thank Keith Lauder who helped me settle in to the Geotechnical Research Group at the University of Dundee as well as all the help and support he gave me throughout the research project.

I would also like to acknowledge and thank the technical staff at the University of Dundee, in particular, David Ritchie and William Truswell who helped me develop apparatus used in the research project. I would also like to thank John Anderson, Alec Anderson and Willie Henderson for their help in the workshop.

Most importantly, I would like to thank my family and friends who have supported and encouraged me throughout my time carrying out this study.

# Table of Contents

# Table of Figures

# Table of Tables

# Chapter 1. Introduction

The oil and gas industry is one of the most lucrative industries contributing billions of pounds to countries wealth. In the United Kingdom, the oil and gas industry is one of the highest employers. In order for the safe transfer of oil and gas from oil rigs in oceans and seas throughout the world, pipelines need to be buried on the sea bed to prevent any interference from human activities and corrosion. To bury a pipeline, an offshore pipeline plough is pulled along the seabed by a towing vessel through the use of a tow wire. When burying these pipelines, it is important to fully understand the soil the plough is being pulled through as it is known that the soil type directly affects the tow force needed to pull the plough. It is extremely important to understand exactly how the soil will affect the plough and the tow force needed to pull it as any underestimations in tow force calculations can prove fatal as towing vessels only have limited towing capacities. Some of the common soil types encountered on the sea bed when ploughing could include sand, silt and clay. However, it is still unknown how fibrous or reinforced soil will affect the plough and tow force needed to pull it. Reinforced soil could consist of tree trunks and branches washed out to sea from rivers, or even a mixture of different soil types. Developing a knowledge and understanding of the effect of fibrous or reinforced soil on a pipeline could be useful to industrial practice as it would be possible to plan and anticipate for this effect, making a project more efficient.

The effect of reinforced soil on offshore pipeline ploughs will be investigated in a controlled laboratory environment through the use of reduced scale models of pipeline ploughs.

## 1.1 Scope of Study

As there are many different combinations of soil reinforcement that could be investigated, it was decided that this study would examine the effect of one type of reinforcement on the plough. This would allow a foundation of knowledge to be created to assist in future testing and possibly used in industrial practice.

## 1.2 Aims and Objectives

- Investigate how the tow force needed to pull the plough and plough depth is affected by different quantities of soil reinforcement through a series of testing at two different scales.

- Investigate if the inclusion of reinforcement in a soil creates an additional rate effect on the plough in comparison to unreinforced soil.

- Investigate the possibility of incorporating the effect of soil reinforcement into current tow force prediction models.

- Create a basic understanding of the effect of reinforced soils on offshore pipeline ploughs for use in industrial practice and future research in the field.

# Chapter 2. Literature Review

The purpose of this literature review is to investigate and discuss previous work looking at the behaviour of fibrous soil and its effect on offshore pipeline ploughs. The papers discussed in this review consist of data taken from actual projects carried out by companies throughout the world and also data which has been obtained from test data which has been carried out in a laboratory or other controlled environments. The effects of fibrous soil on offshore pipeline ploughs is still relatively unknown so it is important to understand the effects of fibrous soil or reinforced soil in other scenarios, such as root reinforcement, in order to help understand its behaviour and how it may affect a plough, this will be discussed in-depth within this section. The typical behaviour of offshore pipeline ploughs will also be discussed in this section as it is vital to fully understand how the plough should behave in other soil conditions.

Pipelines are a practical and efficient way of transferring oil and gas quickly between oil fields, rigs and countries. These pipelines are buried below the seabed to protect them from manmade tools being dragged along the seabed such as anchors and fishing lines as well as providing on-bottom stability, thermal insulation or download to mitigate upheaval buckling (Finch *et al*, 2000). If a fishing line or anchor were to get caught on a pipeline while being dragged along the seabed by a vessel, the pipe could become damaged and affect its performance, worst case scenario being the pipeline is breached and causes a loss. This would have a detrimental effect on the environment as well as costing the company a massive amount of money repairing the pipeline as well as the amount of product that is lost through the leak.

## 2.1 Trenching Method

There are different methods of trenching available when carrying out a project to bury pipelines in the seabed, the main being ploughing or jetting. When selecting the appropriate trenching method, the main properties that need to be considered are soil conditions, pipeline size, pipeline type, trenching specification such as required cover depth, water depth, cost and availability (Finch *et al*, 2000). Both the advantages and disadvantages of each method will be investigated through the use of literature. Methods of trenching which are rarer in their use will also be investigated.

### 2.1.1 Ploughing

When ploughing offshore, the plough is lowered to the seabed and towed by a boat along the sea bed. Ploughs are capable of trenching a wide range of soil conditions from very soft clay to fractured weak rock (Finch *et al*, 2000). An example of a typical offshore pipeline can be seen in the next figure.

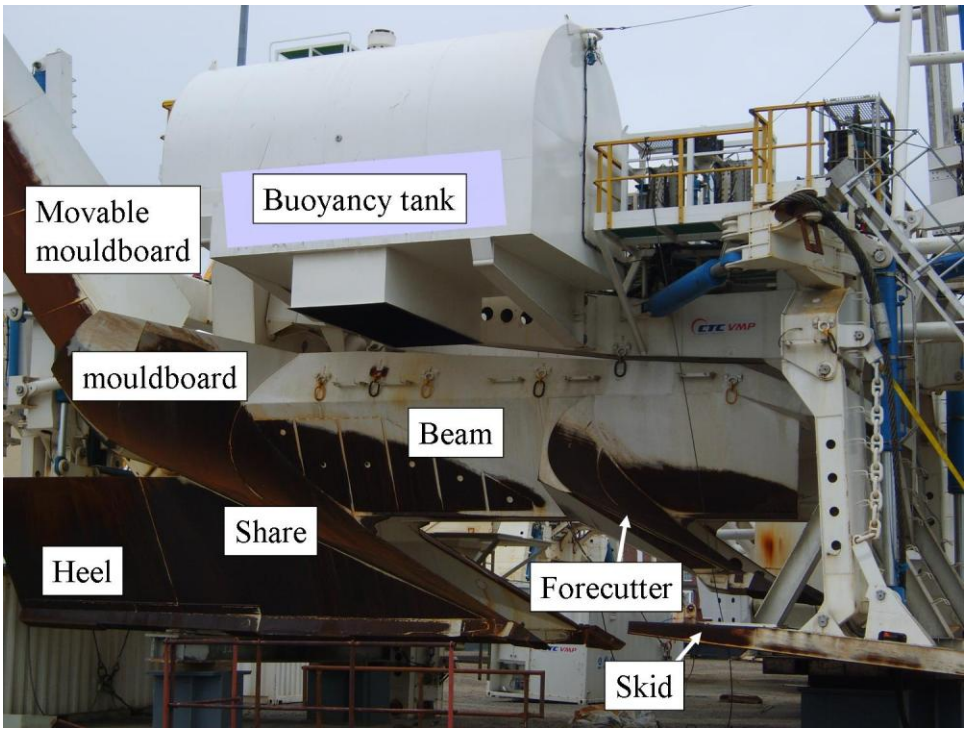


**Figure 1: Offshore Pipeline Plough (Lauder 2011)**

As seen in Figure 1 the main attributes of the plough are labelled on the diagram. The share creates the trench where the pipeline is installed. The mouldboards prevent the soil displaced from the trench from falling back in by creating spoil heaps at either side of the newly created trench. These spoil heaps can then be pushed back into the trench, submerging the pipeline, with a backfill plough. The skids support the weight of the plough and allow it to pivot around their midpoint. By doing this it allows the plough to be raised and lowered to achieve required trench depth and to counteract unforeseen problems below the seabed. The general shape of a trench created by a plough can be seen in Figure 2.

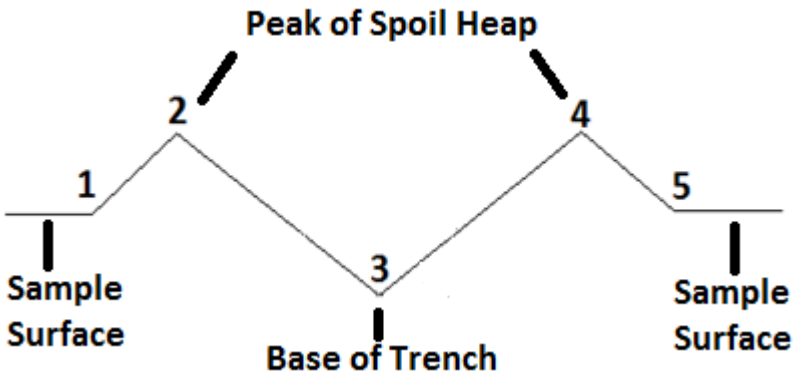


**Figure 2: Generic Shape of Plough Trench (Based on model testing)**

As seen in Figure 2 point 3 indicates the base of the trench, this point is where the pipeline will sit within the trench. Points 2 and 4 are the spoil heaps which are created from the soil displaced by the plough share when cutting the trench. Points 1 and 5 indicate the level of the surface level of the seabed. The inclination of the trench walls is approximately 35 degrees based on model testing (Lauder *et al*, 2008). Finch and Fisher (2000) indicate that it is easier to pull a plough through clays compared to sand as the cuttings are based on un-drained shear failure. They also state that high of ploughing speeds, approximately 100 to 400 m/hr, can be achieved in clays with a relatively low tow force, 100 to 200 tonnes. When pulling the plough through sands, the forces on the plough and its speed are dependent on soil density, particle size and the soils permeability. These variable factors have an effect on the force needed to pull the plough through the material and the speed of the plough. While ploughing in clays, the plough cuts through the clay rapidly enough to allow it to be undrained, meaning that a lower tow force is needed to pull the plough. When working in saturated soils the plough is affected by a 'rate effect' which is determined by the speed of the plough and the drainage path of the water through the soil. This will be discussed in more detail later in the chapter.

### 2.1.2 Jetting

Another method of trenching which can be used is jetting. Jetting tools are usually ROV based and are much smaller than ploughs. It is possible to use a jetting tool in both course and fine grained sands. It is stated by Finch and Fisher (2000) that jetting has become the primary trenching method in deep water where soft soils are prevalent. A trench is created by a jetting tool by liquidising the soil through the use of a high pressure water jet, which reduces the submerged weight of soil in the trenching zone significantly (Finch *et al*, 2000). The pipeline is

then lowered into the liquidised soil, with the fluidised soil reconsolidating after the jetting system has passed. (Finch *et al*, 2000) which submerses the pipeline below the seabed.

## 2.2 Typical Plough Behaviour

It is important to understand the basic behaviour of the plough when working in any soil condition on the sea bed. Palmer (1999) states that the design of an offshore pipeline plough is based on three key design requirements.

- "It must cut to a controlled depth, so that it neither cuts too deep and buries itself, nor cuts too shallow and lifts out of the ground."
- "It must be directionally stable, so that it can make a trench in the desired direction, without zig-zagging or wandering off to one side."
- "The force required to pull the plough must be as small as possible."

Palmer (1999), indicates that the central problem encountered when ploughing on the sea bed is the control of depth. As mentioned previously, depth is controlled by the skid settings and maintained by dynamic equilibrium of moments about the skids due to forces acting on the beam, share and its base (Lauder *et al*, 2008). This is known as the long beam principle of depth control. The long beam principle uses the equilibrium of forces acting on the share of the plough to achieve a constant trench depth, known as steady state behaviour. Steady state behaviour is achieved after the plough has penetrated into the sand until a point where the forces acting on the share were in balance while maintain the same depth as it moves through the soil (Lauder 2011). An example of this principle can be seen in Figure 3 and Figure 4.

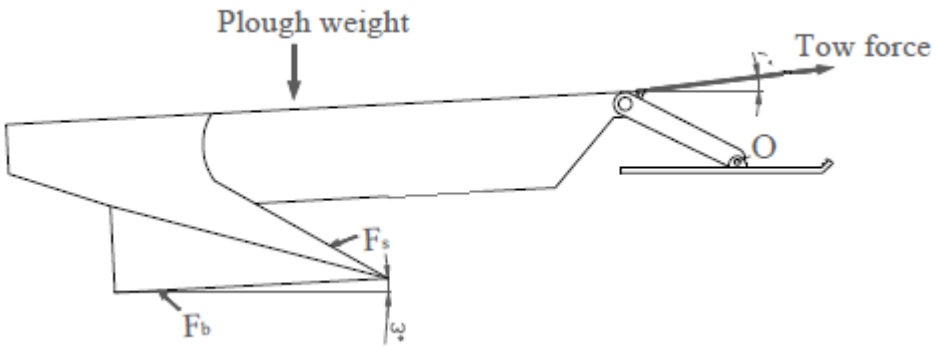


**Figure 3: Plough with Positive (Aft) Pitch (Adapted from Lauder *et al*, 2008)**

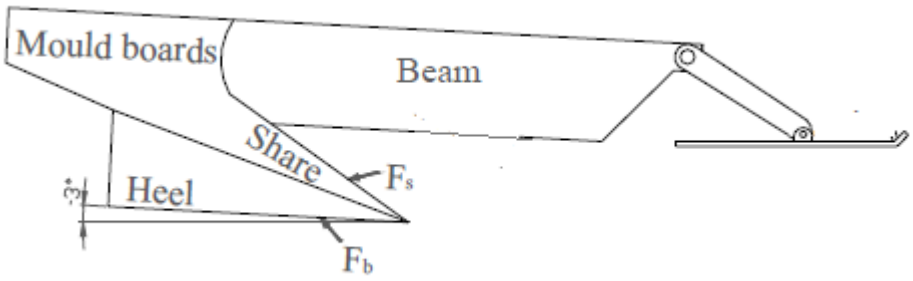


**Figure 4: Plough with Negative (Forward) Pitch (Adapted from Lauder *et al*, 2008)**

When looking at Figure 3 it can be seen that the heel of the plough is deeper than the tip of the share due to the ploughs positive pitch. This means that the plough is trenching too deep. However, the plough would, in this case, dig itself out due to the long beam principle of depth control by finding its equilibrium about the skid centre by clockwise rotation of the plough (Lauder *et al*, 2008). As the plough is trenching too deep, the reaction force in the base of the share, $F_b$, increases greatly, while the force acting on the share, $F_s$, increases only slightly. This will force the plough to rate clockwise until it finds its equilibrium where the heel is horizontal to the base of the trench (Palmer *et al,* 1979). Figure 4 shows the plough in a negative pitch, where the tip of the share is deeper than the heel of the plough which means the plough is too shallow meaning that the plough is attempting to lift itself out of the soil. In this case, the force acting on the share, $F_s$, is greater than the force acting on the base of the share, $F_b$. Due to the long beam principle, the greater force, $F_s$, will cause the plough to rotate anti-clockwise, digging itself deeper into the soil, finding its equilibrium where the plough is horizontal to the base of the trench (Palmer *et al,* 1979). This behaviour can be seen if the plough is placed on the surface of the soil. In this case, the plough would generally start with a negative pitch, which, when towed, will rapidly dig itself into the soil until it reaches the required trench depth of the project. Palmer *et al,* 1979, states that the plough will reach the set trench depth within one plough length, where the plough will then be in its equilibrium due to the long beam principle. Both Palmer *et al,* 1979, and Lauder *et al*, 2008, state that the long beam principle fails if the share is too close to the skids, meaning the length of the beam is reduced, negating the effect of the 'long beam'. The depth of the plough is also determined by the speed of a plough which, in turn, affects the size of force applied to the plough. Bransby et al, 2005, states that when ploughing in granular soils, partial drainage and dilatancy effects result in increasing tow force with increasing speed. Understanding this is essential for the planning of a project when estimating the duration of a project, which if not met, can cost millions of pounds over the

budget of the project. This is known as 'rate effects' which will be discussed in more detail later in the chapter.

## 2.3 Effects of Friction Coefficient, $C_w$ and Passive Pressure Coefficient, $C_s$

Reese and Grinsted, 1986, state that the fundamental problem of all earthmoving machines including ploughs is understanding the relationship between the force, F, necessary to push the blade, the characteristics of the blade and the properties of the soil. Coulomb investigated this problem in 1770 where he found that there were two different types of soil strength, frictional and cohesive, when comparing sand and clay. Coulomb described sand as a simple material to conceive with its main characteristic being that it is frictional and heavy, where the sand particles do not stick together making it a frictional soil. Reese and Grinsted, 1986, developed an equation that attempted to predict the force needed push the share of the plough through a specific soil.

$$F = K_1 \gamma z^2 b \tan \emptyset \quad \textbf{(1)}$$

Where,

- tanΦ is the coefficient of internal friction of sand.
- *γ* is the unit weight of the sand
- *z* is the blade depth
- *b* is the blade width
- $K_1$ is a dimensionless constant depending on the blade rake angle, α

Coulomb found that when cutting a soil, the soil was pushed upwards, with friction being applied on the wedge of soil by the soil to soil and soil to metal, share, interactions. A similar formula to the one seen in Equation 1 was developed by Ivanovic *et al*, 2011 when investigating the influence of object geometry on penetration into the seabed. This can be seen in Equation 2.

$$F = W' \tan \delta + 0.5 K_p \gamma' D^2 L \quad \textbf{(2)}$$

Where,

- *W'*, effective weight of penetrating object.
- *δ*, soil friction angle.
- $K_p$, passive earth pressure coefficient.
- *γ', effective unit weight of soil.*
- *D*, penetration depth below the original ground surface.
- *L*, frontal width of object.

The following data which has tabulated, predicts values of the passive earth pressure coefficient, $K_p$, depending on the front face angle, β, of the object.

| **Front face angle, β (degrees)** | $K_p$ |
|---|---|
| 60 | 10 |
| 90 | 12 |
| 105 | 20 |
| 120 | 30 |
| 150 | 40 |

**Table 1: Passive coefficient, Kp values for different front face angles, β (Ivanovic *et al,* 2011)**

The geometry of the front face angle, β, can be seen in Figure 5.

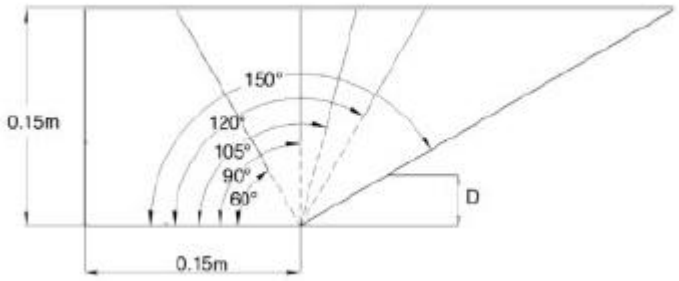


**Figure 5: Geometry of front face angle, β, steel boxes (Ivanovic et al, 2011)**

It can be seen that the lowest front face angle in Table 1 and Figure 5 is 60 degrees, which is higher than the angle of share used on a pipeline plough. A way to solve this, so Equation 2 could be used to predict the drag force when ploughing, would be to interpolate and project the data tabulated in Table 1 to account for lower front face angles, β and $K_p$ values. Equation 2 could then be compared to other force prediction models used for offshore pipeline ploughs to check if this process is applicable. This will be investigated more in depth when analysing test data.

Looking back to Equation 1, found in Reese and Grinsted, 1986, only takes the soil to soil friction into consideration. Cathie and Wintgens, 2001, aimed to develop the theory behind the force needed to move a wedge of soil, as described in Reese and Grinsted, 1986, by attempting to find constant coefficients, dependant on soil properties, which could be used to accurately predict the required tow force for any ploughing project. Cathie and Wintgens, 2001, developed the following equation for static resistance, force, when ploughing in an unsaturated soil.

$$F = C_w W + C_s \gamma D^3 \quad \textbf{(3)}$$

Where,

- $C_W$, is the friction coefficient.
- W, is the weight of the plough.
- $C_S$, is the passive pressure coefficient
- γ, is the unit weight of the soil.
- D, is the plough depth (share depth).

Cathie and Wingens, 2001, developed constant, predicted values for both the friction coefficient, $C_w$, and the passive pressure coefficient, $C_s$. These values were derived from a special data set, derived from 18 different North Sea ploughing projects between 1991 and 1993. These predicted values can be seen in Table 2.

| Tow Force Coefficients Cw and Cs for Cohesionless Soils | | |
|---|---|---|
| **Tow force coefficient** | **Density** | **Value** |
| $C_w$ | All | 0.4 |
| $C_s$ | Loose | 5 |
| | Medium dense | 10 |
| | Dense | 15 |
| | Very dense | 20 |

**Table 2: $C_w$ and $C_s$ Values (Cathie and Wintgens, 2001)**

Cathie and Wintgens, 2001, found that the friction coefficient, $C_w$, is constant regardless of soil density, whereas the passive pressure coefficient, $C_s$, is dependent on soil density, increasing proportionally with soil density from loose to very dense. As mentioned previously, these coefficients were determined from a set of 18 tests which can be seen in Table 3.

| Plough Performance Data: Cohesionless Soils | | | | | | | | | |
|---|---|---|---|---|---|---|---|---|---|
| | | | | $D_{10}$ Range | | | $C_d$ Range | | |
| | Primary Soil | Secondary Soil | Density | Typical (mm) | High (mm) | Low (mm) | Typical (t/m3/hr | High (t/m3/hr | Low (t/m3/hr |
| S1 | SAND | Fine, silty, clayey | Medium dense | 0.04 | 0.08 | 0.2 | 1.5 | 2 | 0.3 |
| S2 | SAND | Fine, silty | Dense | 0.06 | | | 0.8 | 3 | 0.3 |
| S3 | SAND | Fine, silty | Medium dense | 0.06 | | | 0.17 | 0.45 | 0.12 |
| S4 | SAND | Fine, silty locally | Dense | 0.066 | | | 0.18 | 0.25 | 0.12 |
| S5 | SAND | Fine, silty | | 0.07 | | | 0.22 | 0.45 | 0.13 |
| S6 | SAND | Fine | Dense | 0.08 | | | 0.15 | 0.27 | 0.12 |
| S7 | SAND | Fine to medium, silty | Medium dense | 0.08 | | | 0.3 | 0.6 | 0.2 |
| S8 | SAND | Fine, silty | Dense | 0.08 | 0.1 | 0.06 | 0.6 | 1 | 0.4 |
| S9 | SAND | Fine | Dense | 0.09 | | | 0.35 | 0.45 | 0.27 |
| S10 | SAND | Fine | Medium dense | 0.09 | 0.15 | 0.06 | 0.135 | 0.15 | 0.1 |
| S11 | SAND | Fine to medium | Medium dense | 0.09 | | | 0.21 | 0.3 | 0.15 |
| S12 | SAND | Fine | Dense | 0.1 | | | 0.14 | 0.25 | 0.08 |
| S13 | SAND | Fine? | Loose? | 0.1 | | | 0.7 | 3 | 0.5 |
| S14 | SAND | Fine to medium | Medium dense | 0.16 | | | 0.042 | 0.06 | 0.03 |
| S15 | SAND | Medium | Very dense | 0.17 | | | 0.1 | 0.12 | 0.05 |
| S16 | SAND | Fine to medium | Very dense | 0.15 | | | 0.05 | 0.08 | 0.03 |
| S17 | SAND | Gravel, clay | Dense / Very Dense | | | | 0.2 | 0.4 | 0.08 |
| S18 | SAND | Silty, fine, cemented | | | | | 0.4 | 0.8 | 0.2 |

**Table 3: Cathie and Wintgens, 2001, Cohesionless Soils Test Data**

When analysing Table 3 it can be seen that the majority of tests are either medium dense, dense or very dense. It can also be seen that there is only one loose test, marked S13, which is marked in Table 3 as questionable and with poor quality. With there only being one, questionable, loose test in the data set, the accuracy of the passive pressure coefficient, $C_s$, for loose sand in Table 2 could be considered inaccurate. The accuracy of the $C_s$ coefficients for medium dense, dense and very dense sands can also be questioned when analysing Table 3. The reason for this is that for each density, the secondary soil is slightly different. An example of this can be seen when looking at the medium dense tests presented in Table 3, marked S1, S3, S7, S10, S11 and S14. Out of these 6 tests, only 2 tests, S11 and S14, are classed as exactly the same soil. However, even with the same soil type classification, the typical $D_{10}$, which is Hazen's effective grain size in mm, relative to which 10% of the sample is finer, range is significantly different, with the typical $D_{10}$ of the soil in S14 being 0.16 mm compared to the typical $D_{10}$ of the soil in S11, being almost half of the typical $D_{10}$ of S14, at 0.09 mm. This is a very significant difference when taking the permeability of the soil into consideration. The permeability of the soil is affected by its $D_{10}$ size, a soil with a low $D_{10}$ size is more permeable than a soil with a higher $D_{10}$ size. With there being such a small amount of tests used to determine the constant values for the coefficients being recommended by Cathie and Wintgens, 2001, these differences in secondary soils could have a significant effect on the recommended values of $C_s$. Brown *et al*, 2006, investigated the accuracy of Cathie and Wintgens, 2001, predicted coefficients of both $C_w$ and $C_s$ through the use of laboratory tests. The validity of the predicted value of the $C_w$ coefficient, seen in Table 2, was investigated by conducting a series of tests in dry soil using three different plough weights being pulled at approximately the same speed. An average tow force for each plough weight was taken when the plough was in its 'steady state' and was plotted against the resultant force, $R_v$, which is used instead of plough weight to correct for the effect of the tow angle (Brown *et al*, 2006). The resultant force, Rv, is calculated using Equation 4.

$$R_v = W - F \sin \alpha \quad \textbf{(4)}$$

Where,

- W, is the plough weight.
- F, is the tow force.
- α, is the tow angle.

Figure 6 was used by Brown *et al*, 2006, to predict a value of $C_w$.

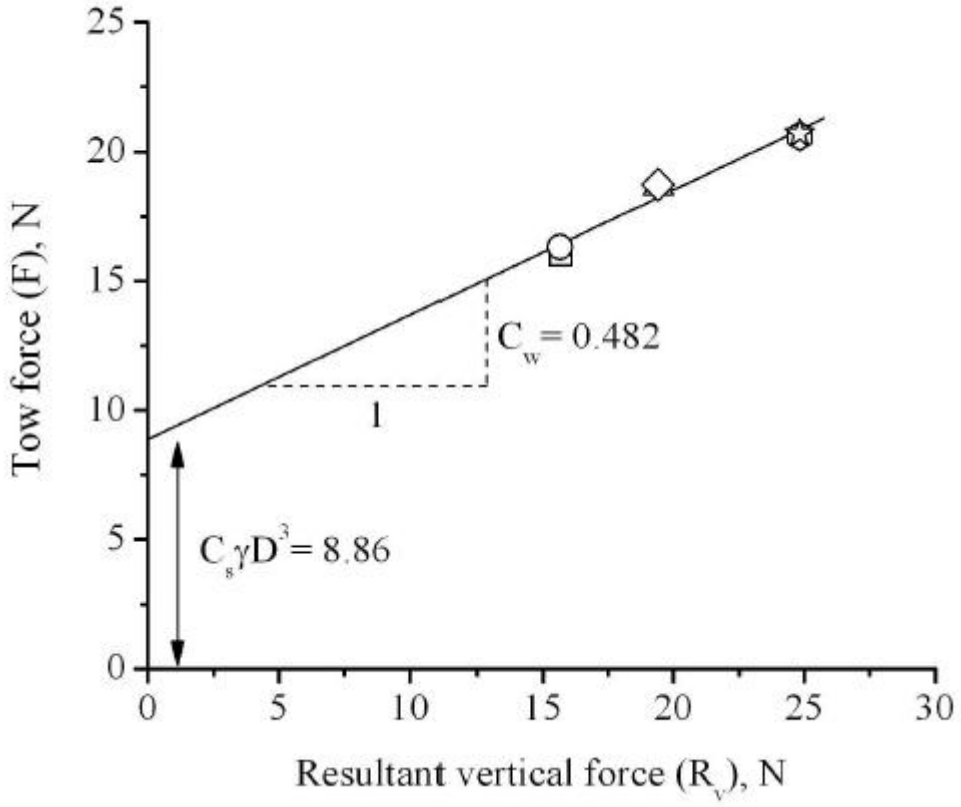


**Figure 6: Prediction of Friction Coefficient, $C_w$ (Brown *et al*, 2006)**

It can be seen in Figure 6 that $C_w$ was found to be 0.482 compared to 0.4 which was found by Cathie and Wintgens (2001), seen in Table 2. Brown *et al*, 2006, generated a $C_s$ coefficient of 30 for these tests, which were carried out in loose dry sands. This is considerably higher than the value recommended for very dense sand by Cathie and Wintgens, 2001. However, Brown *et al*, 2006, states that this difference in $C_s$ may be result from the extrapolation of data to $R_v = 0$ in Figure 6. Brown *et al*, 2006, used the new predicted value of $C_w$, seen in Figure 6, along with $C_s$ of 15 (Cathie and Wintgens, 2001) using Equation 3 to compare it to a test carried out in a saturated dense sand. This produced a scaled tow force of 166.1 tonnes which under predicted the tow force obtained from the actual test of 174.8 tonnes. In order to match the tow force

produced from the test, $C_s$ had to be increased to 17.2 which was closer to the recommended value of $C_s$ in very dense soils by Cathie and Wintgens, 2001. Lauder, 2011, investigated the accuracy of coefficient values given by Cathie and Wintgens, 2001 in Table 2 by carrying out numerous tests using different scales of model ploughs at different densities. Lauder, 2011 used the critical state interface friction angle using two different sands, HST95 (fine grained sand) and HST50 (medium grained sand), to calculate the friction coefficient, $C_w$. The interface friction angle of each sand was obtained through the use of a shear box. A steel block was placed in the bottom of the shear box, with the sand being poured into the box on top of the steel block. The sand was then sheared along the surface of the steel block, allowing the interface friction angle to be calculated from the data obtained from the test. The value of $C_w$ calculated by Lauder (2011) can be seen in Table 4.

| | Interface angle, $\delta$ ($^o$) | Friction coefficient, Cw = $\tan^{-1}\delta$ |
|---|---|---|
| HST95 | 24 | 0.39 |
| HST50 | 27 | 0.44 |

**Table 4: Friction Coefficient, $C_w$ Values (Lauder, 2011)**

When comparing the values of $C_w$ calculated for each sand by Lauder, 2011, in Table 4 to the value of $C_w$ recommended by Cathie and Wintgens, 2001, in Table 2, it can be seen that both are very close to the recommended value in Table 2. The accuracy of the recommended passive pressure coefficient, $C_s$, by Cathie and Wintgens, 2001, was thoroughly investigated by Lauder, 2011, in both saturated and un-saturated sands. The passive pressure coefficient, $C_s$, was calculated from tests in un-saturated soils as Lauder, 2011, wanted to negate the influence of the rate effect, which only occurs in saturated soils as the drainage of water around the share effects the tow force. The rate effect will be discussed in more depth in the following section. The values of $C_s$ found by Lauder, 2011, when testing in dry sand can be seen in Table 5.

| Sand Type | Scale | Forecutter | Very Dense | Dense | Loose |
|---|---|---|---|---|---|
| HST50 | 1/50 | yes | 15.5 | - | 13.9 |
| HST95 | 1/50 | yes | - | 15.4 | 14.1 |
| HST50 | 1/50 | no | 13 | - | 13 |
| HST95 | 1/50 | no | - | 13.6 | 13.4 |
| HST95 | 1/25 | no | - | 10.3 | 6.9 |
| HST95 | 1/10 | no | - | 13.3 | - |

**Table 5: Calculated Values of the Passive Pressure Coefficient, $C_s$, in Dry Sands (Lauder, 2011)**

Lauder, 2011, calculated the $C_s$ values using the following method.

- The passive force, $F_p$, using the following equation, by subtracting the interface friction component from the measured tow force.

$$F_p = F - C_w W$$

- The passive force was calculated, which determines the value of $C_s$ through the use of the following equation.

$$C_s = \frac{F_p}{\gamma \times D^3}$$

When looking at values of $C_s$ compiled by Lauder, 2011, in Table 5 it can be seen that tests were carried out with and without a forecutter. This is a smaller share placed in front of the main share which is designed to reduce the drainage path when cutting in a saturated soil. The forecutter cuts a smaller trench ahead of the main share of the plough meaning that the main share has to cut through less soil, which means the drainage path is reduced. This will be discussed in more depth in the following section. In Table 5 it can be seen that the $C_s$ values calculated by Lauder, 2011, for both dense and very dense sands are lower than the recommended values given in Table 2 by Cathie and Wintgens, 2001. It can also be seen that all but one of the values for $C_s$ in loose sand calculated by Lauder, 2011, are significantly higher than what is recommended by Cathie and Wintgens. Table 5 also indicates that density does not have a significant effect on $C_s$, with each sand having very similar values of $C_s$ regardless of density. It can also be seen that the forecutter has a detrimental effect on the passive pressure coefficient when cutting in dry sands. Table 5 shows that values of $C_s$ are slightly higher with the forecutter attached compared to a test using the same sand and density where the forecutter has been removed. This indicates that the tow force needed to pull the plough

would increase when using a forecutter in dry sand. The results of $C_s$ calculated in saturated sands by Lauder, 2011, can be seen in Table 6.

| Sand | Cs | Density | Forecutter |
|---|---|---|---|
| HST95 | 10.1 | Dense | No |
| | 10.7 | Medium | No |
| | 10.1 | Loose | No |
| HST 50 | 9.9 | Dense | No |
| | 10.2 | Medium | No |
| Redhill 110 | 13.1 | Medium | No |
| HST 95 | 14.7 | Dense | Yes |
| | 15.5 | Medium | Yes |
| HST50 | 14.5 | Dense | Yes |
| | 12.8 | Medium | Yes |

**Table 6: Calculated Values of the Passive Pressure Coefficient, $C_s$, in Saturated Sands (Lauder, 2011)**

It can be seen that the results for $C_s$ found by Lauder, 2011, in Table 6 once again do not corroborate with the recommended values of the $C_s$ given by Cathie and Wintgens, 2001, in Table 2. Similarly to the values of $C_s$ found by Lauder, 2011, in dry sand, Table 6 suggests that the density of the soil has little effect on the value of $C_s$. Table 6 also indicates that the inclusion of a forecutter increases the values of $C_s$ when ploughing in saturated soils. However, its effect on rate effect will be discussed in the following section. Lauder, 2011, compiled the values of $C_s$ obtained from testing at $1/50^{th}$ scale in both saturated and unsaturated sands and compared them to the values recommended by Cathie and Wintgens, 2001, depending on density. This can be seen in Figure 7.

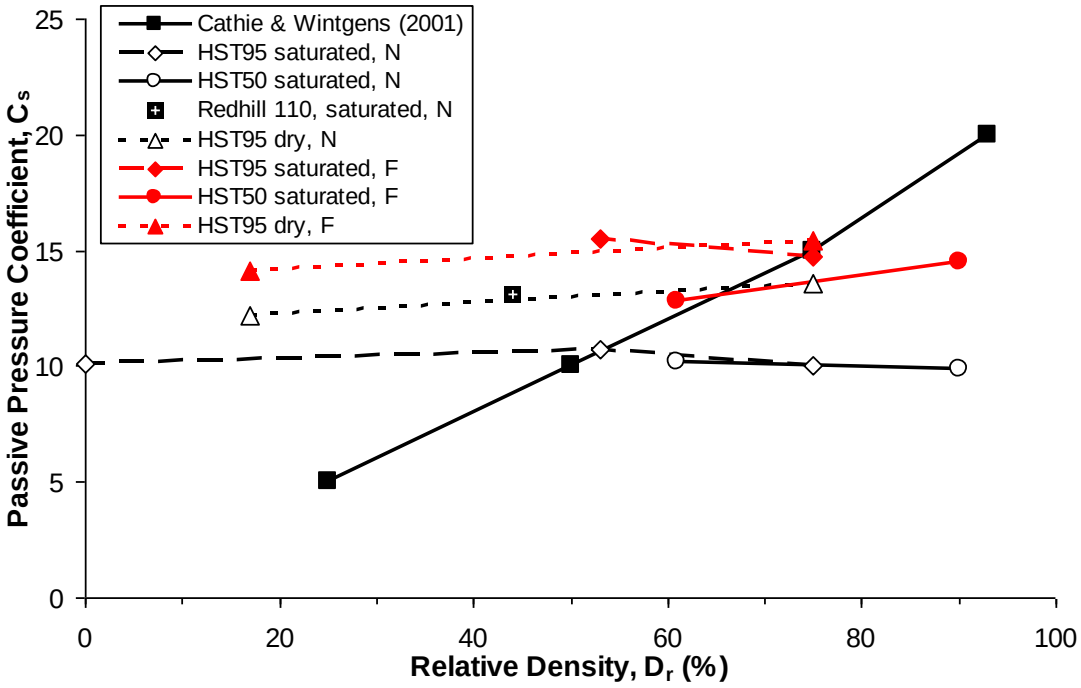


**Figure 7: Comparison of $C_s$ Values in 1/50th Scale Tests with Cathie and Wintgens, 2001, model (Lauder, 2011).**

In Figure 7 tests carried out with a forecutter are marked with an F and tests without a forecutter are marked with an N. When looking at Figure 7 it can be clearly seen that the values of $C_s$ calculated by Lauder, 2011, indicate that $C_s$ is not depend on density, which severely contradicts the Cathie and Wintgens, 2001, model. Lauder, 2011, suggests that if his results are to be relied upon, a recommended $C_s$ value of 15 should be used when a forecutter is attached to the plough and a value of 10 should be used when it has been removed.

## 2.4 Influence of Rate Effects

Bransby *et al* (2005) state that, when ploughing in saturated soils, an increase in tow force will occur with an increase in plough velocity compared to the same speed in unsaturated soils, this is known as the 'rate effect'. The rate effect occurs when the soil dilates when sheared, creating voids between the particles which are filled by water (Palmer, 1999). The reason for this is due to water being practically incompressible, which will increase the force needed to pull the plough through the saturated soil. This theory is backed up by Reese and Grinsted, 1986, where it is also stated that the increase in cutting force with increased speed, primarily depends on the amount of dilation of the soil and the resistance to water flow through the soil, which is the soils permeability. When considering the plough speed, Palmer (1999) indicates that if the

deformation of the soil is slow, slow plough speed, there is ample time for the fluid to fill the increased void space, meaning only a small pressure gradient is needed to drive the flow. Resulting in the pore pressure changes within the pore fluid are small, in turn, having little effect on the effective stresses within the soil. In contrast to this, Palmer (1999) states that if the deformation is faster, the water has to flow rapidly moves to fill the void space caused by the increased amount of dilation. This relationship between speed and pulling force can be seen in Figure 8.

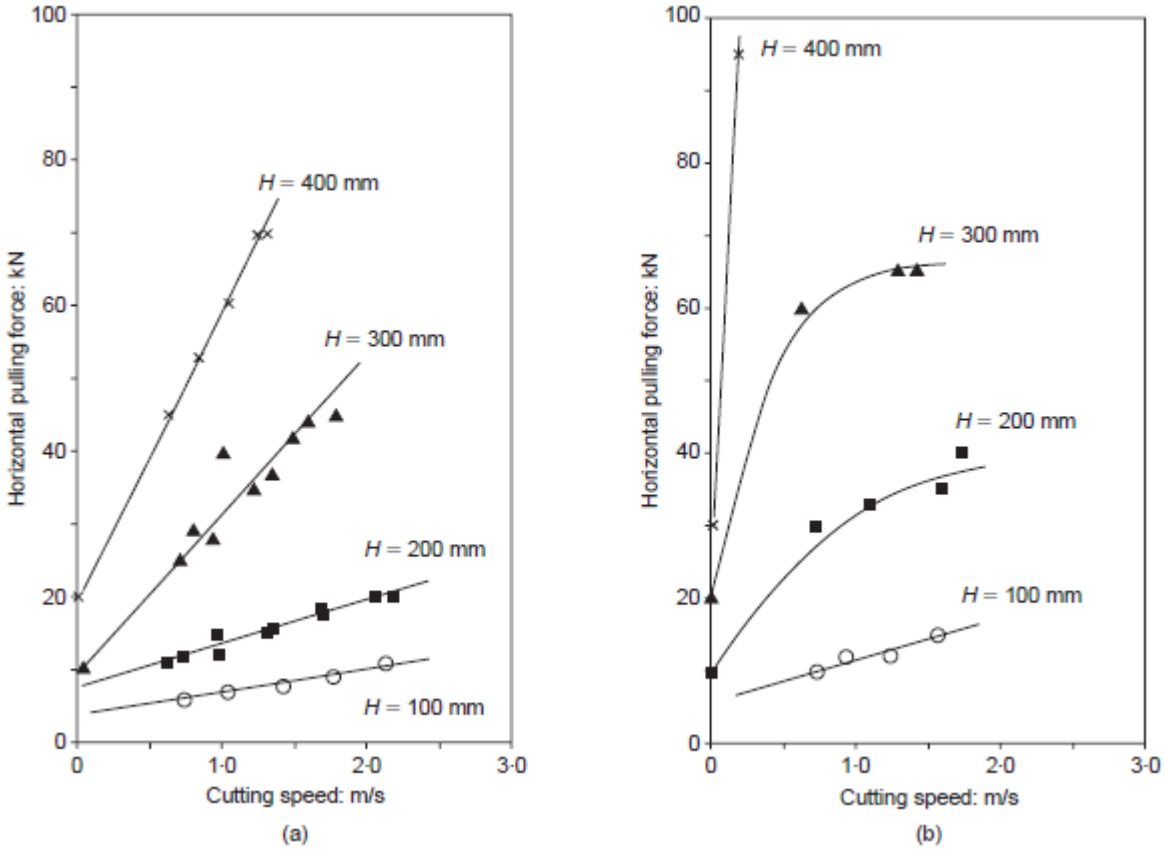


**Figure 8: Relationship Between Speed and Pulling Force (Reece and Grinsted, 1985): (a) Creswell Site (coarse sand); (b) Solway Site (fine, silty sand)**

In the most heavily deformed areas of the soil, the pore pressure has to drop dramatically in order for there to be a large enough pressure gradient to drive the flow. The suction in the fluid, caused by the increase in pressure gradient, presses the soil particles more firmly together, making it harder for the plough to cut through the soil, resulting in an increase in tow force. The relationship between plough speed and tow force can be seen in Figure 9 taken from Lauder, 2011.

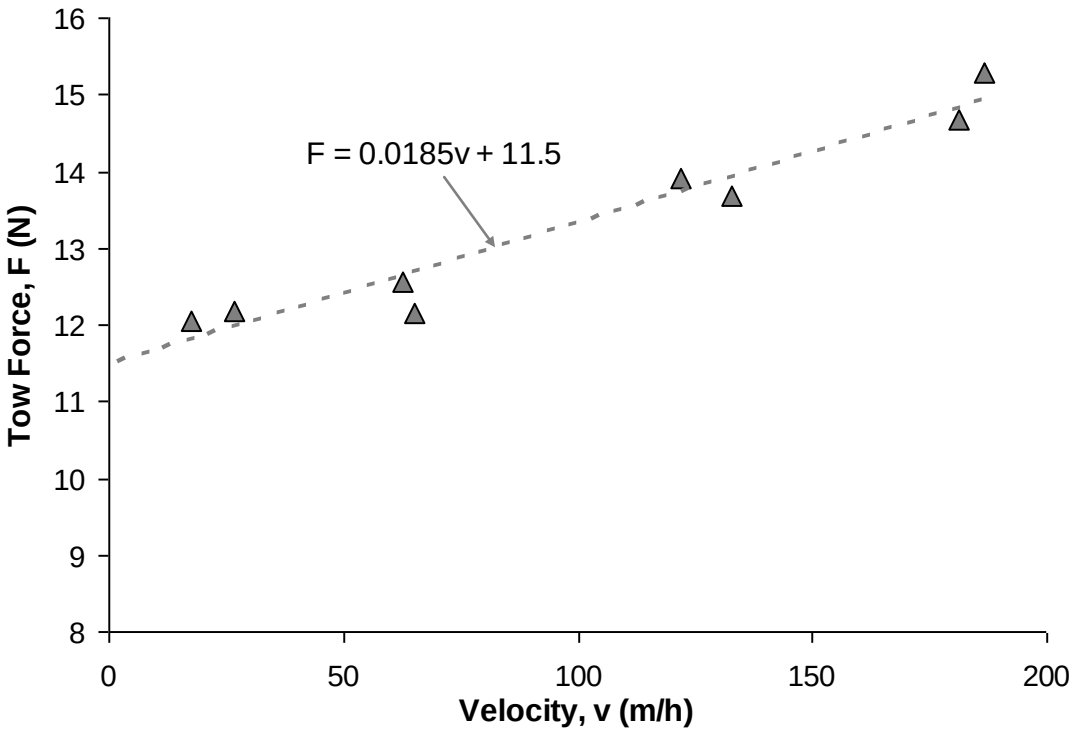


**Figure 9: Increase in Tow Force with Increasing Plough Velocity (Lauder, 2011)**

The effects of increasing plough velocity on corresponding tow force can clearly be seen in Figure 9, suggesting that as plough velocity increases, so does the tow force. There is also a similar effect to this seen when ploughing in dense soils compared to that of loose as indicated by Reese and Grinsted (1986) which can be seen in Figure 8. This is due to a greater amount of dilation occurring in dense soils than loose soils when sheared, meaning the water has to move more rapidly to fill the void space. This results in an increase in soil strength due to suctions, meaning a greater tow force is needed to pull the plough through the soil.

Rate effects have caused many problems during plough projects in the North Sea. Palmer (1999) states that in one instance, a contractor ploughing in silty sand expected easy ploughing conditions, not taking the rate effect into consideration. Instead finding the plough speeds set in the project design resulted in much higher tow forces than anticipated. This unexpected increase in tow force caused a weak link in the towing system to break, meaning that the project missed the deadline by days. It was also found that another major influence on the rate effect is the effect of cavitation. This occurs when the pore pressure in the pore water falls to a low value, just above zero (Palmer, 1999). This means that if the pore pressure ahead of the cutter reduces, the absolute pressure within the pore water pressure reduces to zero, the pore

water cavitates, reducing the rate affect, in turn, reducing the force needed to pull the plough through the soil due to the pore pressure being unable to reduce further. This indicates that it would be beneficial to reach cavitation when ploughing in saturated soils in order to combat the rate effect and reduce the force needed to pull the plough. However, it is only realistically possible to initiate cavitation in shallow waters, as is thought that the effect of cavitation is suppressed in deep water due to the increase in hydrostatic pressures on the seabed (Reese and Grinsted, 1986).

Cathie and Wintgens (2001) developed the effect of the rate effect by finding a relationship between tow force and rate effect through the use of a coefficient by adding to Equation 3.

$$F = C_w W + C_s \gamma D^3 + C_d v D^2 \quad \textbf{(5)}$$

Where,

- $C_d$, is the dynamic resistance coefficient or the rate effect coefficient.
- v, is the velocity of the plough.
- D, is the plough depth.
- The $C_w$ and $C_s$ terms have already been described when discussing Equation 3.

The dynamic resistance coefficient is determined by the soils $D_{10}$ size, which is obtained from a chart created by Cathie and Wintgens (2001). After an analysis of correlations between $D_{10}$, $D_{20}$ and $D_{50}$ with $C_d$, Cathie and Wintgens (2001) found $D_{10}$ to provide the best correlation with $C_d$, even though $D_{10}$ is the most sensitive and variable of the three soil grain size specifications. The $D_{10}$ of a soil is also important as it is an indication of the soils permeability. If a soil is less permeable, it means that it is harder for it to drain, resulting in an increase of rate effect within the soil, meaning more force is needed to pull the plough through it. The effect of $D_{10}$ size on tow force when pulling the plough at different speeds can be seen in Figure 10.

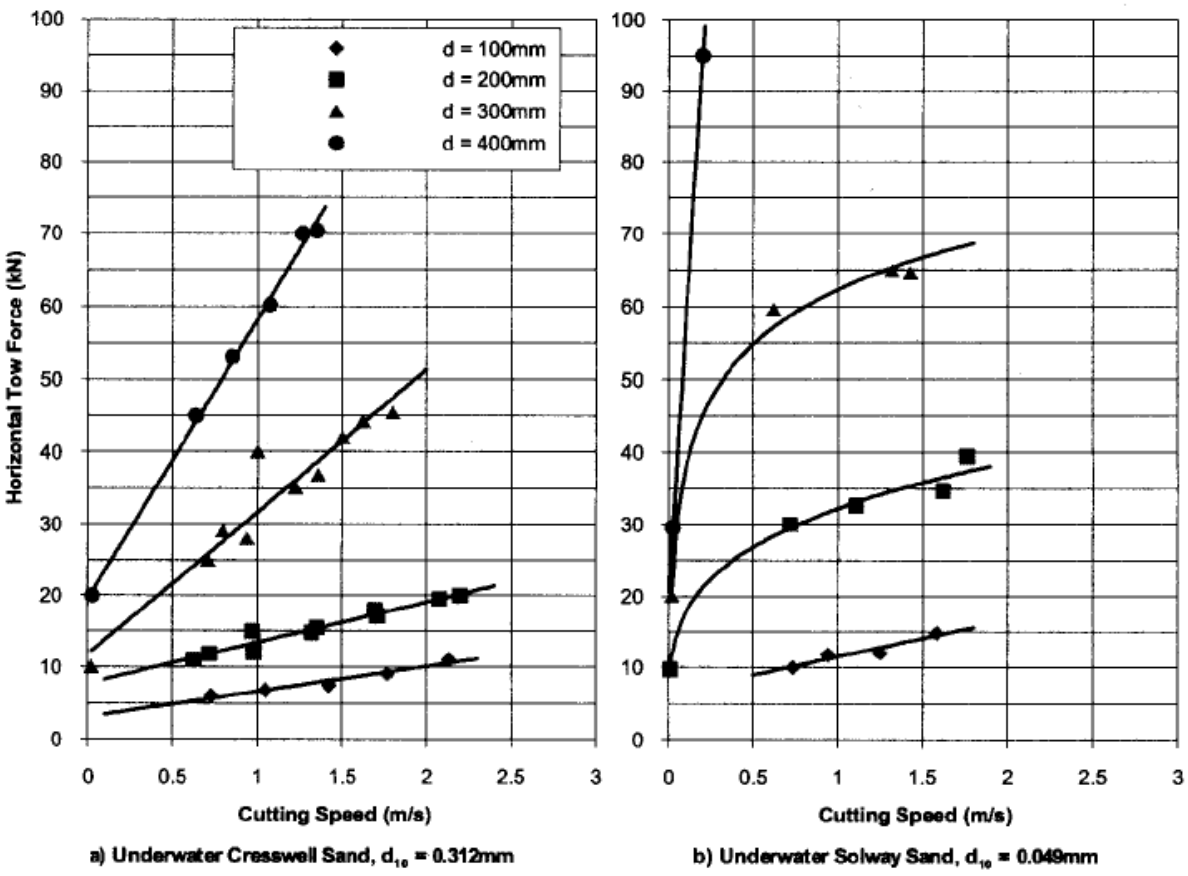


**Figure 10: Relationship Between Speed and Pulling Force (Cathie and Wintgens, 2001): (a) Creswell Site (coarse sand); (b) Solway Site (fine, silty sand) with $D_{10}$ size (Adapted from Reese and Grinsted, 1985)**

When comparing the results from the Cresswell sand to the Solway sand in Figure 10 it can be seen that more force is needed to pull the plough through the Solway sand at the same depth as pulling a plough through the Cresswell sand, assuming that both sands are at the same relative density. This is because the Solway sand has a significantly smaller $D_{10}$ particle size compared to the Cresswell sand meaning it is much more permeable. This means that the Solway sand is much harder to drain, meaning there is a higher rate effect on the plough, increasing the force needed to pull the plough through the sand at the same speed as the corresponding test in the Cresswell sand at the same plough depth. Cathie and Wintgens, 2001, used a collection of data which attempted to show the relationship between $D_{10}$ and $C_d$ can be seen in Figure 11.

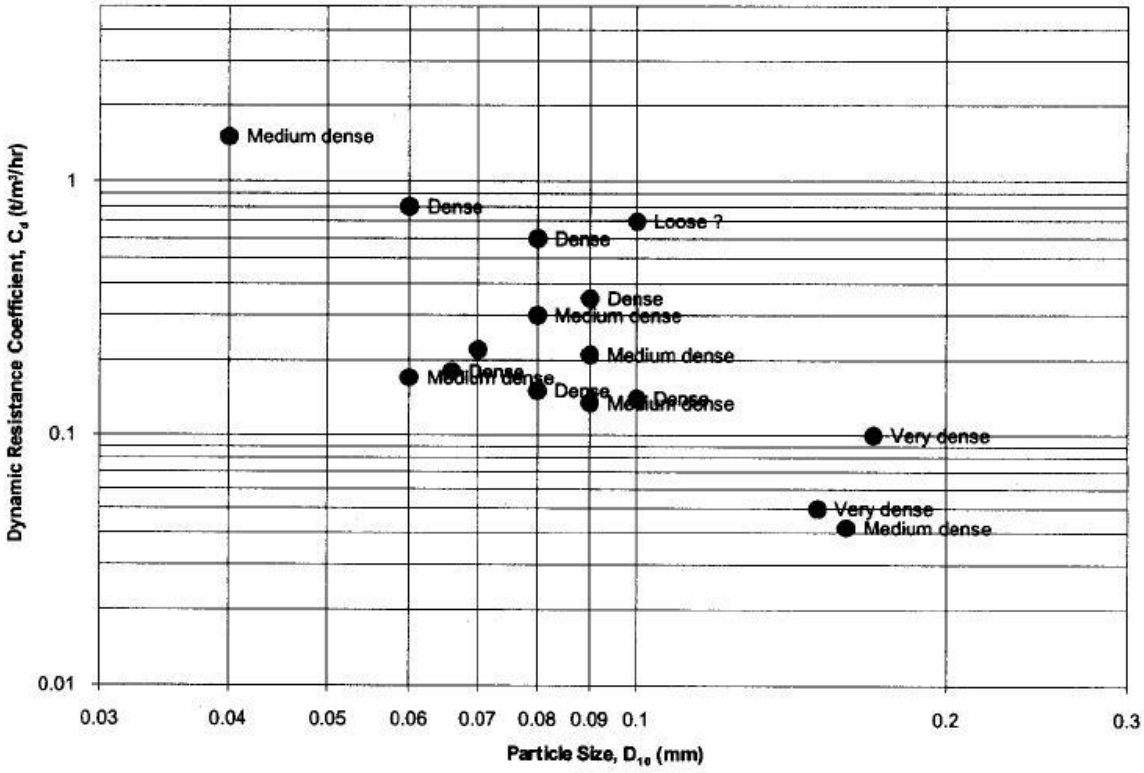


**Figure 11: $C_d$ Dependant on Soil Density (Cathie and Wintgens, 2001)**

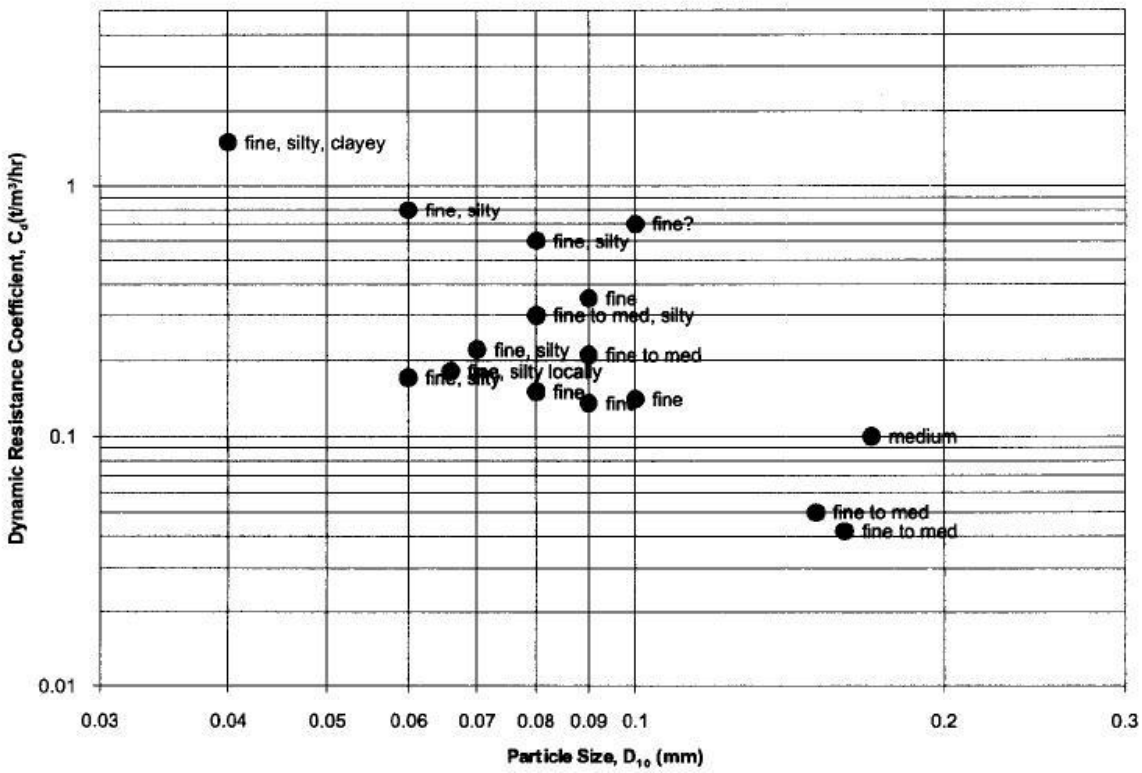


**Figure 12: $C_d$ Dependant on Soil Type (Cathie and Wintgens, 2001)**

The data seen in both Figure 11 and Figure 12 was obtained from field data indicate that the value of $C_d$ generally ranges between 0.1 and 0.8. In order to allow a user to interpret a value of $C_d$ for a new project, Cathie and Wintgens (2001) created a chart through the use of the data seen in both Figure 11 and Figure 12. This chart can be seen in Figure 13.

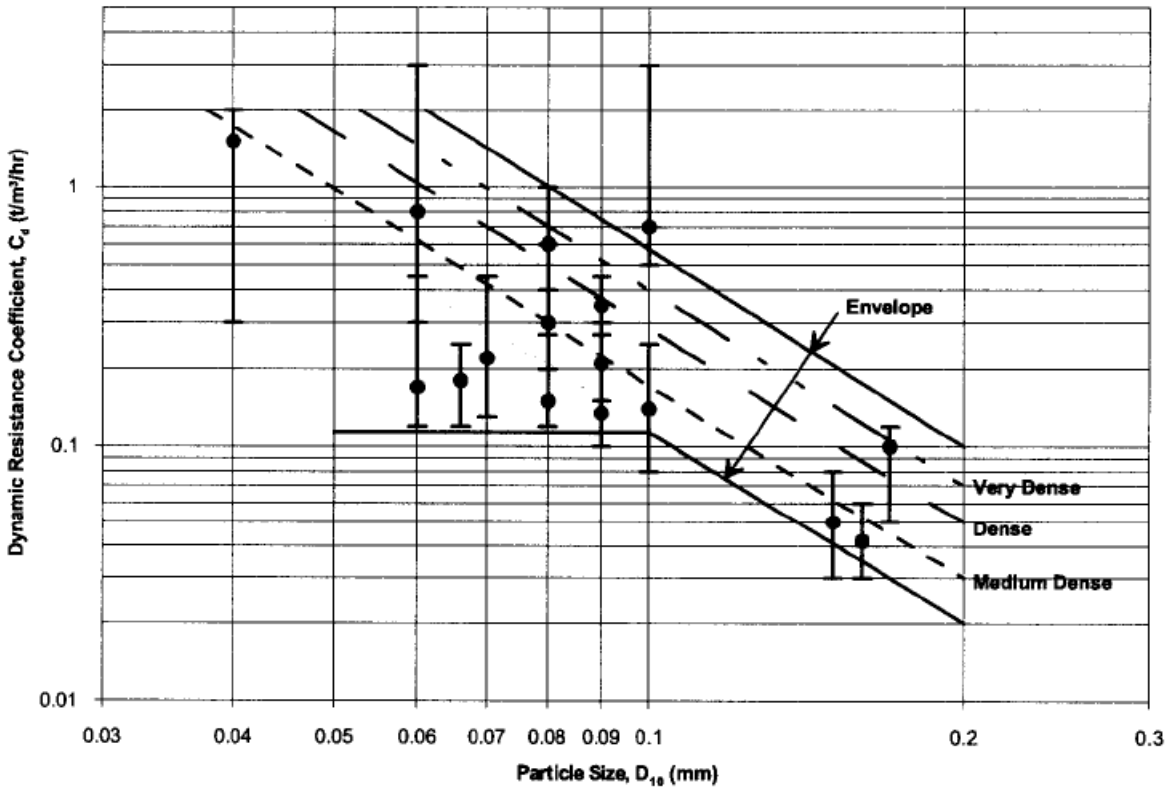


**Figure 13: Dynamic Resistance Coefficient, $C_d$ – Interpretation**

Figure 13 allows the user to predict a value of $C_d$ through the use of the $D_{10}$ particle size of the soil and the density of the soil in which they are ploughing in. However, the chart seen in Figure 13 is created by projecting a best fit line through each soil density. This method is questionable as it can be seen in Figure 11 and Figure 12 that the data is fairly random. An example of this can be seen in Figure 11 where the position of the medium dense and dense data points seem to have no distinguishable relationship with a $D_{10}$ particle size of 0.08 mm. It can be seen that the two dense data points do not correlate with each other, even though both points have the same density and $D_{10}$ particle size.

## 2.5 Fibrous Soil /Soil Reinforcement

The following section will discuss the effect of soil reinforcement or fibrous soil has on the strength and behaviour of a soil. By investigating this, it will be possible to predict how a plough will behave in reinforced or fibrous soil as it has never been studied before. However, it has been encountered in projects throughout the world, severely affecting the trench depth and project length, potentially costing millions more than budgeted for. For this reason alone it is extremely important to try and understand how the plough will behave in a reinforced soil in

order to help counteract the problem, which, in turn would help improve the efficiency of a project. Jewell and Wroth, 1987, investigated the difference between unreinforced and reinforced direct shear tests on sand and the implications of the tests for reinforced soil design. Jewell and Wroth, 1987, reinforced sand in the direct shear tests with close coiled tension springs to model circular, rough, perfectly elastic reinforcement bars. The reinforcement was positioned in the sand sample at predetermined orientation. A simple layout of this can be seen in Figure 14.

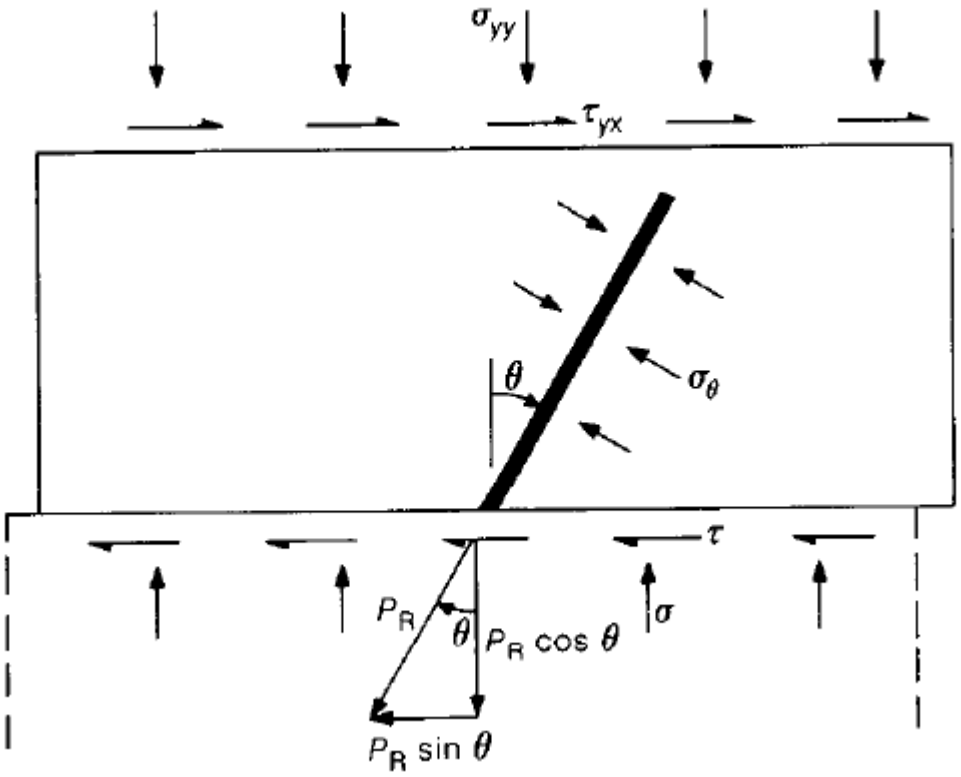


**Figure 14: Reinforced Sand Direct Shear Test Layout (Jewell and Wroth, 1987)**

The reinforcement is placed in a single plane at an angle $\pi/2 - \theta$ to the horizontal plane with half of the reinforcement being placed equally either side of the horizontal plane which has been displayed in Figure 14. The orientation of the reinforcement is extremely important and its effect has been investigated by Jewell and Wroth, 1987, in order to find the optimum angle of reinforcement which produces the most shear resistance. This can be seen in Figure 15.

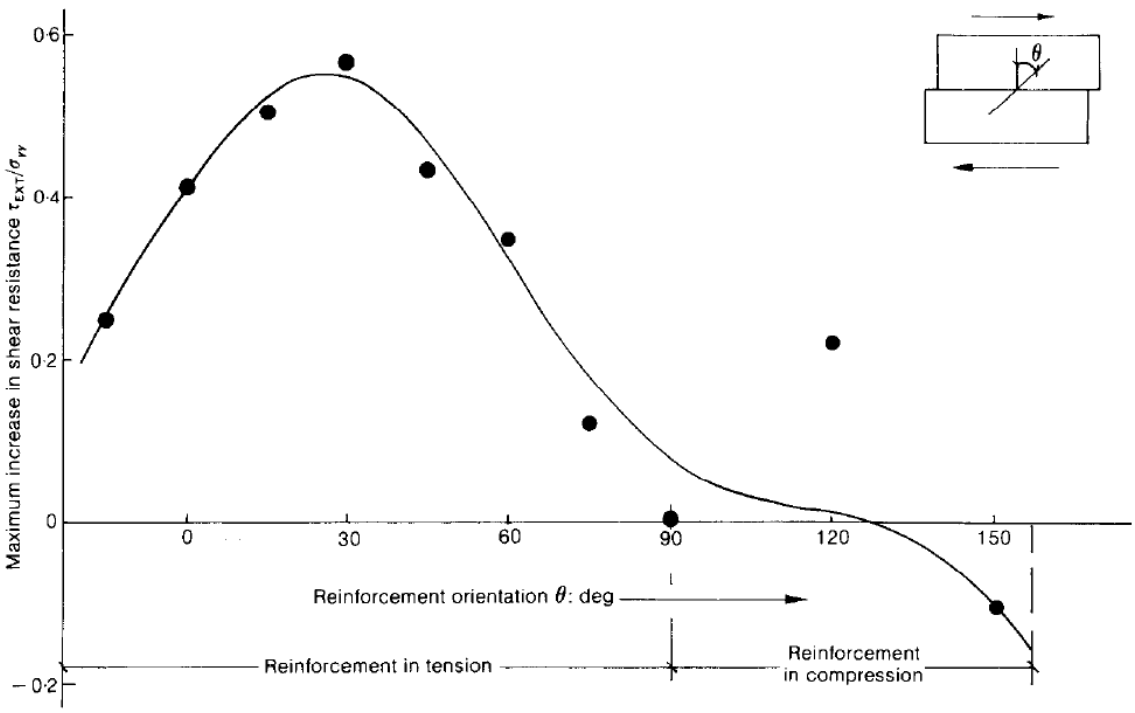


**Figure 15: The Effect of Reinforcement Orientation on the Increase in Maximum Shear Resistance (Jewell and Wroth, 1987)**

Figure 15 shows that the maximum increase in shear resistance occurs when the reinforcement is orientated at an angle of approximately 25 degrees to the vertical. With the effect of reinforcement on shear resistance reducing as the angle of reinforcement placed in the sample approaches the horizontal of the shear box. The reason for this is that reinforcement is most effective when in tension, as the angle of reinforcement approaches the horizontal of the shear box, it gets closer to being in compression, reducing its effectiveness within the sample. It can also be seen that if the reinforcement is placed at 120 degrees or more to the vertical it actually reduces the shear resistance measured in the test.

Three tests were carried out by Jewell and Wroth, 1987 at the same normal effective stress but one was unreinforced, one with extensible reinforcement within the sample and one with inextensible reinforcement. The reinforcement was placed in both samples at an angle of 25 degrees to the vertical. These results can be seen in Figure 16.

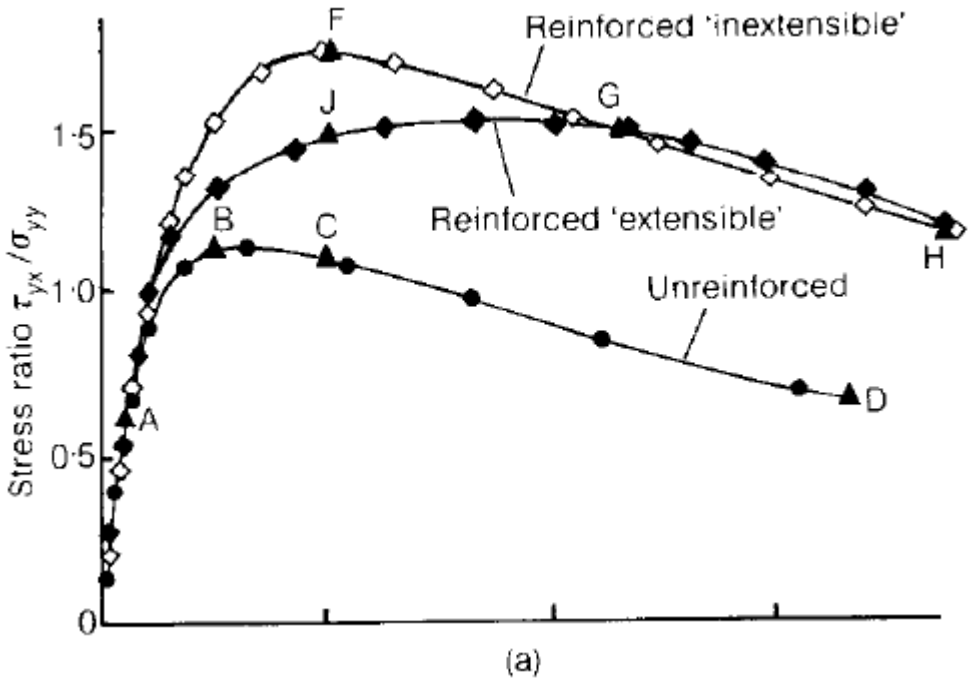


**Figure 16: Results of Direct Shear Tests on Reinforced and Unreinforced Sands (Jewell and Wroth (1987))**

Figure 16 clearly shows an increase of more than 50 % when comparing unreinforced and reinforced inextensible peak shear ratio, which is the ratio between the measured shear stress and the normal effective stress applied to the sample. It can also be seen that the shear ratio in the reinforced inextensible sample peaks quicker than the reinforced extensible sample. However, the reinforced extensible sample stays at its peak shear ratio for a longer period of time than the reinforced inextensible sample. A reason for this could be that due to the extensible reinforcement having the ability to stretch when in tension, it will slowly reach an inextensible state. This means that the stress ratio of the extensible reinforcement sample will increase for a longer period of time as the reinforcement stretches out to its point of inextensibility, before reaching its peak. In contrast to this, as inextensible reinforcement is very stiff and rigid, it is unable to stretch out while being sheared, resulting in the shear ratio peaking rapidly before reducing towards the samples ultimate state. Jewell and Wroth (1987), found that it was also important to analyse the vertical displacement, or dilatancy of a reinforced sample. Three tests were used to analyse the effect of this, one is unreinforced (test 62Y), one with extensible reinforcement (test S9Y) and one with inextensible reinforcement (test 62Y). This can be seen in Figure 17.

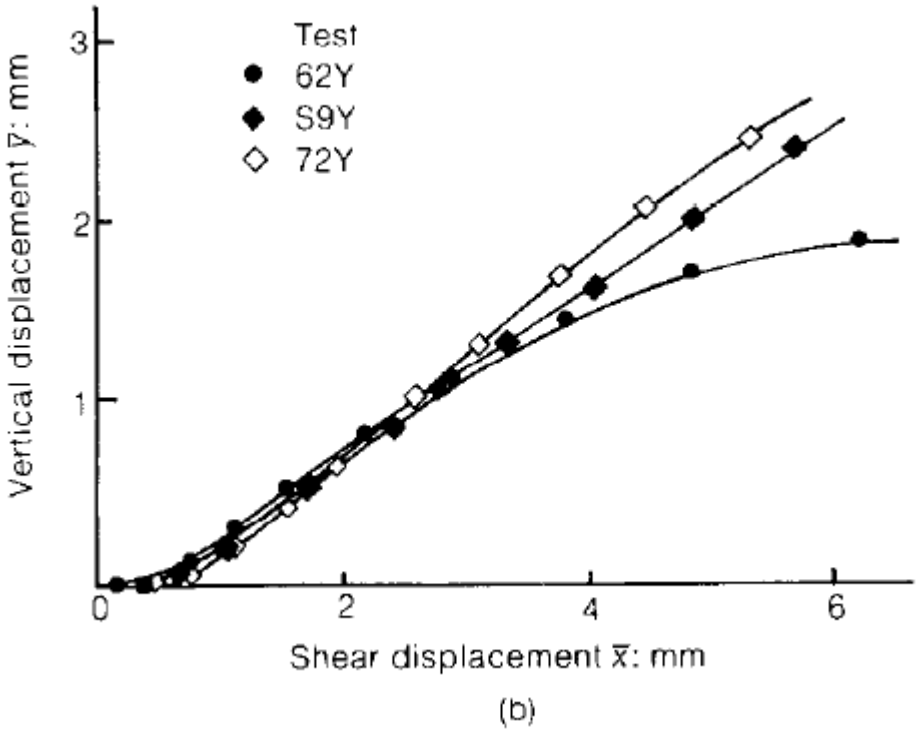


**Figure 17: Effects of Reinforcement on Vertical Displacement in Direct Shear Tests (Jewell and Wroth (1987))**

Figure 17 shows that a sample with reinforcement present will dilate more when being sheared compared to an unreinforced sand sample. It can also be seen that a sample using inextensible reinforcement will dilate more than a sample with extensible reinforcement. Jewell and Wroth (1987), found that reinforcement causes more sand to deform and helps resist localized shear deformation, which, is reflected in Figure 17 by more dilation occurring within the reinforced sand samples compared to the unreinforced sand samples. The increase in dilation, when comparing reinforced sands to unreinforced sands, is of similar behaviour to shearing different densities of sands, where more dilation occurs when shearing dense sand compared to loose sand. Jewell and Wroth (1987), also found that an explanation for the increase in stress and vertical displacement of the sample when comparing reinforced and unreinforced sands could be due to the increase in volume expansion in the deforming soil immediately surrounding the reinforcement. This increase in volume can cause additional confining stresses to be generated, meaning that it is harder to shear the sand around the reinforcement, increasing the measured shear force while testing. Jewell and Wroth (1987), created an equation which aimed to predict the extra shearing resistance due to reinforcement.

$$\tau_{EXT} = \frac{P_R}{A_S}(\cos\theta \tan\emptyset + \sin\theta)$$

**(6)**

Where,

- $\tau_{EXT}$, extra shearing resistance due to the reinforcement
- $P_R$, reinforcement force
- $A_S$, area on the central plane in direct shear apparatus
- $\theta$, angle of reinforcement from the vertical direction in the direct shear apparatus
- $\emptyset$, mobilised angle of friction

This effectiveness and accuracy of Equation 6 will be investigated through the use of test data and discussed in a later chapter. It must be noted that even though it is highly unlikely that a plough would encounter such rigid reinforcement on the seabed, Jewell and Wroth (1987), gives a solid understanding of the behaviour of reinforced sand while being sheared. However, a study on shear strength of sands reinforced with randomly distributed fibres carried out by Yetimoglu (2002) contradicted the results found by Jewell and Wroth (1987). It could be argued that randomly distributed fibres are more likely to be found in soils around the world compared to manually placing reinforcement in a specific direction for testing purposes. Yetimoglu (2002) used Duomix F20/5.1 polypropylene fibres produced by Bekaert in Belgium for testing that was carried out in a 60 x 60 mm shear box. Testing found that randomly distributed fibres never had a significant effect on peak shear strength of the soil when comparing it to an unreinforced sample with the same relative density. This can be seen in Figure 18.

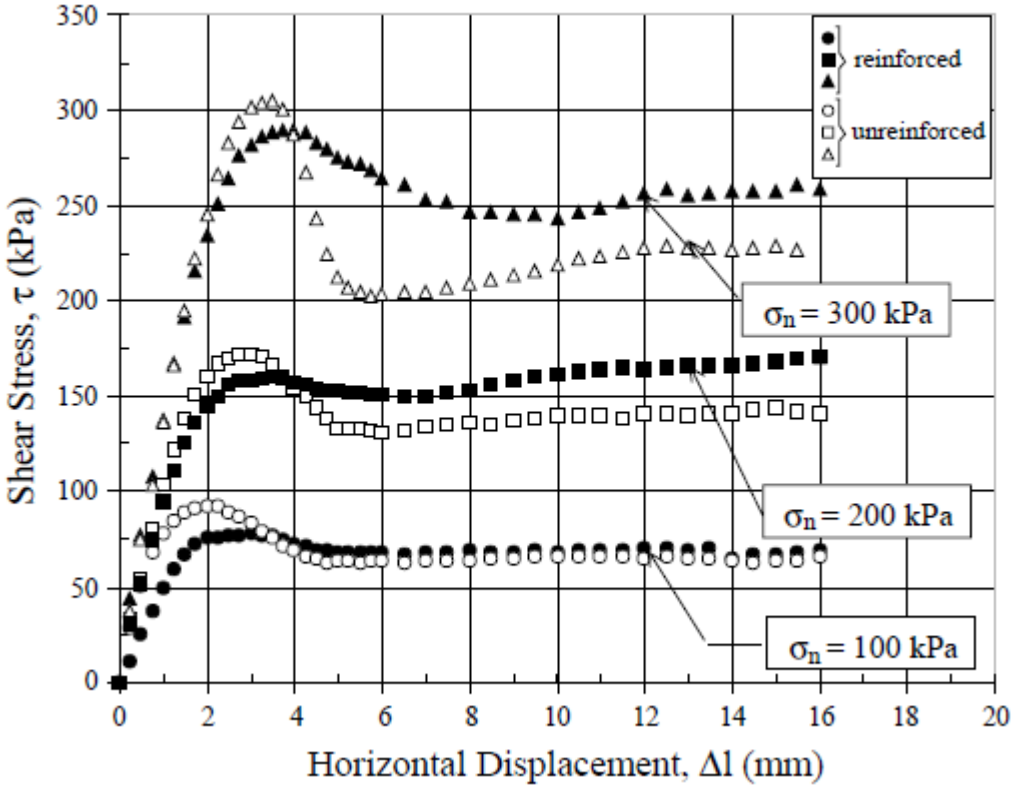


**Figure 18: Comparison of Unreinforced and Reinforced Sand with a 1 % Fibre Content (Yetimoglu, 2002)**

However, Figure 18 shows that randomly distributed fibres has a more significant effect on the residual strength of the sand when analysing the each test pair at different normal effective stress. With the increase in residual strength in reinforced sands becoming larger as the normal effective stress placed on a test increases with each pair when comparing the results to the corresponding unreinforced test. This means that the reinforced sands have a smaller reduction in post-peak strength meaning the behaviour of the sand becomes more ductile, compared to a more brittle behaviour seen in unreinforced sands. The increase in residual strength also results in the residual shear strength angle, or ultimate friction angle, increasing. It can also be seen in Figure 18 that the randomly distributed fibres have little to no effect of the initial stiffness of the sand as the shear stress increases at the same rate as the unreinforced sands. It could be argued that the rate of shear increases faster in unreinforced sands compared to reinforced sands when looking at the results in Figure 18 with the horizontal displacement of each comparable test being similar at the point of peak shear stress. Gray and Ohashi (1983) investigated the mechanics of fibre reinforcement in sand through the use of direct shear tests using similar reinforcement to Yetimoglu (2002). The difference between the test carried out by

Yetimoglu (2002) and Gray and Ohashi (1983) was that Gray and Ohashi (1983) distributed fibres in a fairly regular pattern at approximately equal spacing to each other compared to the random distribution method used by Yetimoglu (2002). Four different types of fibre reinforcement were used when testing; reed (which is commonly used to make baskets), plastic (PVC), Palmyra (which is a tough fibre which is taken from the African Palmyra palm which is often used as to construct heavy duty brooms) and a copper wire. The properties of the different fibres used in tests carried out by Gray and Ohashi (1983) can be seen in Table 7.

| Type of reinforcement (1) | Diameter DR, in millimetres (2) | Skin friction angle, $\delta$, in degrees (3) | Tensile strength, $T_R$, in pounds per square inch (4) | Youngs Modulus $E_R$, in pounds per square inch x $10^6$ (5) |
|---|---|---|---|---|
| #2 reed | 1.8 | 30 | 4,860 | 0.22 |
| Plastic (PVC) | 2.2 | 23 | 4,500 | 0.3 |
| Palmyra | 1.2 | 30 | 25,800 | 2.4 |
| Copper (wire | 1.0 | 21 | 29,000 | 8.5 |

**Table 7: Properties of Fibre Reinforcement (Gray and Ohashi, 1983)**

It was found through the use of direct shear tests that general fibre reinforcement increases the peak shear strength of the sand and limits the reduction in post peak shearing resistance.

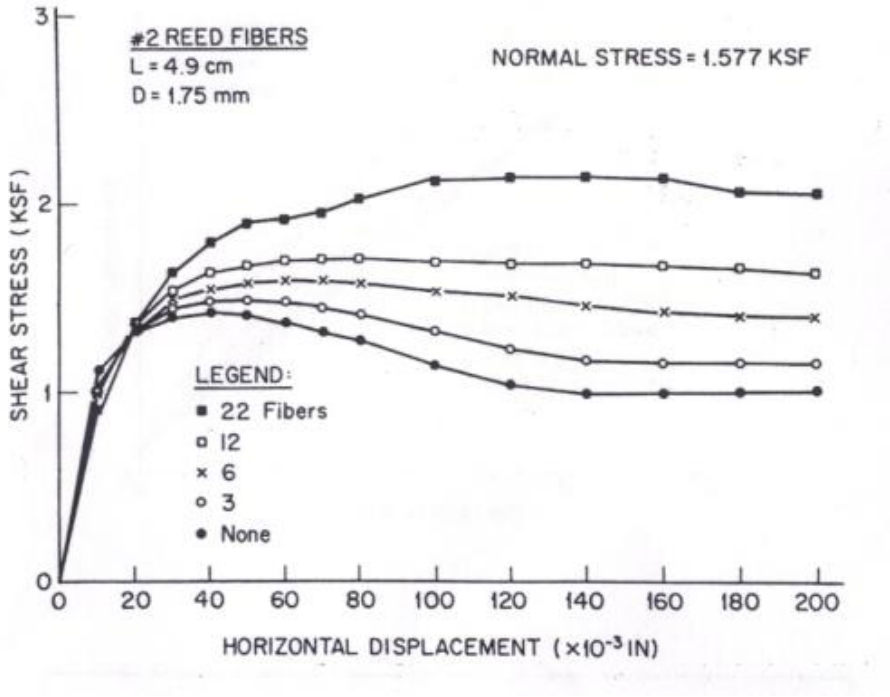


**Figure 19: Effect of Different Amounts of Reinforcement on Shear Stress (Gray and Ohashi, 1983)**

This indicates that the inclusion of reinforcement increases the strength of the soil when comparing it to an unreinforced sand of similar density, which contradicts the results found by Yetimoglu (2002) seen in Figure 18. This suggests that the direction that the fibres are placed in are as equally important as the angle that the fibres are placed in the sample in relation the shear plane that was found by Jewell and Wroth (1987) which be seen in Figure 15. Figure 19 also suggests that the amount of fibres or fibre ratio within the soil has a significant effect on shear stress. This indicates that measured shear stress will increase when the soil is reinforced with a higher fibre ratio, or in this case, more fibres present within the soil. The length of fibre and its effect on shear strength increase was also investigated by Gray and Ohashi (1983). It was found that increasing the length of fibres used for reinforcement increase the shear strength of the soil. However, the increase in shear strength only occurred up to a point as each of the fibres used did not reach its full mobilization of tensile strength due to some of the fibres being longer than the shear box. The effect of fibre length on shear stress can be seen in Figure 20.

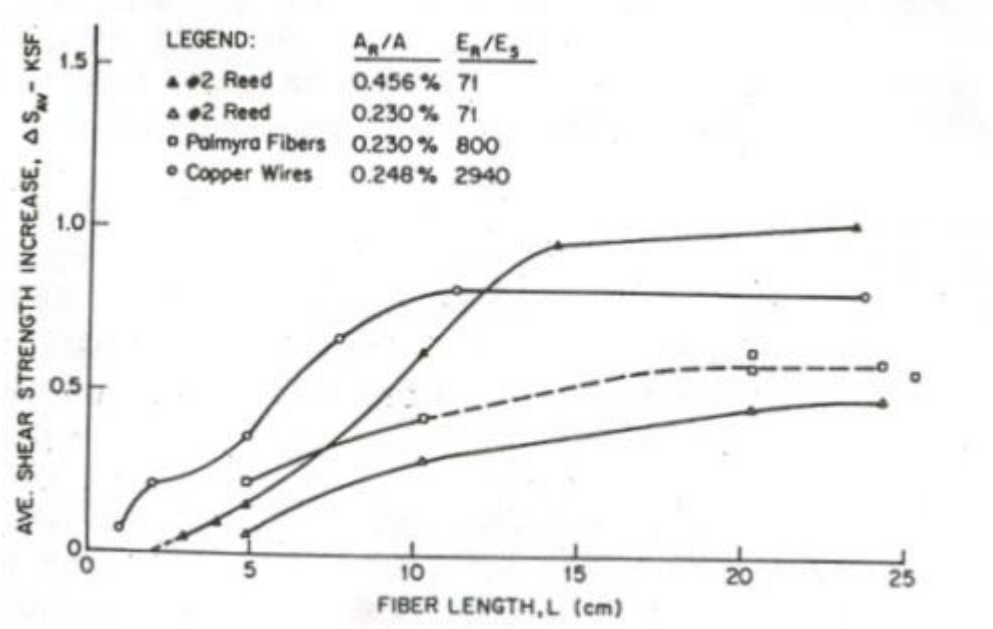


**Figure 20: Influence of Fibre Length on Shear Strength Increase (Gray and Ohashi, 1983)**

As mentioned earlier the angle in which the fibres are placed to the shear plane has a significant effect on shear strength. Gray and Ohashi (1983) found that the maximum shear strength increase occurred when fibres were placed at 60 degrees to the horizontal, or 30

degrees to the vertical as described by Jewell and Wroth (1987). The effects of fibre orientation found by Gray and Ohashi (1983) can be seen in Figure 21.

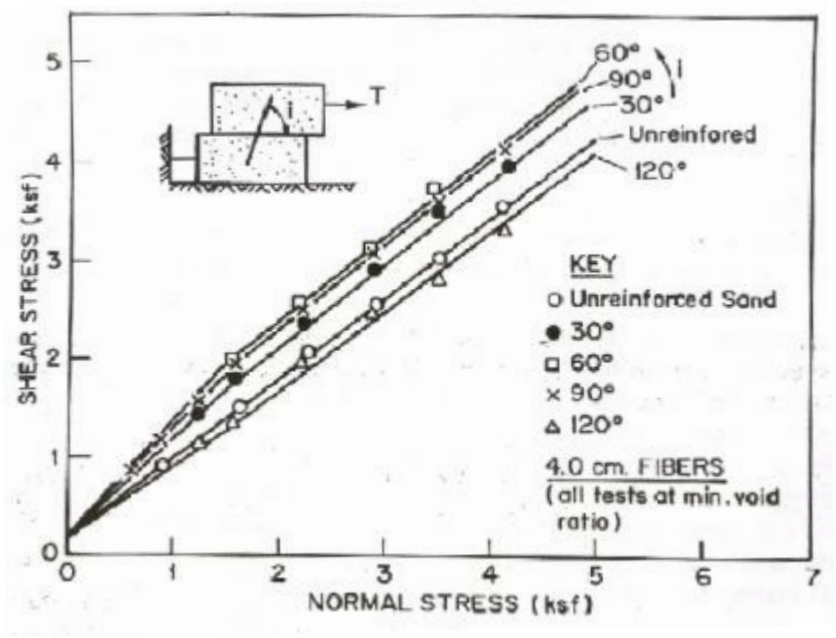


**Figure 21: Influence of Fibre Orientation on Shear Stress (Gray and Ohashi, 1983)**

It can be seen that the optimum angle of fibre orientation of 60 degrees to the horizontal in Figure 21 backs up the results found by Jewell and Wroth (1987) in Figure 15 where it was also found that the biggest increase in shear stress occurs when fibres are orientated at 60 degrees to the horizontal, or 30 degrees to the vertical as indicated in Figure 15. Similarly to Figure 15, it can be seen from the work carried out by Gray and Ohashi (1987) that when fibres are orientated at an angle of 120 degrees the soil seems to be weakened. This is because the fibres are now in compression rather than in tension, where they are most effective. When a fibre is in compression it has little to no effect as they are not rigid, meaning they will bend and crush when being compressed. Diambra *et al* (2008) investigated the effects of sand reinforced with short polypropylene fibres and how it behaved in conventional triaxial and extension tests. One of the main findings was that the volumetric behaviour, or dilatancy, of the sample is affected by the addition of fibres, with the dilation of the sample increasing with fibre content. This suggests that the angle of dilatation is dependent on both density of the sample and its stress level. Diambra *et al* (2008) also found that an increase in fibre ratio will increase the strength of the sample which backs up results found by Gray and Ohashi (1983). A reason for this could be that the addition of fibres within the sample effects restricts the movement of

sand grains while being sheared due to the physical presence of the fibres. This means that the strength of the sample will increase as it is harder for the grains to move while being sheared resulting in more force needed to move them, explaining why the strength of a sample increases with higher fibre ratios. The effect of different fibre ratios on sample strength and its corresponding volumetric behaviour found by Diambra *et al* (2008) can be seen in Figure 22.

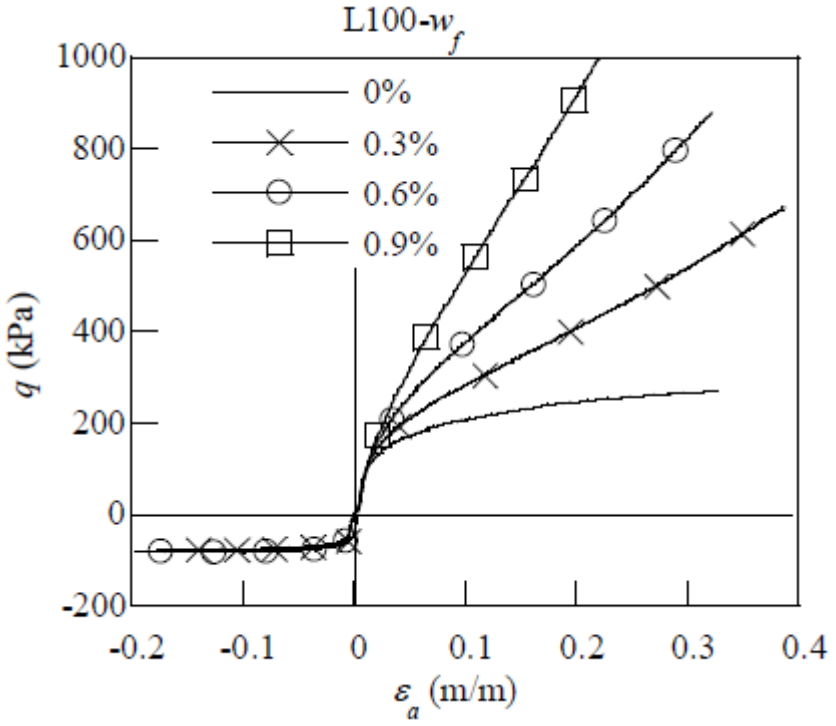


**Figure 22: Deviator Stress-axial Strain for Drained Tests at Different Fibre Ratios (Diambra *et al*, 2008)**

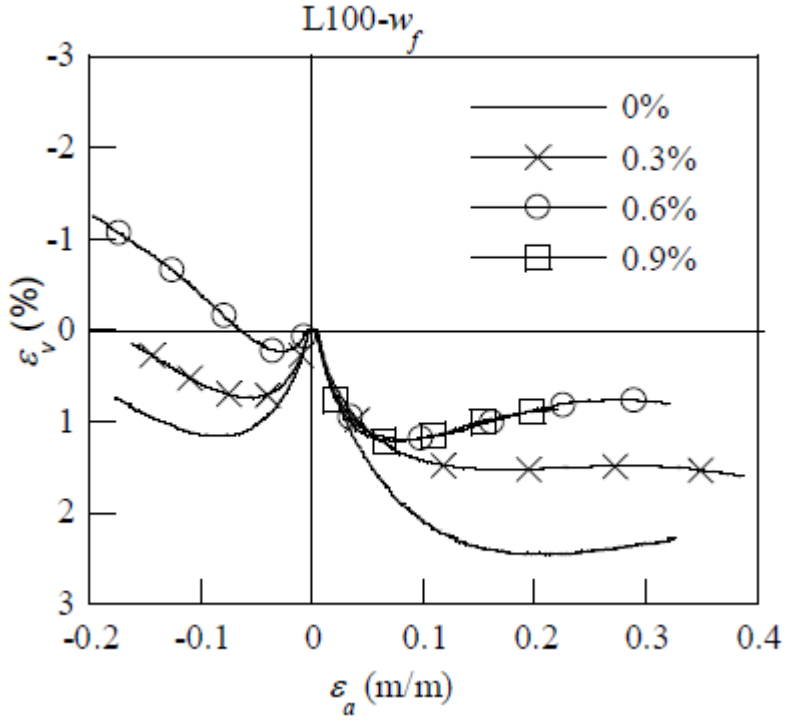


**Figure 23: Volumetric Behaviour for Drained Tests at Different Fibre Ratios (Diambra *et al*, 2008)**

Similarly to Gray and Ohashi (1983), Diambra *et al* (2008) found that the inclusion of fibres has a negative effect on the strength of a sand when being compressed. This can be seen in Figure 22 where the stress measure for each test is negative while the strain of the sample is negative, or in compression. It was also found by Diambra *et al* (2008) that the addition of fibres results in a significant increase in the angle of friction and cohesion intercept. These increases can be seen in Table 8.

| at failure $\varepsilon_a$ = 20 % | | | | | | | | |
|---|---|---|---|---|---|---|---|---|
| Test series | Fibre content (%) | | | | | | | |
| | 0 | | 0.3 | | 0.6 | | 0.9 | |
| | c (kPa) | 0 (°) | c (kPa) | 0 (°) | c (kPa) | 0 (°) | c (kPa) | 0 (°) |
| (L) tests | 4.8 | 33.5 | 21.4 | 36.2 | 46.3 | 38.5 | 68.9 | 42.7 |
| (M) tests | 8.5 | 33.1 | 38.2 | 34.5 | 77.4 | 36.9 | - | - |
| (D) tests | 2.4 | 35.9 | 40.7 | 38.9 | - | - | - | - |
| $\varepsilon_r$ = 15 % | | | | | | | | |
| (L) tests | 4.8 | 33.5 | 35.7 | 39.2 | 59.4 | 43.7 | 79.3 | 49.4 |
| (M) tests | 8.5 | 33.1 | 36.9 | 38.6 | 84.0 | 41.5 | - | - |
| (D) tests | 2.4 | 35.9 | 43.1 | 38.7 | - | - | - | - |

**Table 8: Angle of Friction and Cohesion Intercept of all Series of Tests in Compression at Failure (Diambra *et al*, 2008)**

Table 8 clearly shows how both the cohesion intercept and friction angle of each test increases with fibre content. The strength envelopes of each test which produced the cohesion intercepts for the L test series can be seen in Figure 24.

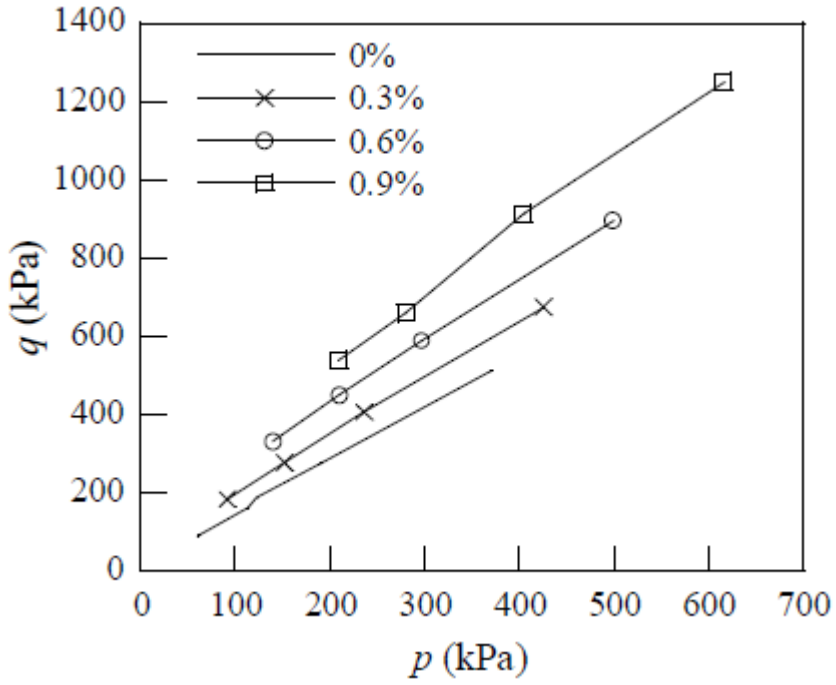


**Figure 24: Deviatoric Strength Envelopes for (L) Test Series (Diambra *et al*, 2008)**

A report by the University College Dublin investigated the effect on soil strength through the use of laboratory tests carried out on fibrous sand and organic clay from the Adriatic Sea. The soil tested was taken from the route of a submarine pipeline to an LNG terminal. Similarly to what was found by Jewell and Wroth (1987) and Gray and Ohashi (1983), the results of tests carried out by the University College Dublin showed that compared to unreinforced samples, the fibre reinforced tests reach a higher peak shear stress and the post peak shear stress remains larger until very large strains. The UCD report also found that while fibres do not influence the stiffness of the soil at small strains, they have a significant influence on the shear strength for intermediate to large strains. This could explain the reason that the measured stress in both unreinforced and reinforced samples initially increases at the same rate until the point where the unreinforced soil begins to reach its peak stress and the measured stress in the reinforced sample continues to increase, which can be seen in Figure 18, Figure 19 and Figure 22.

## 2.6 Areas for Further Investigation

- Use direct shear tests to further investigate the effects of reinforced sands on shear stress.
- Investigate the effects of reinforced sand on offshore pipeline plough performance at different fibre ratios.
- Investigate the rate effect on an offshore pipeline plough when working in reinforced or fibrous sand.
- Analyse different models mentioned in previous sections that predict the increase in shear strength when working with reinforced soils. Investigate if any of these models can be used to predict the effect of reinforced sand on offshore pipeline ploughs or if they can be modified and added to the Cathie and Wintgens (2001) model.

# Chapter 3. Methodology

The following chapter will discuss the apparatus and methods used while investigating the effects of reinforced sand on an offshore pipeline plough. Two different tanks were used for investigating the behaviour of the plough in reinforced sand with two different scale model ploughs. Element testing was also carried out to investigate the characteristics of reinforced sand and how it will affect the plough.

## 3.1 Testing Apparatus

### 3.1.1 Sand Bed Tanks

Two tanks were used for testing 1/25$^{th}$ and 1/50$^{th}$ scale model ploughs. The tank used for the 1/25$^{th}$ scale test was 2500 mm long, 1500 mm wide and 750 mm deep. The tank was manufactured on site at the University of Dundee based upon designs by Keith Lauder (Lauder *et al*, 2008). The tank was welded together then sealed using silicon to allow for saturated tests to be conducted. It was important to have a tank that was of sufficient length to allow the plough to reach its steady state zone after transitioning in order to get an accurate understanding of how the plough behaves in each test. The 1/25$^{th}$ scale tank had two parallel tracks that were installed on each wall spanning its length with two perpendicular I-beams. The two I-beams were connected at a set distance apart of 165 mm by bolting two metal plates on either side of the I-beams. The 1/25$^{th}$ tank can be seen in Figure 25.

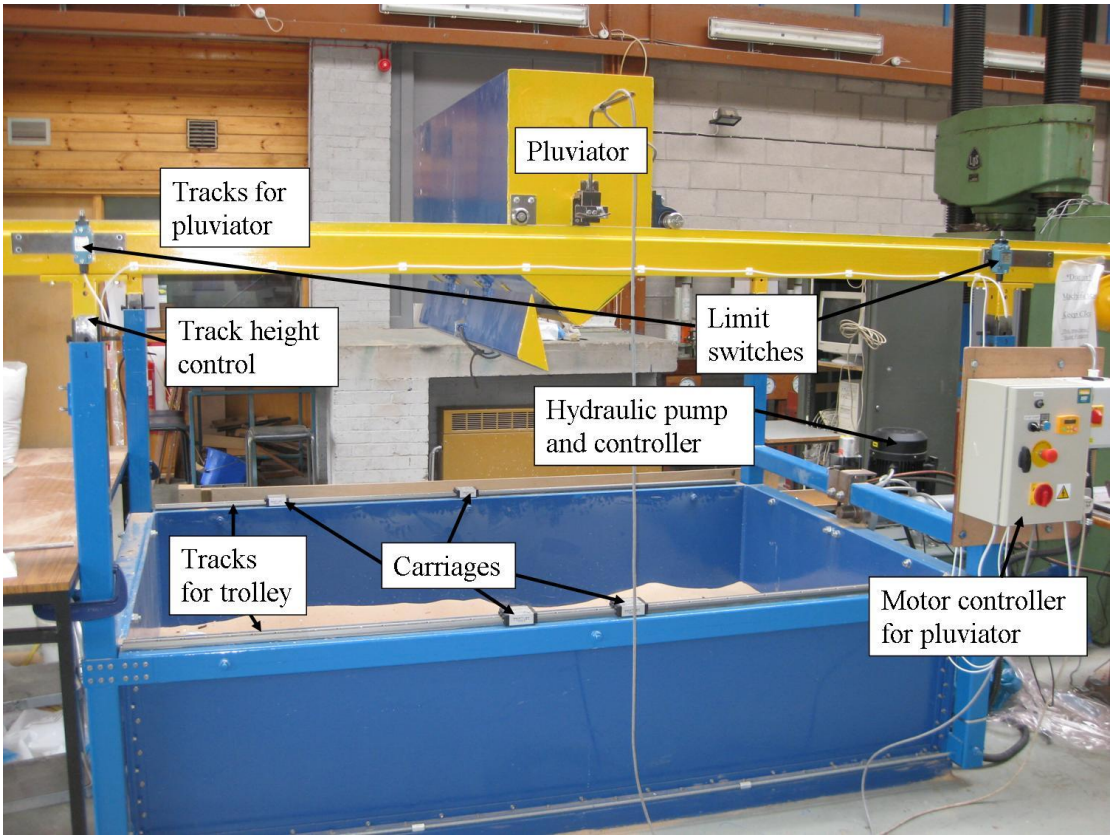


**Figure 25: 1/25th Scale Tank Test Apparatus (Lauder, 2011)**

The reason for fixing the I-beams at a set distance was to help prevent the beams twisting relative to each other whilst on the track. The I-beams (trolley system) that were used to pull the plough when testing in the 1/25th scale tank can be seen in Figure 26.

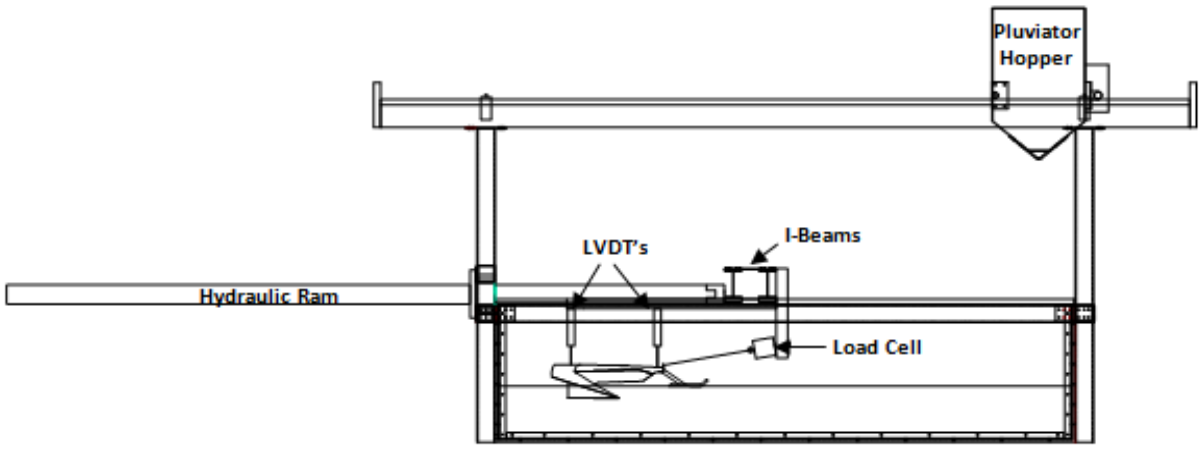


**Figure 26: Diagram of 1/25th Scale Tank Apparatus (Lauder, 2011)**

The I-beams were connected to the track by a set of Drylin T linear carriage runners manufactured by Igus that were bolted to each end of the I-beams. These runners were used as they produce low friction when being pushed along the track. The runners had a carriage width of 25 mm and a length of 96 mm. The I-beams (Figure 26) were pushed the length of the tank by a hydraulic actuator that was placed at one end of the tank which can be seen in Figure 25. The speed and direction of the actuator was controlled manually through the use of a proportional speed controller at the side of the tank.

To allow sand bed preparation by pluviation, two rails that span the length of the tank, were also installed above the tank at height of 950 mm above the tank wall. These rails held an automated pluviation system that travelled back and forth along the rails at a speed of 100 mm/s. The pluviation system consisted of a sand hopper, which was moved along the track by an electric motor connected to wheels, with interchangeable slot widths to change sand density which was positioned at a constant height of approximately 800 mm above the sand bed to particles being poured to reach terminal velocity. The 1/25$^{th}$ hopper had a width of 2 mm which poured a sample with a relative density of approximately 75 % when moving at a speed of 100 mm/s. Four sensors were placed at each of the rails which changed the direction of the hopper once touched. More detail about the pluviation system used in testing can be found in Lauder, 2011.

A series of pipes were installed in the bottom of the tank that was connected to a tap in the laboratory that allowed for tests to be saturated. These pipes were then covered by a layer of gravel to allow the water, to spread evenly around the base of the tank before coming into contact with the sample. The gravel layer was then separated from the sample by a layer of fabric and mesh. The fabric and mesh was used to prevent sand particles falling into the gravel layer and to allow for a relatively flat sample to be created from the sand being poured by the pluviation system.

The tank used for the 1/50$^{th}$ scale tests was 2000 mm long, 400 mm wide and 500 mm deep which was previously used by Bransby *et al* (2005), Brown *et al* (2006), Tovey (2009) and Lauder (2011). Similarly to the 1/25$^{th}$ scale tank it was important for the tank to be long enough to allow for the plough to comfortably reach its steady state. One wall of the tank was made from clear Perspex. This allowed for easier viewing of the testing process. A schematic of the 1/50$^{th}$ scale tank can be seen in Figure 27.

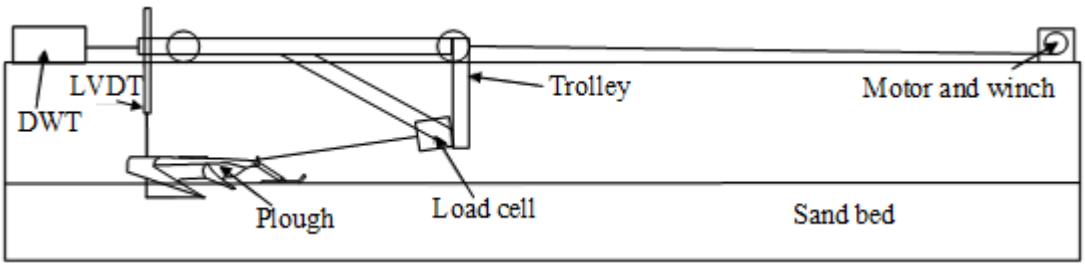


**Figure 27: Elevation and Plan View of 1/50th Scale Tank (Adapted from Lauder, 2011)**

A pulley system was connected to a trolley seen in Figure 28 and Figure 29, which was constructed using dexion frame and plastic wheels, to pull the plough throughout the test at a constant speed. This system was pulled by a D.C geared electric motor which was powered by a variable power supply. The power supply varied from 2v to 20v, which allowed the option of variable tow speeds for testing. A picture of the trolley used in 1/50th scale tank testing can be seen in Figure 28.

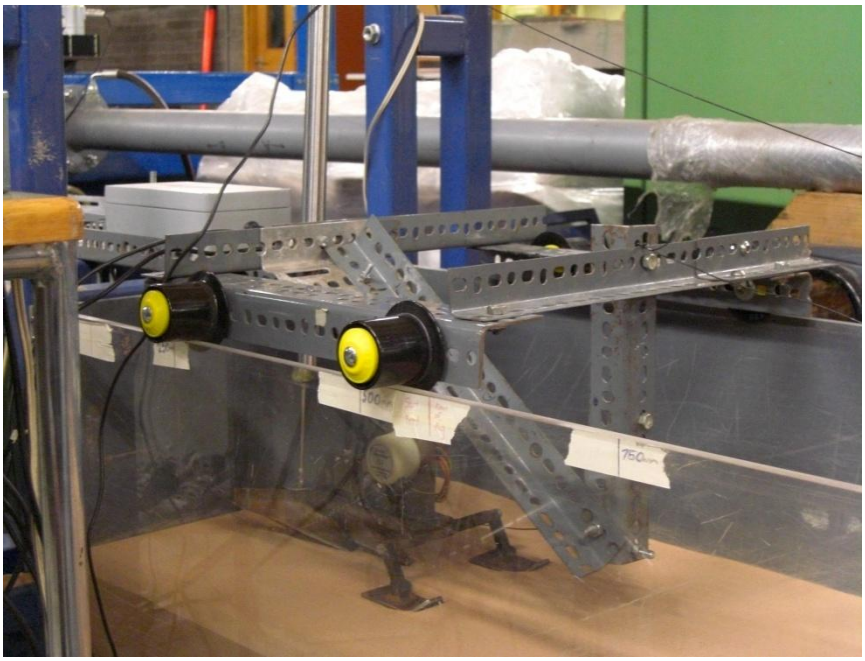

**Figure 28: 1/50th Scale Tank Trolley System**

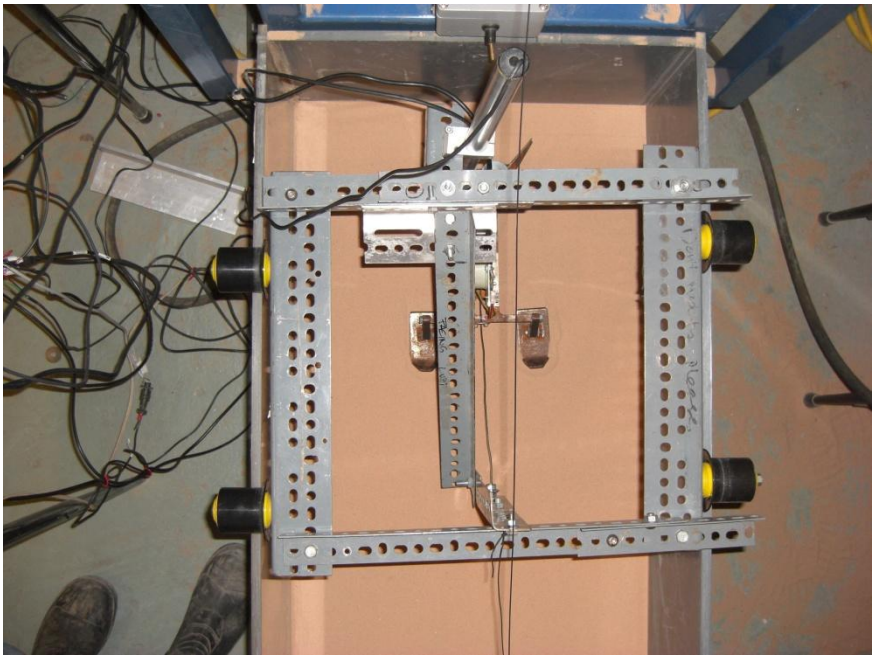

**Figure 29: 1/50th Scale Tank Trolley System (Plan View)**

Two railings, spanning the length of the tank, were attached to the top of the frame, so that a hopper could run back and forth above the tank for the pluviation of sand. The hopper can be seen in Figure 30.

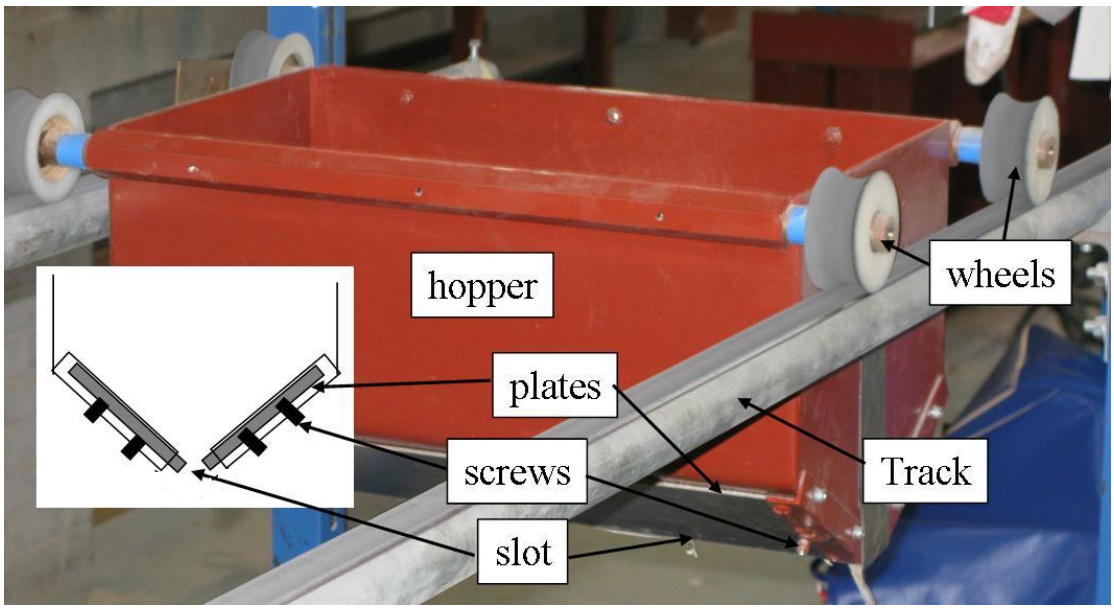


**Figure 30: 1/50th Pluviation Hopper (Lauder, 2011)**

The hopper was placed 800 mm above the 1/50th scale tank to allow for the sand particles to reach terminal velocity. The width of the slots, seen in Figure 30, could be varied manually to

dictate the density of sand poured from the hopper with a typical width of 0.5-4 mm (Lauder, 2011). However, this hopper was moved back and forth along the length of the tank manually at a velocity of approximately 150 mm/s when preparing a sample. A hose valve was also connected to the tank by a valve so that the sand could be saturated and drained when carrying out saturated tests, later on in the testing process. This valve was placed below the surface of the drainage layer to allow the water to spread evenly throughout the gravel before coming into contact with the sample.

## 3.2 Ploughs

Two ploughs were constructed at 1/25$^{th}$ and 1/50$^{th}$ scale based on engineering drawings provided by CTC Marine. The ploughs were modelling the Advanced Pipeline Plough (APP) with a full scale weight of 190 Te (1893.2 kN) and dimensions of 17.5m long, 10m wide and 8.5 m high. The models constructed for testing were simplified and ignored pipeline grabs, buoyancy tanks and hydraulics. The two scale ploughs were constructed by Houston's of Cupar with minor modifications being made at the University of Dundee. Each model plough had a removable forecutter, which was not used in testing, and adjustable skid height control which dictates plough depth. A 1/10$^{th}$ scale plough was also constructed but wasn't used in the project.

## 3.3 Measurement Apparatus

A number of different measurement apparatus were required in order to log and produce data on the ploughs performance throughout each test. When testing in the 1/25$^{th}$ and 1/50$^{th}$ scale tanks a Draw Wire Transducer (DWT), two Linear Variable Displacement Transducers (LVDTs) and a load cell were connected to the I-beams and to the plough. The basic setup of apparatus for the 1/25$^{th}$ scale tests can be seen in Figure 31 and Figure 32

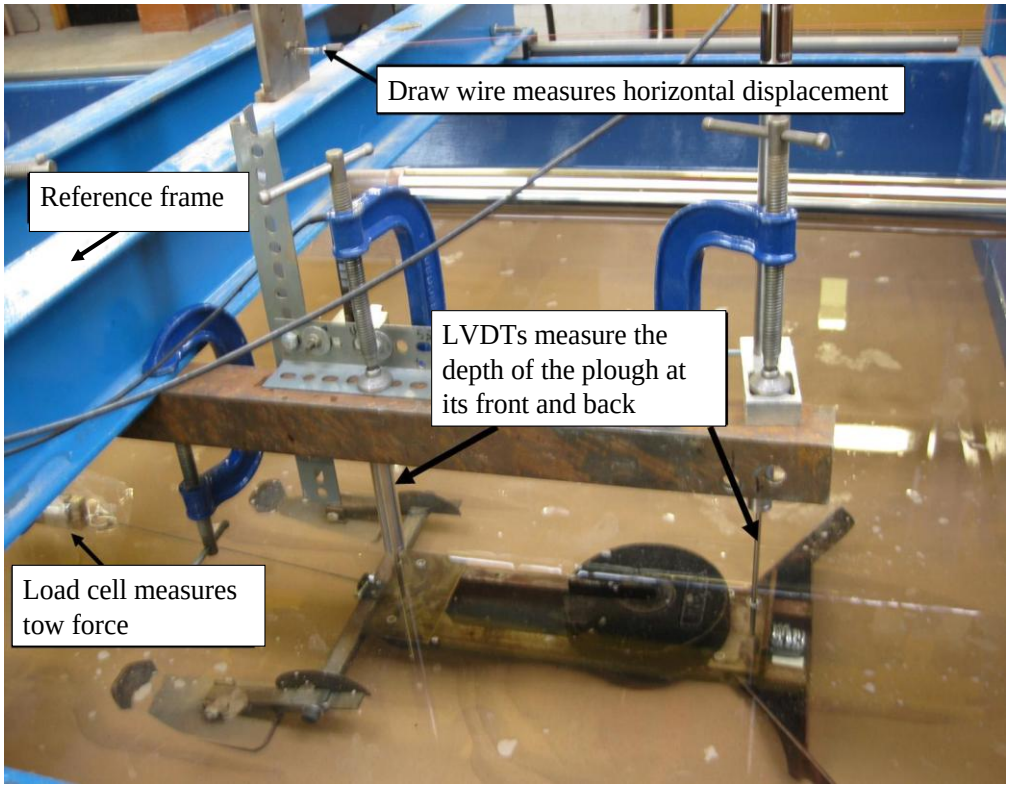


**Figure 31: Basic 1/25th Scale Test Measurement Apparatus Setup (Lauder, 2011)**

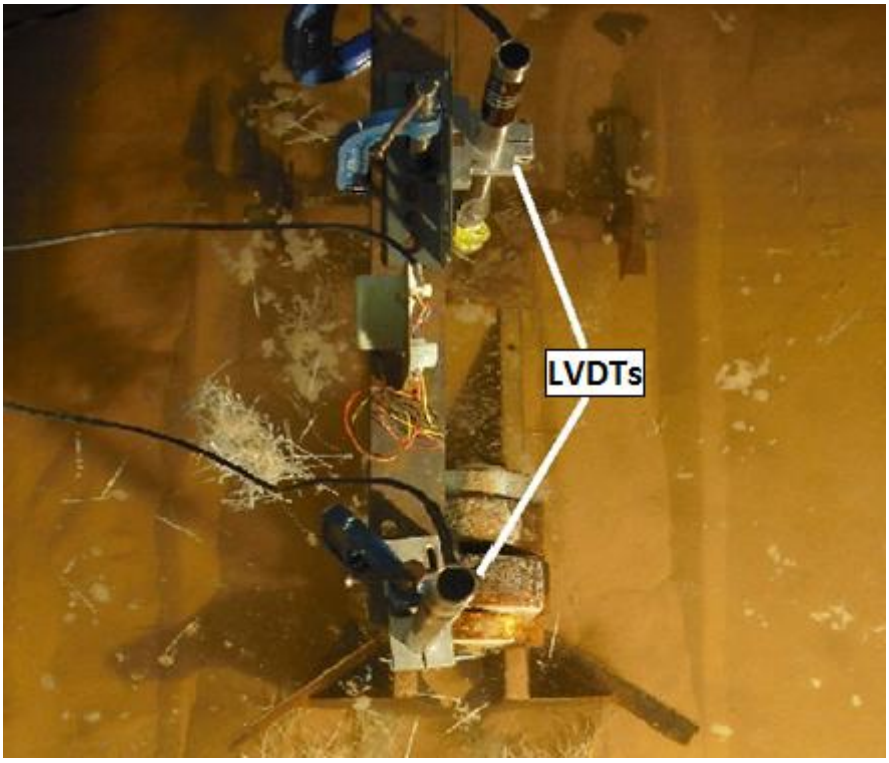


**Figure 32: Basic 1/25th Scale Test Measurement Apparatus Setup (Plan View)**

The general setup of apparatus used in the 1/50$^{th}$ scale tests can be seen in Figure 27.

The load cell used in the 1/25$^{th}$ scale tank was a RLT Tension Load Cell with a capacity of 50 kg. The load cell used in the 1/50$^{th}$ scale tank was the same model of load cell but with a capacity of 20 kg. Both load cells were manufactured by RDP Electronics LTD. The LVDTs used in both tanks were LDC Series DC to DC LVDT Displacement Transducers which were also manufactured by RDP Electronics.

## 3.4 Shear Box Apparatus

The apparatus used for shear box testing consisted of two LVDT's and a load cell. The load cell used was a 250 kg capacity S-Bend load cell manufactured by Tadea Huntleigh and two LDC Series DC to DC LVDT Displacement Transducers manufactured by RDP Electronics. The effective stresses used in testing were applied by adding weights to a hanger which was connected to the lid of the shear box. The normal effective stresses used in testing will be discussed in the shear box preparation section later in the chapter.

## 3.5 Soil Properties

The soil used in all of the tests carried out in the project was uniform fine silica sand. The dense samples used were prepared using a slot pluviator. The sand properties can be seen in Table 9.

| | | |
|---|---|---|
| $D_{50}$ | 0.18 | mm |
| $D_{10}$ | 0.10 | mm |
| $\rho_{min}$ | 1461 | kg/m$^3$ |
| $\rho_{max}$ | 1760 | kg/m3 |
| $\theta'_{crit}$ | 30.8 | degrees |

**Table 9: Properties of Sand Used in Testing**

Figure 33 displays the particle size distribution (PSD) curves for Redhill 110, HST95 and HST50 sands.

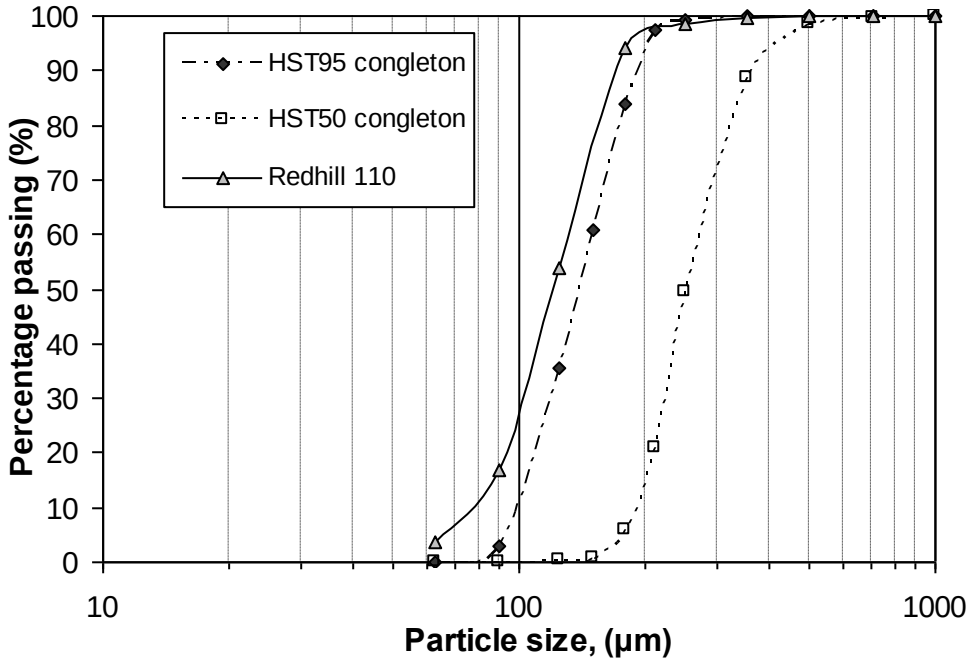


**Figure 33: Particle Size Distribution Curves - HST50, HST95 and Redhill 110**

## 3.6 Fibre Properties

The fibres used in the project were Strux 90/40 macro fibre reinforced (Grace Construction Limited). These fibres are designed to limit shrinkage cracking in concrete. Before deciding to use Strux 90/40 in the project, many different materials were considered at the beginning of the project. Initially, it was though that natural fibres would be best suited, such as jute, string and wood. However, due to practicality issues these materials could not be used as it would be near impossible to produce the large numbers of fibres for each fibre layer. Other man made materials were also considered such as Loksand by Drake Extrusion ltd which is used as reinforcement when installing artificial turf. This material was very hard to separate which would prove to be a problem when creating fibre layers. Therefore, it was decided that Strux 90/40 would be the most practical material to use in the project. The scale length of Strux 90/40 in the $1/25^{th}$ and $1/50^{th}$ scale tank was approximately 1 m and 2m respectively. The properties of the fibre can be seen in Table 10.

| | | |
|---|---|---|
| Length | 40 | mm |
| Width | 2 | mm |
| Thickness | 0.1 | mm |
| Specific Gravity | 0.92 | |
| Modulus of Elasticity | 9.3 | GPa |
| Tensile Strength | 620 | MPa |

**Table 10: Strux 90/40 Fibre Properties (Grace Construction Products)**

## 3.7 Sample Bed Preparation

Each test carried out in the 1/25$^{th}$ and 1/50$^{th}$ scale tanks consisted of fibre layers within the sand sample. These layers were based on percentage volume approach where each layer was calculated by working out the percentage of sand being replaced by fibre. One layer consisted of two passes of the hopper along the length of the tank while pouring the sand, with a layer being approximately 13 mm in depth. It was decided that five different fibre volume ratios would be used throughout testing (f = 0.5, 1, 1.5, 2, 4 %). These percentages were chosen due to practicality issues with fibre and sample bed preparations. A fibre volume ratio of higher than 4 % would be unpractical when preparing each test due to it being extremely time consuming and sheer volume of fibres needed.

### 3.7.1 1/25$^{th}$ Scale Bed Preparation

Each sample bed was prepared using an automated pluviating system with the hopper set to pour dense sand in dry conditions as mentioned previously. Initially a 60 mm deep unreinforced sand zone was poured to negate any influence on the fibre layers caused by the fabric filter layer. Each fibre layer was pre-measured to allow for an accurate percentage of fibre per layer and separated into a plastic sample bag. The tank was then split into two halves as it is possible to run two tests in one sample bed due to the width of the tank. To show the effect of fibres on the plough a 1 m zone (from the back of the ploughs starting point to the start of fibre zone, which is approximately 720 mm from the front of the plough to the start of the fibre zone) of unreinforced sand was placed in front of the fibre zone. This unreinforced sand zone allowed the plough to reach its steady state behaviour before being affected by the fibre zone. Figure 34 is an example of how these zones were arranged.

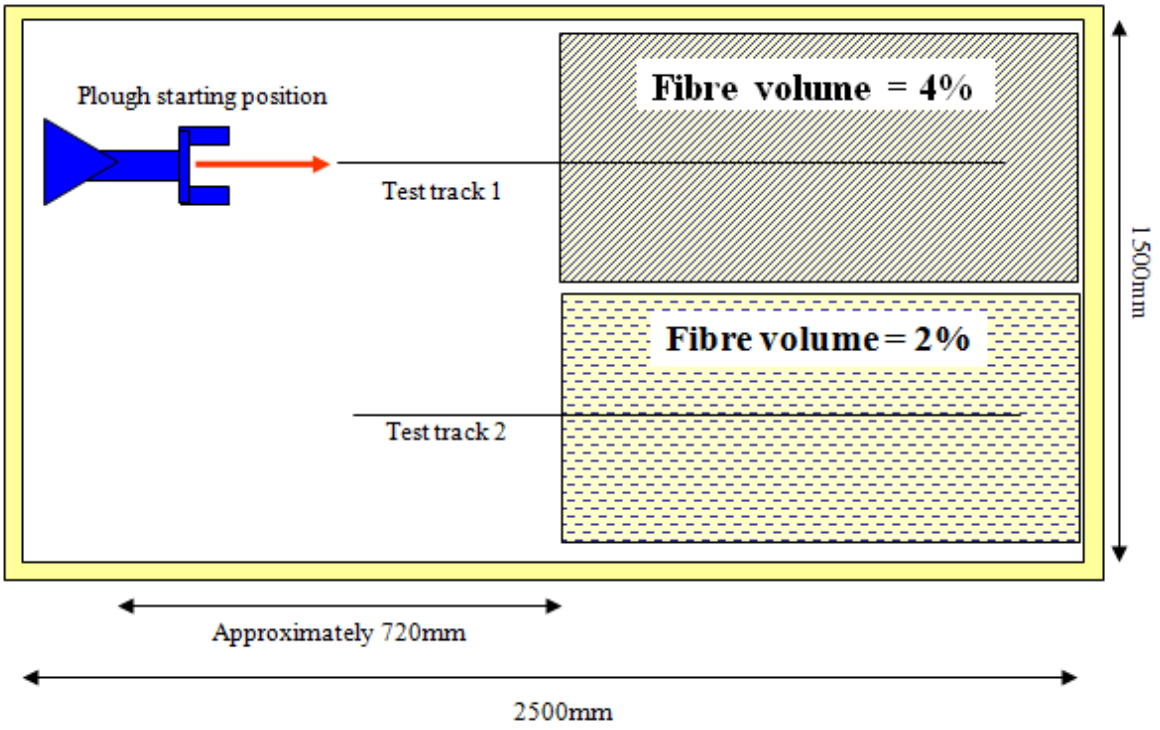


**Figure 34: Layout of 1/25th Scale 2 & 4 % Fibre Volume Test (Brown,M.J., Bransby, M.F., Tovey, S. & Lauder, K., (2010) – Experimental Investigation of Pipeline Plough Performance in Reinforced Soils)**

Each fibre layer was created by spreading out the pre-measured fibres evenly by hand throughout the set fibre zone area. This procedure was refined by carrying out several trial runs in smaller tank before preparing the first sample bid. Each layer consisted of 13 mm depth of sand poured by the hopper and the pre-measured fibre percentage distributed randomly throughout the fibre zone. The slot width of the hopper was set to pour sand at a relative density of 75 %.This procedure was repeated until a total bed depth of 390 mm was achieved. This total depth consisted of 100 mm drainage layer, 60 mm unreinforced sand zone and a 230 mm reinforced zone. However, the reinforced zone for the 2% and 4% tests were 300 mm deep. This increase in sample depth had no effect on testing, it simply increased the depth of the fibre layer when compared to other beds. A fibre layer during preparation can be seen in Figure 35. The sample bed being prepared consisted of 2% and 4% fibre volume ratios, with the annotated red line indicating the border between reinforced and un-reinforced sand zones.

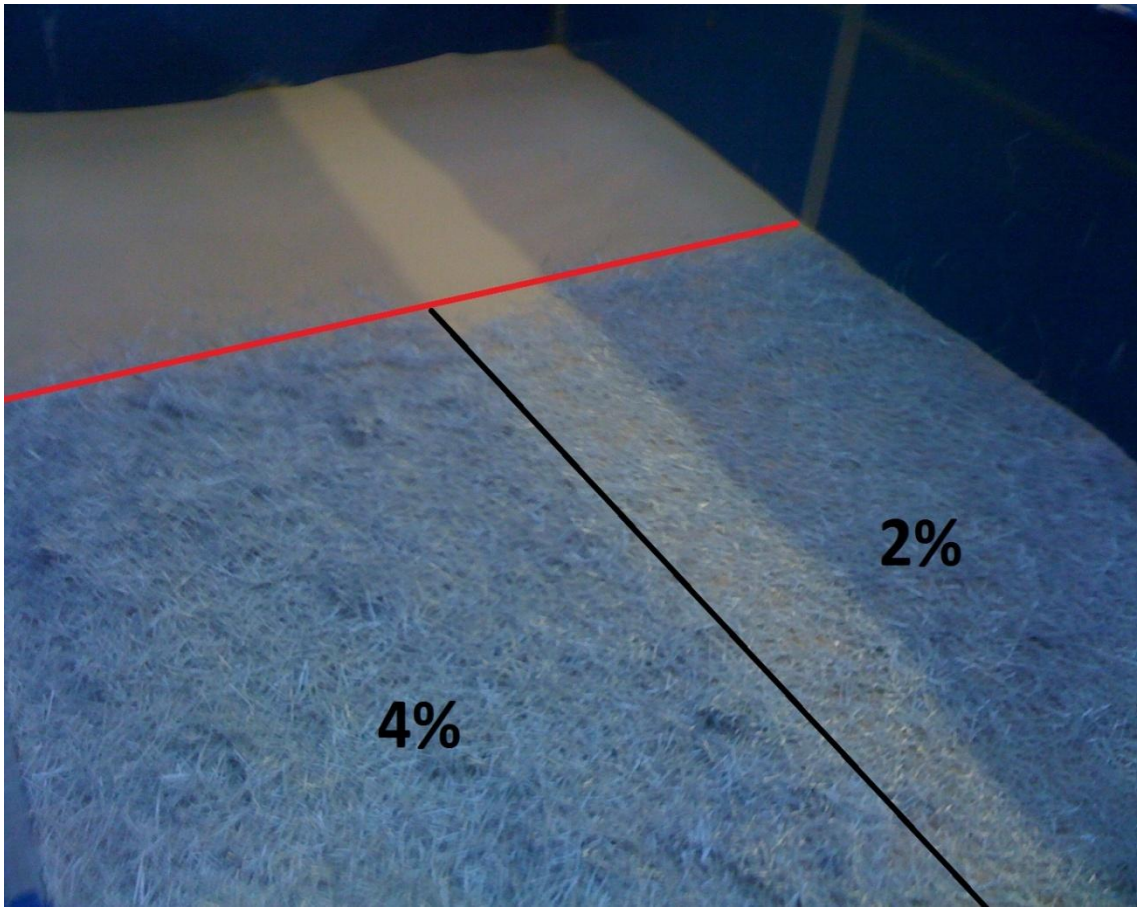


**Figure 35: Example of a Fibre Layer - 2 & 4 % Fibre Volume Ratio – 1/25$^{th}$ Scale**

Once the sample bed had been successfully prepared, the surfaced was levelled. This was done by connecting a 25.5 mm Perspex sheet to the I-beams (trolley) which was then skimmed along the sample bed surface, by the hydraulic ram pushing the trolley along the length of the tank, to produce a flat sample bed. Once the surface had been levelled, the sample bed was then saturated. The saturation process took approximately 2-3 hours until there was a head of water of 300 mm above the sand surface. The tank was then left for at least 24 hours to allow the sample to fully saturate. Once fully saturated the sample bed was ready for testing.

When preparing the 1/50$^{th}$ scale box, it was decided that the sample would be fully reinforced along the length of the bed rather than having an un-reinforced zone in order for the plough to reach its steady state behaviour before passing into a reinforced zone. The fibre and sand were the same as that which was used in the 1/25$^{th}$ scale tank, meaning the fibres had a scale length of 2 m in the 1/50$^{th}$ scale tank. The 1/50$^{th}$ scale box consisted of a 65 mm drainage layer, a 50 mm deep un-reinforced sand zone and 95 mm deep reinforced zone. Similarly to the 1/25$^{th}$

scale sample bed, the reinforced zone consisted of layers. When testing in the 1/50$^{th}$ scale, it was decided that the fibre volume ratio for each test would be kept constant at 2%. Pre-measured bags of fibre for each layer were spread out evenly over the length of the tank. This process was repeated until the reinforced fibre zone was 95 mm thick. The sample bed was then levelled by skimming a piece of Perspex along the whole tank by hand. Once the sample had been levelled, the sample bed was saturated. This process took approximately 1-2 hours until there was head of 140 mm above the sand surface. A prepared sample in the 1/50$^{th}$ scale tank, prior to saturation, can be seen in Figure 36.

**Figure 36: Example of Prepared Sample Bed - 1/50 Scale - Pre Saturation**

## 3.8 Shear Box Preparation

Multiple direct shear tests were carried out using a standard 60 mm square shear box. Nine tests were carried out at three different normal effective stresses, 4.7 kPa, 8.8 kPa and 17 kPa, with three different fibre volume ratios at each effective stress. The fibre volume ratios used were 0, 1 and 2 %. It was found that it was not practical to prepare a test with a fibre volume ratio any higher than 2 %. In order for the shear box to simulate the shear plane produced by

the share of the plough, the fibre layers were installed at 20 degrees to the normal. This was achieved by having a steel wedge manufactured at exactly 20 degrees so that it was possible to incline the shear box when preparing a sample. The fibres were mainly placed in a direction so that they were being pulled out in tension. The setup of the shear box when preparing a sample can be seen in Figure 37.

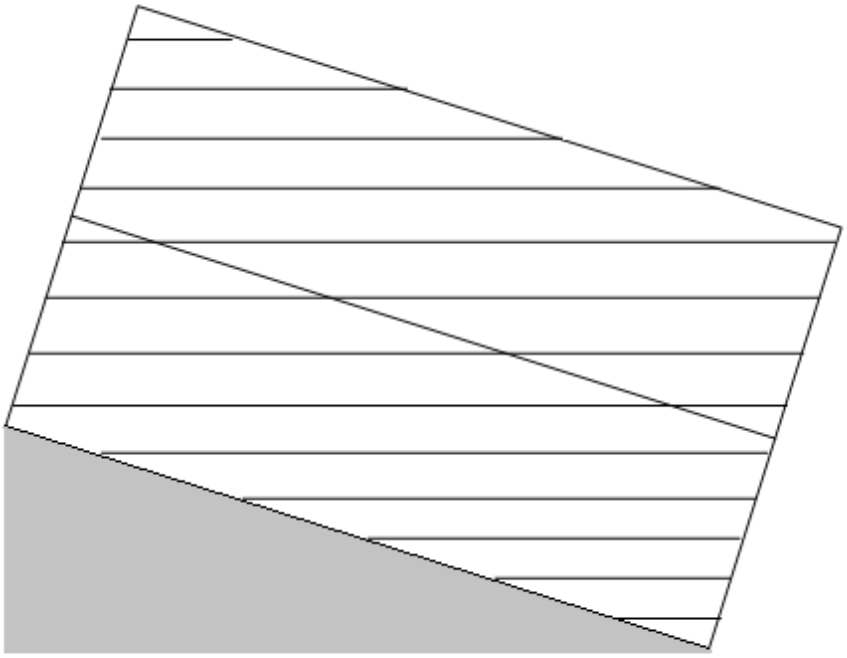

**Figure 37: Incline Shear Box (Not to Scale)**

Each Sample had a target relative density in unreinforced sand of approximately 70 – 75 %. A sample in the shear box consisted of multiple layers which consist of 5 mm of sand and a pre-measured volume of fibre depending on the required fibre volume ratio. A self adhesive template that had multiple lines at 20 degrees spaced 5 mm apart was placed on the inside wall of the shear box so that each layer was poured to the correct depth . Each pre-measured layer of fibre had to be counted by hand so that there was an accurate amount of fibre in the layer to achieve the required ratio. The pre-measured fibres were spread across each layer to be consistent with samples in the $1/25^{th}$ and $1/50^{th}$ scale tanks. After filling the shear box up with the 5 mm fibre layers, the sample was then levelled off. It was then weighed on a set of accurate electronic scales to determine the sample density. Once in the shear box, a lid with small steel ball on top was placed on the top of the sample so that a hanger and pre-decided

weight (normal effective stress) can be applied to the sample. Two LVDT's are connected to the box to measure horizontal and vertical displacement of the sample. A load cell was also connected to the shear box by a small steel rod to measure the force needed to shear the sample. Each test was carried out at a speed of 0.031 mm/s which can be set on the shear box through the use of gears.

## 3.9 Testing

### 3.9.1 1/25th and 1/50th Scale Tank

When setting up a 1/25$^{th}$ scale test, the plough was pre-embedded to a depth of approximately 90 mm below the sand surface. The load cell was connected to a small steel beam that was connected vertically to the trolley system that is pushed by the hydraulic ram. The load cell is then connected to the plough, through the use of a steel tow wire, set at a constant angle of 10 degrees to the horizontal. Once connected, the tow wire is tensioned by slowly pushing the trolley forward using the hydraulic ram, stopping the ram before the plough begins to move. The DWT is fixed to the end of the tank and is connected to the back of the trolley in order to measure horizontal displacement. Two LVDTs are then connected to the trolley and placed on the front and back of the plough at hand measured heights above the plough and sand surface. It is important to know the difference in height between where the LVDTs rest on the plough and the surface of the sand as the surface is used as a reference point for plough depth. The distance between each LVDT is measured and also the distance from the LVDT placed at the front of the plough and where the DWT connects to the trolley. The LVDT placed at the back of the plough is used to measure plough depth. Also, by having an LVDT placed at the front and back of the plough, it is possible to calculate plough pitch.

Setting up a test in the 1/50$^{th}$ scale test is very similar to a 1/25$^{th}$ scale tests. However, due to the scale differences, the 1/50$^{th}$ plough was pre-embedded to a depth of approximately 40 mm below sand surface. Once again the tow wire is kept at a constant tow angle of 10 degrees, two LVDT's are placed at the front and back of the plough and the DWT is connected to the back of the 1/50$^{th}$ scale trolley. The trolley is pulled in 1/50$^{th}$ tests using a pulley system compared to being pushed when testing in the 1/20$^{th}$ scale tests. The 1/50$^{th}$ scale tank test setup can be seen in Figure 27.

### 3.9.2 Shear Box

Once the sample had been successfully prepared shear box was placed in the shearing machine, a lid with small steal ball on top is placed on the top of the sample so that a hanger and pre-decided weight (normal effective stress) can be applied to the sample. Two LVDT's are connected to the box to measure horizontal and vertical displacement of the sample. A load cell is also connected to the shear box by a small steel rod to measure the force needed to shear the sample. Each test is carried out at a speed of 0.031 mm/s which can be set on the shear box through the use of a gear system.

## 3.10 Data Logging

The data logging system used in the $1/25^{th}$ and $1/50^{th}$ scale tanks was called LABview. This piece of software converted data measured in voltages, which is recorded through the use of measurement apparatus mentioned earlier in the chapter, into actual values of displacements and forces. The sample rate for each test in both tanks was one data sample per second.

The data logging system software used in shear box element testing was called Hewlett-Packard Vee 5.0. This piece of software also converted data from voltage into actual measurements of displacement and force.

### 3.10.1 Calibration

To convert the data recorded using the data logging system from voltages to actual measurements, a calibration factor is needed for each piece of measurement apparatus. These calibration factors are achieved by moving displacement measuring instruments a known distances, or in the case of the load cell, known weights are applied to the load cell. The voltages recorded during this calibration process were then placed in a graph against the known changes in distance or weight applied to the measurement apparatus, with the gradient of the line produced by the data being the calibration factor for the specific piece of apparatus. Once these factors have been calculated, they can either be inserted into the data logging system to allow the user to see the actual measurements on their screen as they are testing. It is also possible to convert the data in a spreadsheet, after the test has taken place.

## 3.11 Measuring Trench

It is imperative to the project that the trench depth is measured after every test as the LVDT's placed on the plough during a test only measures plough depth. The surface of the sample is surveyed after it is has been levelled out. The reason for this is to have an accurate reference point when manually measuring trench depths. There is a significant difference between plough depth and trench depth, mainly due to fall back of sand within the trench. A basic trench produced by ploughing can be seen in Figure 2. Points one and five seen in the sketch are the sample bed surface, points two and four are the peaks of the spoil heaps and point three indicates the bottom of the trench produced by ploughing. Each point seen on the sketch is measured to vertically and horizontally from a pre-determined reference point. The reference point for measuring each point is the top of tank wall for vertical measurements and the left side wall of the tank for horizontal measurements. In the 1/25$^{th}$ scale tank each of these measurements were taken at 200 mm longitudinal intervals in the un-reinforced zone and 100 mm intervals in the reinforced zone for 1400 mm along the length of the tank. In the 1/50$^{th}$ scale tank the measurements were taken at 250 mm intervals for 1200 mm along the length of the tank. A picture of an actual trench produced by a plough can be seen in Figure 38.

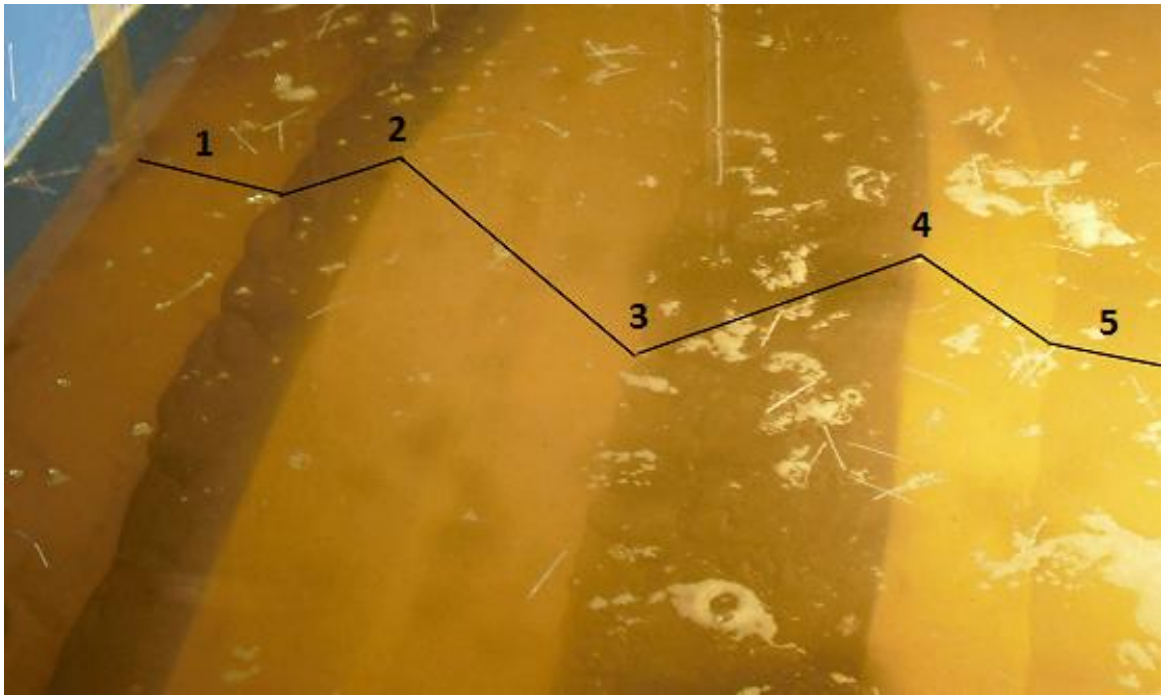


**Figure 38: Trench Shape Example**

## 3.12 Scaling Test Results

It is important to be able to convert results from in testing using the model plough to compare the forces that would be encountered by actual offshore pipeline ploughs. As the ploughs used in this project were designed at two different scales, 1/25$^{th}$ $(1/N)$ and 1/50$^{th}$, compared to an actual prototype plough, it is possible to calculate the scaled forces and depth encountered during testing. The scaling method used in this project is the same as was used by Lauder, 2011 where forces were scaled by multiplying by the scale factor cubed, $N^3$, and the depth by the scale factor, N. This method was also used by Brown *et al*, 2006, when scaling results using the 1/50$^{th}$ scale plough. It must be noted that the rate effects were not scaled in this project as the effect was found to be inconclusive through a series of tests carried out by Lauder, 2011.

# Chapter 4. Element Testing

The following chapter will discuss the effect of different fibre volume ratios of fibre reinforcement on the shear strength of sand measured during the direct shear test. The results of tests will be compared to models that predict an increase in shear stress due to reinforcement which have been discussed earlier in the literature review chapter.

## 4.1 Results and Discussion

Nine tests were carried out at three different normal stresses with the intent to give a clear indication on the behaviour of sand samples reinforced by fibres. As mentioned in the methodology chapter, three different fibre volume ratios are used during testing; 0, 1 and 2 %. Low effective stresses of 4.7, 8.8 and 17 kPa were applied with the intention of giving a good indication of how an offshore pipeline plough would be affected by the different volume ratio of fibre as the normal stresses produced when ploughing are relatively low at around 18 kPa based on a plough depth of 1.8 m and normal submerged unit weight of $\gamma' = 10$ kN/m$^3$ (Lauder, 2011). Figure 39 and Figure 40 consist of three tests with fibre volume ratios of 0, 1 and 2 % which had an applied normal effective stress of 4.7 kPa.

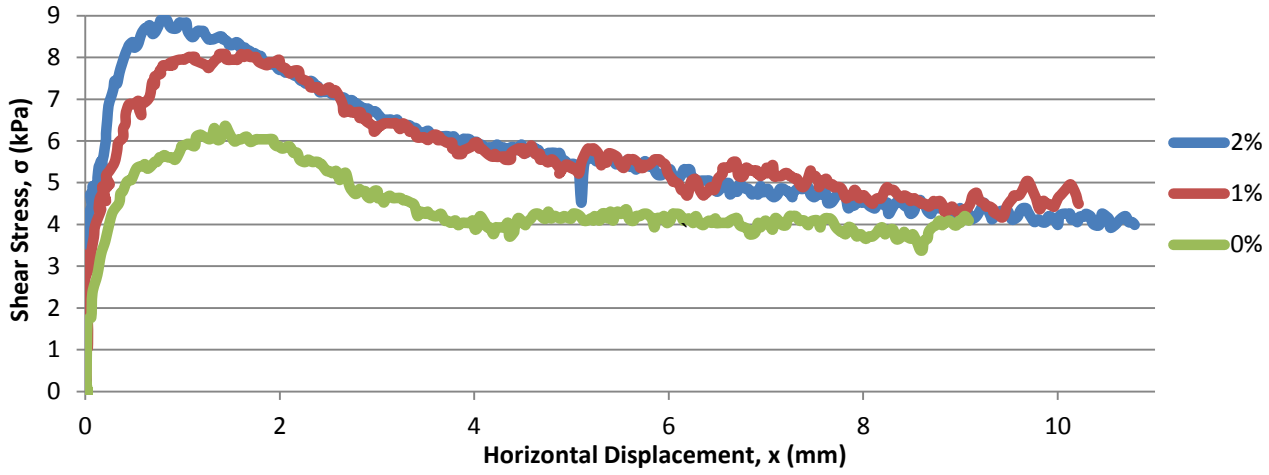


**Figure 39: Shear Stress vs. Horizontal Displacement 0, 1 and 2 % Fibre Volume Ratios - 4.7 kPa ($D_r$ = 69 %)**

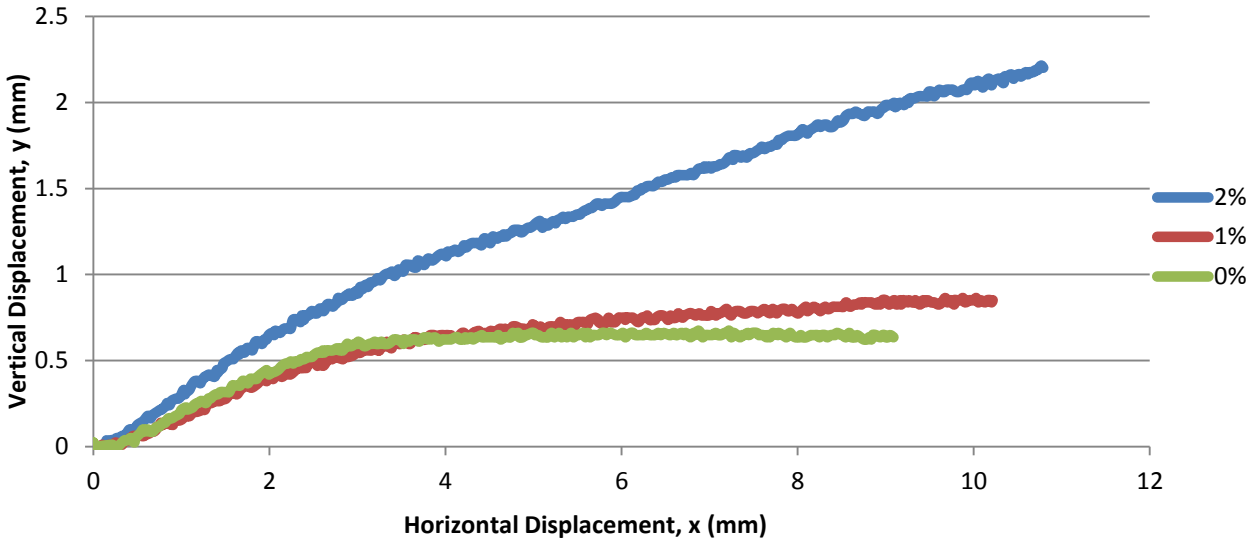


**Figure 40: Vertical Displacement vs. Horizontal Displacement 0, 1 and 2 % Fibre Volume Ratios - 4.7 kPa ($D_r$ = 69 %)**

| | Peak Shear Stress, kPa | Peak Friction Angle, $\phi_{pk}$ | Ultimate Shear Stress, kPa | Ultimate Friction Angle, $\phi_{ult}$ | Dilation Angle, $\Psi$ |
|---|---|---|---|---|---|
| 0% | 6.37 | 53.49 | 3.80 | 38.90 | 11.67 |
| 1% | 8.08 | 59.74 | 4.55 | 44.01 | 12.58 |
| 2% | 8.90 | 62.09 | 4.13 | 41.21 | 16.71 |

**Table 11: Reinforced and Unreinforced Direct Shear Tests: Summary of Results - 4.7 kPa ($D_r$ = 69 %)**

Where dilation angle is calculated using Equation 7.

$$\Psi = (\phi_{pk} - \phi_{ult}) \times 0.8 \quad \textbf{(7)}$$

| Fibre Volume Ratio | $D_r$ |
|---|---|
| 0% | 69.8% |
| 1% | 69.1% |
| 2% | 65.0% |

**Table 12: Summary of Sample Relative Densities – 4.7 kPa**

The results in Figure 39 show that peak shear stress increases with fibre volume ratio which backs up what was described by Gray and Ohashi (1983) and Jewell and Wroth (1987). However, both Gray and Ohashi (1983) and Jewell and Wroth (1987) found that the post peak shear stress, or ultimate shear stress, remains higher than a corresponding unreinforced

sample for the remainder of the test. It can be seen in Figure 39 that the post peak shear stress for both the 1 and 2 % samples is higher than seen in the 0 % sample for the majority of the test before matching the ultimate shear stress of the unreinforced sample at the end of each tests. A reason for the ultimate shear stress reducing in both reinforced samples until it approximately equals the critical state recorded in the unreinforced sample at the end of each test could possibly be due to the majority of the fibres being partially or completely pulled out of the shearing zone. This may not have been observed in test results by Gray and Ohashi (1983) because they used significantly longer fibres than the strux 90/40 used for the test shown in Figure 39. It could be possible that if the tests carried out by Gray and Ohashi (1983) and Jewell and Wroth (1987) were sheared for long enough, the post peak shear stress measured in the reinforced sample would finally reach the ultimate shear stress, or critical state, of the unreinforced test much like what is seen in Figure 39. Figure 40 shows the effects of reinforcement on the dilation of the sample. It can be seen that the inclusion of fibres increases the amount of dilation within the sample, with the effect increasing with fibre volume ratio. It can be seen in Figure 40 that the 2 % volume ratio test dilates 61 % more than the 1 % test, which dilates only 22 % more than the unreinforced sample. A reason for the significant difference in the amount of measured dilation between the 1 and 2 % samples could be that as there is double the amount of fibres in the 2 % sample, there is less room for the sand particles to move while being sheared, meaning that each particle will be displacing more dramatically to move over other sand particles as well as the fibre reinforcement within the sample, resulting in a higher vertical displacement being measured compared to what was seen in the 1 % test. The effect of fibre volume ratio on dilation can be clearly seen in Table 11 where the dilation angle of the 2 % test is much higher than the 1%, whereas the dilation angles for both the 1 and 0 % tests are fairly similar. The relationship between peak shear stress and normal effective stress used to determine the peak friction angle for each fibre volume ratio test carried out with a normal effective stress of 4.7 kPa can be seen in Figure 41.

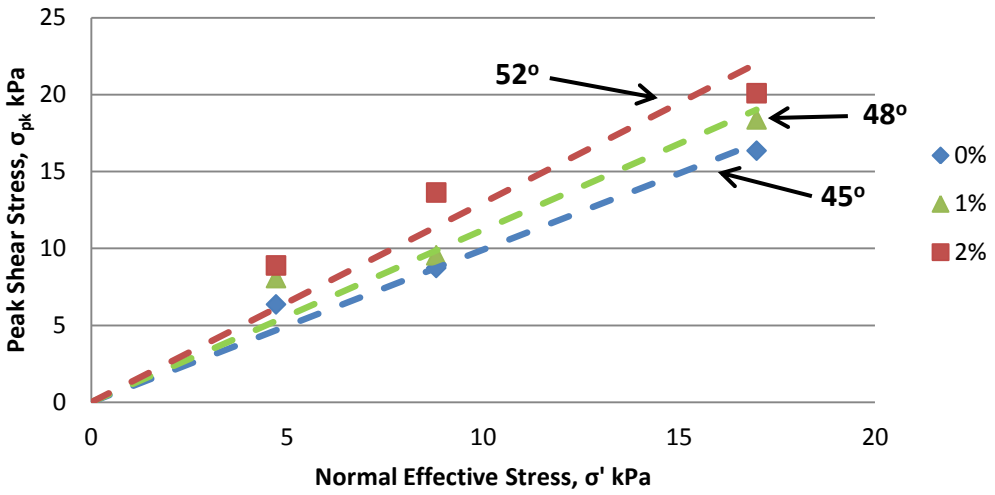


**Figure 41: Peak Friction Angle: 0, 1 and 2 % Fibre Volume Ratios ($D_r$ = 69 %)**

The following results are taken from three tests reinforced with 0, 1 and 2 % fibre volume ratios carried out with an applied normal effective stress of 8.8 kPa.

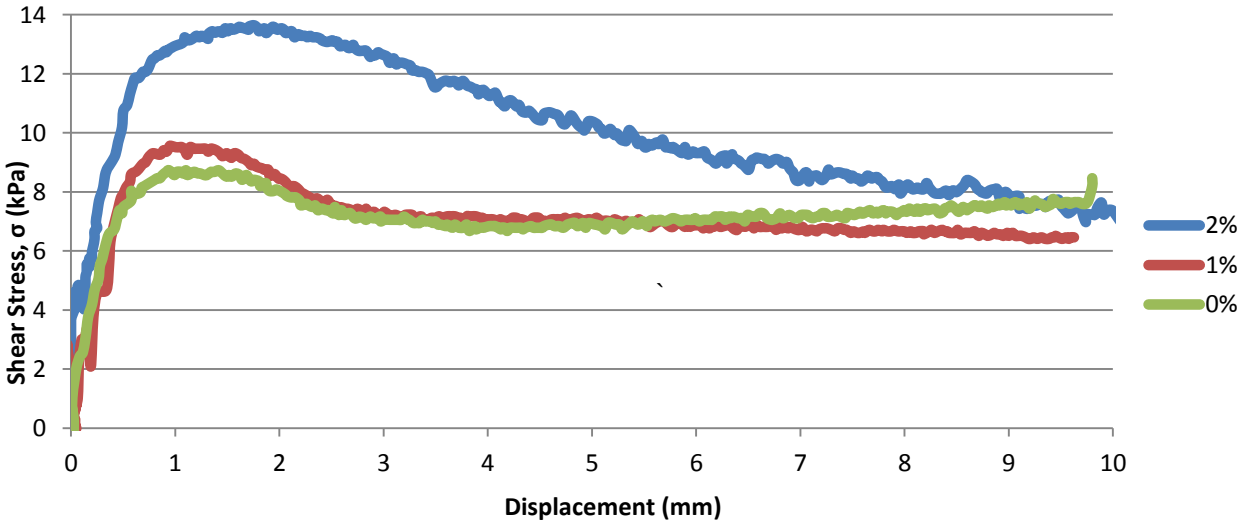


**Figure 42: Shear Stress vs. Horizontal Displacement 0, 1 and 2 % Fibre Volume Ratios - 8.8 kPa ($D_r$ = 69 %)**

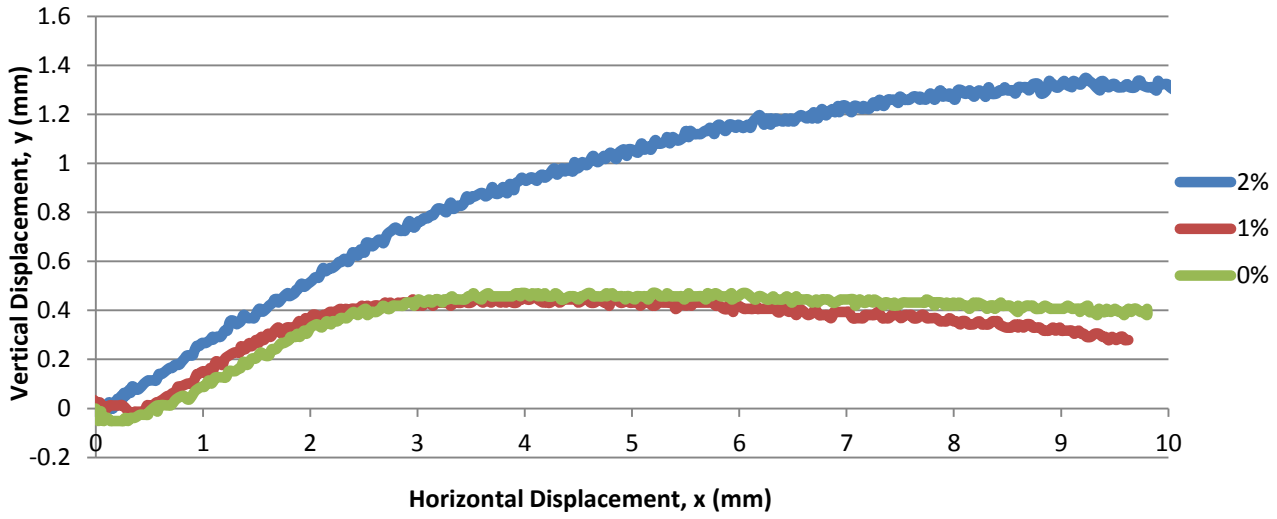


**Figure 43: Vertical Displacement vs. Horizontal Displacement 0, 1 and 2 % Fibre Volume Ratios - 8.8 kPa ($D_r$ = 69 %)**

| | Peak Shear Stress, kPa | Peak Friction Angle, $\Phi_{pk}$ | Ultimate Shear Stress, kPa | Ultimate Friction Angle, $\Phi_{ult}$ | Dilation Angle, $\Psi$ |
|---|---|---|---|---|---|
| 0% | 8.73 | 44.78 | 7.58 | 40.75 | 3.22 |
| 1% | 9.56 | 47.36 | 6.54 | 36.64 | 8.58 |
| 2% | 13.64 | 57.17 | 7.49 | 40.40 | 13.41 |

**Table 13: Reinforced and Unreinforced Direct Shear Tests: Summary of Results – 8.8 kPa ($D_r$ = 69 %)**

| Fibre Volume Ratio | $D_r$ |
|---|---|
| 0% | 67.8% |
| 1% | 69.8% |
| 2% | 66.1% |

**Table 14: Summary of Sample Relative Densities - 8.8 kPa**

It can be seen in Figure 42 that the peak shear stresses measured while shearing the sample on the 0 % test is very similar to the 1 % test whereas the 2 % test peaks at approximately 5 kPa higher than the other two tests. The reason for the 1 % test having a minimal effect on increased peak shear stress and post peak stress compared to the unreinforced test could be explained from what was found by Yetimoglu (2002) where the distribution of fibres within a sample was investigated. As described in the Literature Review section, Yetimoglu (2002) found that when fibres are randomly distributed within a sample, they have little to no effect on peak shear stress and the post peak shear stress at low normal effective stresses when comparing

results to an unreinforced test. When preparing a reinforced shear box test which provided the results seen in Figure 42, the fibres were mostly placed in the direction of the shearing action so that the majority were in tension. Therefore, it is possible that the distribution of fibres within the 1 % test seen in Figure 42, where a low normal effective stress is applied to each sample, was slightly more random than the distribution of fibres in the 2 % test explaining why there is a smaller difference in peak and ultimate shear stress between the 0 and 1 % tests. It can also be seen in Figure 42 that in each test the ultimate shear stresses are approximately similar at the end of each test. This effect was also seen in Figure 39 where the post peak shear stresses in the both reinforced tests were significantly higher than the unreinforced sample for the majority of the test before each test seemed to settle at a similar ultimate shear stress.

The following test results consist of test with 0, 1 and 2 % fibre volume ratio with an applied normal effective stress of 17 kPa.

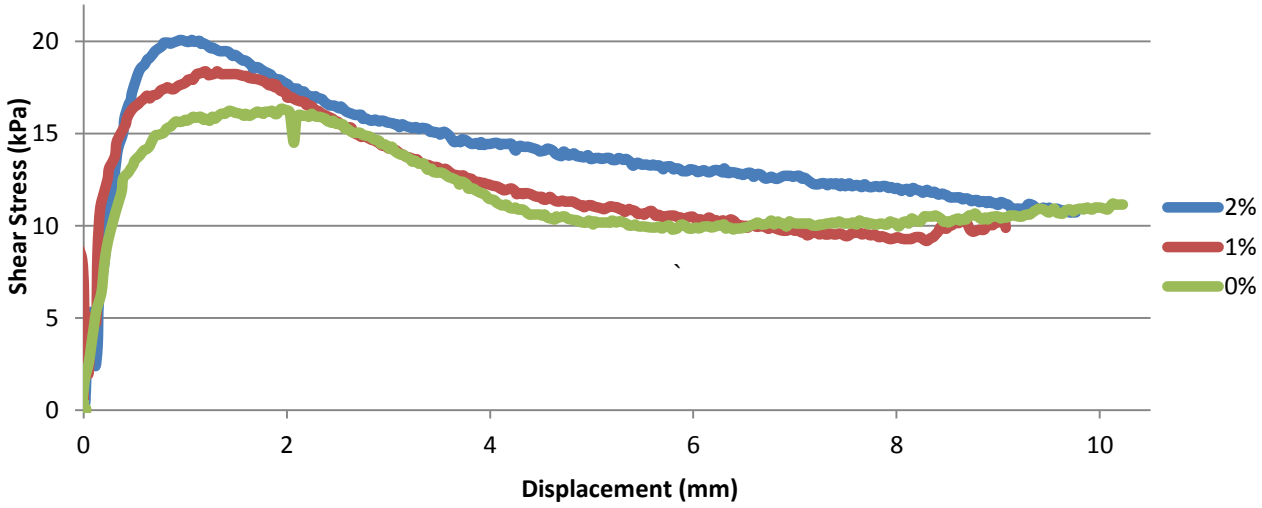


**Figure 44: Reinforced and Unreinforced Direct Shear Tests: Shear Stress vs. Horizontal Displacement 0, 1 and 2 % - 17 kPa ($D_r$ = 70 %)**

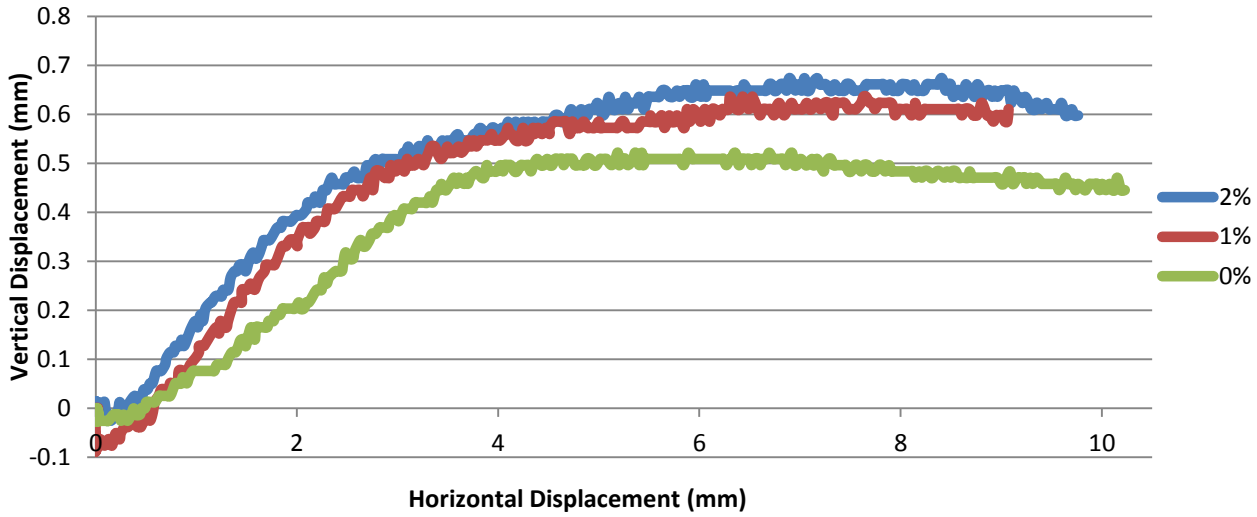


**Figure 45: Reinforced and Unreinforced Direct Shear Tests: Vertical Displacement vs. Horizontal Displacement 0, 1 and 2 % - 17 kPa ($D_r$ = 70 %)**

| | Peak Shear Stress, kPa | Peak Friction Angle, $\Phi_{pk}$ | Ultimate Shear Stress, kPa | Ultimate Friction Angle, $\Phi_{ult}$ | Dilation Angle, $\Psi$ |
|---|---|---|---|---|---|
| 0% | 16.36 | 43.94 | 10.47 | 31.68 | 9.81 |
| 1% | 18.39 | 47.29 | 9.86 | 30.16 | 13.71 |
| 2% | 20.09 | 49.81 | 11.32 | 33.70 | 12.88 |

**Table 15: Reinforced and Unreinforced Direct Shear Tests: Summary of Results – 17 kPa ($D_r$ = 70 %)**

Figure 44 shows that there is a difference in 2 kPa peak shear stress between each of the tests. However, it can be seen that the post peak shear stress for the 0 and 1 % tests are very similar for the remainder of the test until the both reach their respective ultimate shear stresses. One explanation for this could be similar to what was seen when analysing the 0 and 1 % tests in Figure 42 where the results have been affected by the distribution of fibres within the 1 % sample. The distribution of fibres within the 1 % test seen in Figure 44 could be slightly more random than the 2 % test meaning that the full strength of the reinforcement within the sample is not achieved as only the peak shear stress has been increased compared to an unreinforced test. However, the amount of measured dilation for the 1 and 2 % tests seen in Figure 45 are very similar, with the 1 % test having a slightly higher dilation angle which can be seen in Table 15. A reason for this is that the 2 % shear stress does not level out and reaches its ultimate shear stress because the shear box reaches its maximum horizontal displacement before the sample has reached its critical state. Therefore, a higher value of ultimate shear

stress than what would be used if working in a larger shear box is used to calculate the dilation angle of the sample, resulting in a lower than expected dilation angle. As discussed when analysing the results in both Figure 39 and Figure 42, it was found that regardless of fibre volume ratio, each test seems to level out at approximately the same ultimate shear stress. It could be assumed that the shear stress measured in the 2 % test in Figure 44 would reduce and reaches an ultimate shear stress similar to what was measured for both the 0 and 1 % tests. If the ultimate shear stress for the 2 % followed this trend, it would have a value of approximately 10 kPa, which reduces ultimate friction angle to 30.5 degrees from 33.7 degrees seen in Table 15. This results in a new dilation angle of 15.44 degrees using Equation 7 which is similar to the dilation angle calculated for the 1 % test.

When analysing all of the tests carried out to investigate the effect of fibre reinforcement on shear strength in sand it is clear that fibre inclusion has a significant effect on peak shear stress and post peak shear stress which supports what was found by both Gray and Ohashi (1983) and Jewell and Wroth (1987). The importance of fibre distribution within the sample has also been highlighted. The 1 % tests seen in Figure 42 indicated that if the majority of fibres are not placed in the direction of the shearing action, little to no effect is seen on the measured peak and post peak shear stresses which corroborate what was found by Yetimoglu (2002). Through the tests carried out, it has also been found that the shear stress at the end of each test reduces to approximately the same ultimate shear stress. This indicates that even with the inclusion of fibres, each sample has the same critical state as an unreinforced test.

## 4.2 Comparison of Shear Strength Increase Models Due to Reinforcement

It is possible to compare each of the direct shear results to a model created by Jewell and Wroth (1987) which predicts the limiting bond force $P_{RL}$ of the reinforcement in a sample. In theory the difference in measured peak shear force between a reinforced and unreinforced direct shear test should sit on or below the limiting bond force. The limiting bond force of the reinforcement (Jewell and Wroth (1987)), $P_{RL}$ in the reinforcement can be seen in Equation 8.

$$P_{RL} = \sigma_\theta \times A_r \times \tan\delta \quad \textbf{(8)}$$

Where,

- $\sigma_\theta$, is the inclined applied normal force.
- $A_r$, is the surface area of the reinforcement bonding with the soil
- $\delta$, is the angle of surface friction between the soil and the reinforcement.

It must be noted that $A_r$ is taken as the surface area of the shear box. This was used as more testing would need to be carried out to analyse the actual area of the surface area of the soil as the fibres are distributed throughout each layer randomly.

The inclined applied normal force is calculated using Equation 9.

$$\sigma_\theta = \sigma_{yy} \frac{1 + \sin \emptyset_{ps} \sin(\emptyset_{ps} + 2\theta)}{\cos^2 \emptyset_{ps}} \quad \textbf{(9)}$$

Where,

- $\sigma_{yy}$, is the vertical normal effective stress applied to the sample.
- $\emptyset_{ps}$, is the plane strain angle of friction.
- $\theta$, is the angle of fibre inclination within the sample to the vertical.

It must be noted that when comparing this model to the test results, $\emptyset_{ps}$ was taken as the peak angle of friction in each case. As there were nine tests carried out at three different normal effective stresses, this allows for six different cases to be compared to the limiting bond force which can be seen in Equation 8. The data for each case was calculated by subtracting an unreinforced test from a reinforced test, resulting in two cases per applied normal effective stress. For example, the two cases which will be compared to Equation 8 at a normal effective stress of 17 kPa consist of '2 % - 0%' and '1 % - 0 %'.

The comparison of Jewell and Wroth's (1987) limiting bond equation, seen in Equation 8 to the '2 % - 0 %' case at an applied normal effective stress of 17 kPa can be seen in Figure 46.

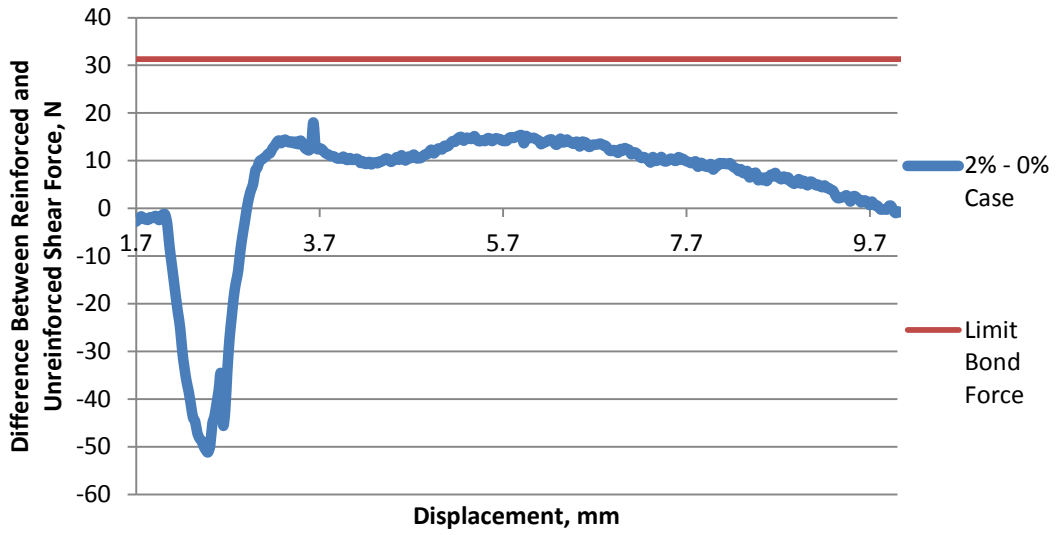


**Figure 46: Comparison of Test Results to Calculated Limiting Bond Equation; 2 % - 0 % at 17 kPa**

| | | |
|---|---|---|
| Normal Effective Stress, $\sigma_{yy}$ | 16.98 | kPa |
| Fibre Inclination (to vertical), $\theta$ | 80 | degrees |
| Fibre Surface Interface Friction Angle, $\delta$ | 19 | degrees |
| Peak Friction Angle, $\emptyset_{ps}$ | 49.81 | degrees |
| Fibre/Soil Surface Area | 0.06 | m2 |
| Inclined Effective Stress, $\sigma_\theta$ | 25.28 | kPa |
| Peak Force Difference | 18.06 | N |
| Limiting Bond Force, $P_{RL}$ | 31.34 | N |
| $P_{RL}$- Peak Force | 13.28 | N |

**Table 16: Summary of Results; 2 % - 0 % at 17 kPa**

It must be noted that an interface friction angle, $\boldsymbol{\delta}$ of 19 degrees was used in Table 16. This value was obtained from Gray and Ohashi (1983).

When analysing both Figure 46 and Table 15 it is clear the peak shear force is significantly lower than the limiting bond force. A reason for this could be due to the distribution of fibres within the soil not all being in the direction of the shearing action. As mentioned previously, Yetimoglu (2002) found that if fibres are randomly distributed in the sample, the reinforcement has a minimal effect on the shear strength of the soil as the majority of the fibres are not in tension where they are most effective. Therefore, it is possible to conclude that the reinforcement will

achieve its full strength increase potential if the fibres are only placed in the exact direction of the shearing action. This means that the reason for the peak shear force, seen in Figure 46 being significantly lower than limiting bond force could be due to the distribution of the fibres within the sample is preventing the reinforcement from reaching its full strength potential.

The comparison of Jewell and Wroth's limiting bond equation to the '1 % - 0 %' case at 17 kPa can be seen in Figure 47.

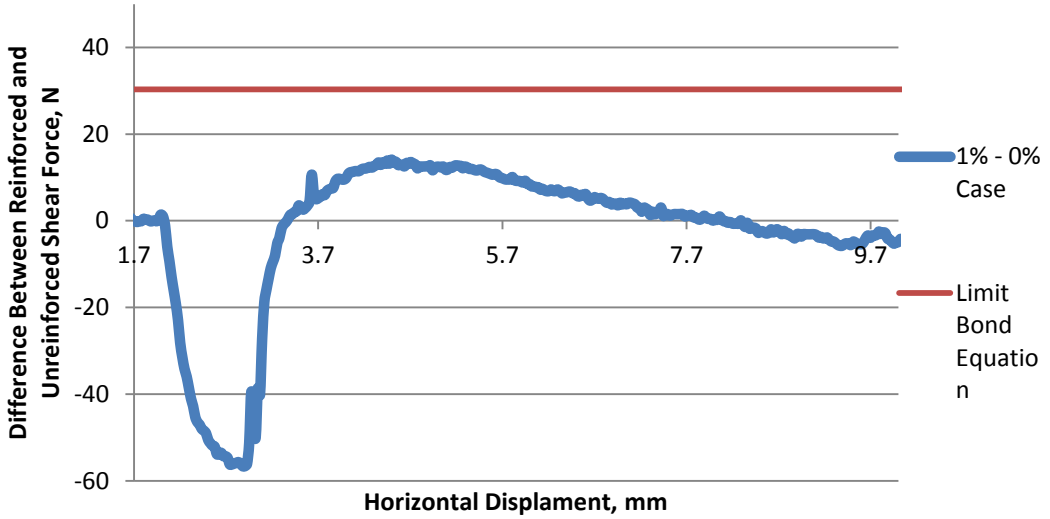


**Figure 47: Comparison of Test Results to Calculated Limiting Bond Equation; 1 % - 0 % at 17 kPa**

| | | |
|---|---|---|
| Normal Effective Stress, $\sigma_{yy}$ | 16.98 | kPa |
| Fibre Inclination (to vertical), $\theta$ | 80 | degrees |
| Fibre Surface Interface Friction Angle, $\delta$ | 19 | degrees |
| Peak Friction Angle, $\emptyset_{ps}$ | 47.29 | degrees |
| Fibre/Soil Surface Area | 0.06 | m2 |
| Inclined Effective Stress, $\sigma_{\theta}$ | 24.47 | kPa |
| Peak Force Difference | 14.11 | N |
| Limiting Bond Force, $P_{RL}$ | 30.33 | N |
| $P_{RL}$- Peak Force | 16.22 | N |

**Table 17: Summary of Results; 1 % - 0 % at 17 kPa**

The comparison of Jewell and Wroth's (1987) limiting bond equation, seen in Equation 8 to the '2 % - 0 %' case at an applied normal effective stress of 8.8 kPa can be seen in Figure 48.

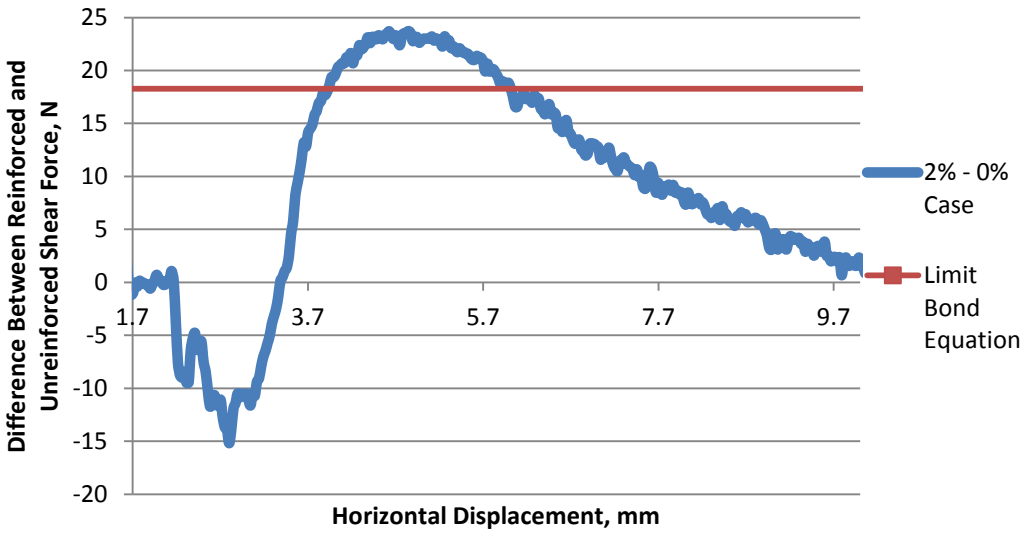


**Figure 48: Comparison of Test Results to Calculated Limiting Bond Equation; 2 % - 0 % at 8.8 kPa**

| | | |
|---|---|---|
| Normal Effective Stress, $\sigma_{yy}$ | 8.80 | kPa |
| Fibre Inclination (to vertical), $\theta$ | 80 | degrees |
| Fibre Surface Interface Friction Angle, $\delta$ | 19 | degrees |
| Peak Friction Angle, $\emptyset_{ps}$ | 57.17 | degrees |
| Fibre/Soil Surface Area | 0.06 | m2 |
| Inclined Effective Stress, $\sigma_{\theta}$ | 14.74 | KPa |
| Peak Force Difference | 23.72 | N |
| Limiting Bond Force, $P_{RL}$ | 18.27 | N |
| $P_{RL}$- Peak Force | -5.45 | N |

**Table 18: Summary of Results; 2 % - 0 % at 8.8 kPa**

It can be seen in Figure 48 and Table 18 that the limiting bond force equation seen in Equation 9 is exceeded by the test data in Figure 48 by 5.45 N. This will be discussed after the remainder of the test data has been displayed.

The comparison of Jewell and Wroth's limiting bond equation to the '1 % - 0 %' case at 17 kPa can be seen in the following figure.

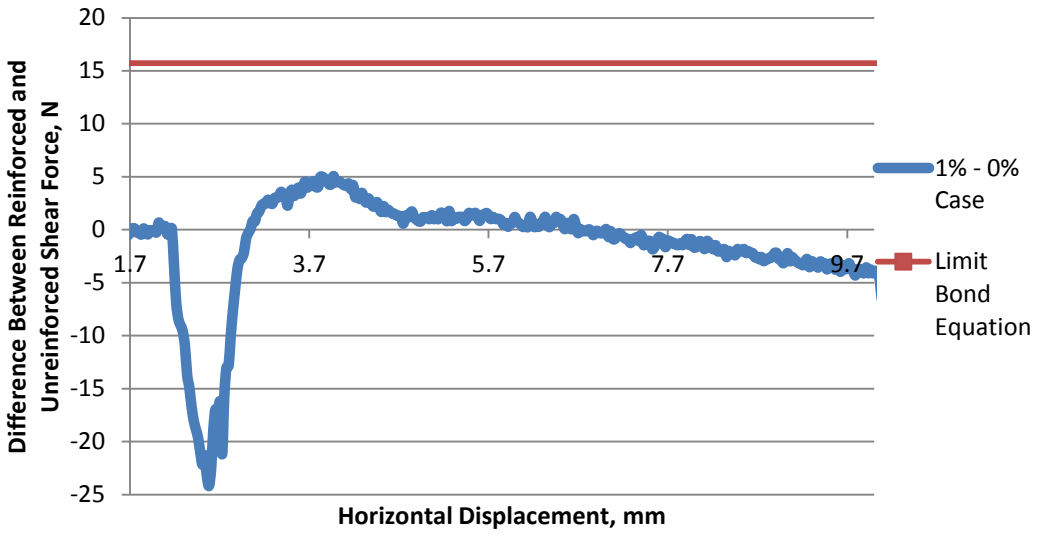


**Figure 49: Comparison of Test Results to Calculating Limiting Bond Equation; 1 % - 0 % at 8.8 kPa**

| | | |
|---|---|---|
| Normal Effective Stress, $\sigma_{yy}$ | 8.80 | kPa |
| Fibre Inclination (to vertical), $\theta$ | 80 | degrees |
| Fibre Surface Interface Friction Angle, $\delta$ | 19 | degrees |
| Peak Friction Angle, $\emptyset_{ps}$ | 47.36 | degrees |
| Fibre/Soil Surface Area | 0.06 | m2 |
| Inclined Effective Stress, $\sigma_{\theta}$ | 12.70 | KPa |
| Peak Force Difference | 5.06 | N |
| Limiting Bond Force, $P_{RL}$ | 15.74 | N |
| $P_{RL}$- Peak Force | 10.68 | N |

**Table 19: Summary of Results; 1 % - 0 % at 8.8 kPa**

As discussed previously in the chapter, the difference between the 1 % and the 0 % fibre volume direct shear test results was minimal, resulting in the peak force difference seen in Table 19 being relatively small. An explanation for this was that the fibres within the 1 % test were distributed in a more random fashion compared to the other reinforced direct shear tests, resulting in the difference in shear stress between the 1 % and unreinforced sample being minimal which backs up what was found in Yetimoglu (2002).

The comparison of Jewell and Wroth's (1987) limiting bond equation, seen in Equation 8 to the '2 % - 0 %' case at an applied normal effective stress of 4.7 kPa can be seen in the following figure.

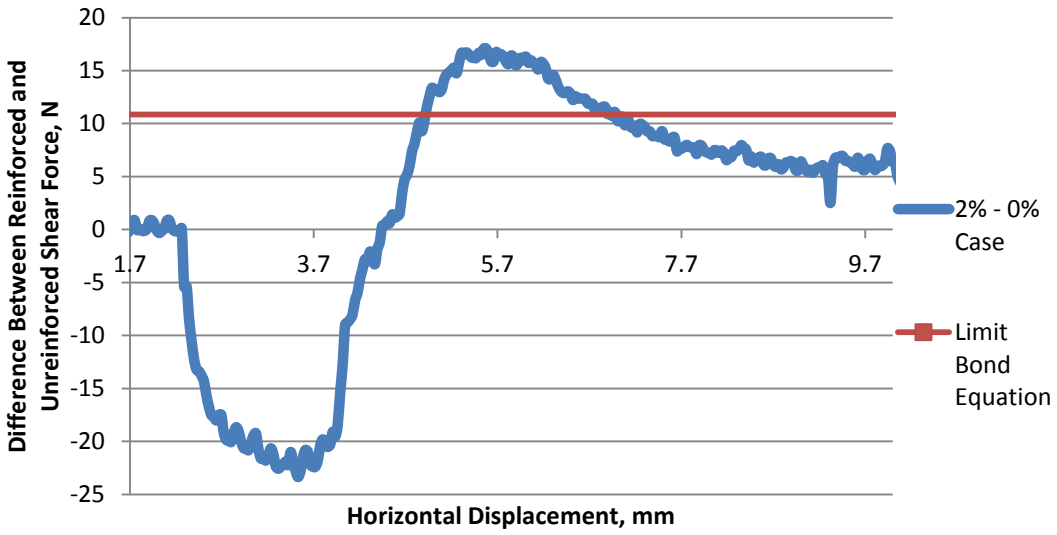


**Figure 50: Comparison of Test Results to Calculating Limiting Bond Equation; 2 % - 0 % at 4.7 kPa**

| | | |
|---|---|---|
| Normal Effective Stress, $\sigma_{yy}$ | 4.71 | kPa |
| Fibre Inclination (to vertical), $\theta$ | 80 | degrees |
| Fibre Surface Interface Friction Angle, $\delta$ | 19 | degrees |
| Peak Friction Angle, $\emptyset_{ps}$ | 62.09 | degrees |
| Fibre/Soil Surface Area | 0.06 | m2 |
| Inclined Effective Stress, $\sigma_{\theta}$ | 8.77 | KPa |
| Peak Force Difference | 17.06 | N |
| Limiting Bond Force, $P_{RL}$ | 10.87 | N |
| $P_{RL}$- Peak Force | -6.19 | N |

**Table 20: Summary of Results; 2 % - 0 % at 4.7 kPa**

The comparison of Jewell and Wroth's limiting bond equation to the '1 % - 0 %' case at 4.7 kPa can be seen in Figure 51.

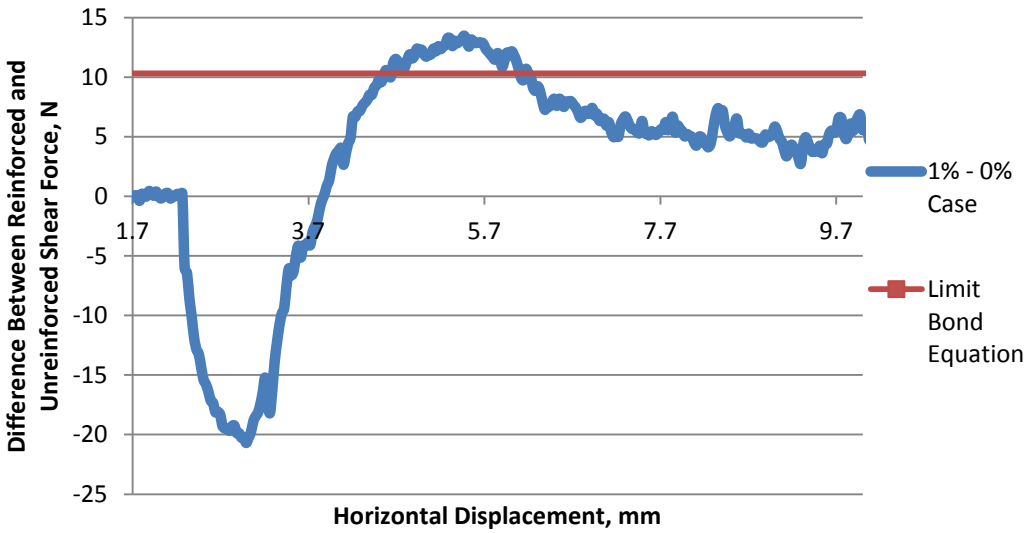


**Figure 51: Comparison of Test Results to Calculating Limiting Bond Equation; 1 % - 0 % at 4.7 kPa**

| | | |
|---|---|---|
| Normal Effective Stress, $\sigma_{yy}$ | 4.71 | kPa |
| Fibre Inclination (to vertical), $\theta$ | 80 | degrees |
| Fibre Surface Interface Friction Angle, $\delta$ | 19 | degrees |
| Peak Friction Angle, $\emptyset_{ps}$ | 59.74 | degrees |
| Fibre/Soil Surface Area | 0.06 | m2 |
| Inclined Effective Stress, $\sigma_{\theta}$ | 8.31 | KPa |
| Peak Force Difference | 13.47 | N |
| Limiting Bond Force, $P_{RL}$ | 10.30 | N |
| $P_{RL}$- Peak Force | -3.17 | N |

**Table 21: Summary of Results; 1 % - 0 % at 4.7 kPa**

Figure 48, Figure 50 and Figure 51 all show that the limiting bond force, which is calculated using Equation 9 under predicts the peak difference in shear force in each case. This could be due to the shear box not giving accurate results at low normal effective stresses due to its size. Another reason for this could be the model is incapable of dealing with low effective stresses as it was only used by Jewell and Wroth (1987) when using normal effective stresses far greater than what is encountered by a plough. When carrying out direct shear tests it is common practice to use higher normal effective stresses when investigating the effect of a foundation for example on compared to the low effective stresses used to simulate ploughing on the seabed. However, as these results are being used to predict what effect fibre reinforcement would have on an offshore pipeline plough on the sea bed it was decided that low effective stresses were used because a plough works at relatively low effective stresses. The accuracy of the surface area of the reinforcement bonding with the soil may also be having a detrimental effect on the results seen in Figure 48, Figure 50 and Figure 51. Due to the complexity of the reinforcement within the sample, it is difficult to estimate the area of the reinforcement bonding with the soil. As mentioned previously, for investigation purposes a surface area of 0.06 $m^2$ was used as this is the area of the direct shear box used in testing. A lower bonding surface area is likely to be used which incorporates the effect of a fibre volume ratio would be more effective, however, due to time restrictions, it wasn't possible to investigate this possibility further. However, the possibility of adapting this model to predict the increase in tow force that the plough encounters when working in reinforced soils will be investigated further in the following chapter.

# Chapter 5. Results and Discussion

The following section will analyse the results and trends of data accumulated through a series of tests using 1/25$^{th}$ and 1/50$^{th}$ scale ploughs. An in depth analyses will be carried out on the influence of fibre reinforced soil on plough behaviour and how they affect ploughing performance. The effect of fibre reinforcement on sand during shearing will also be investigated by analysing tests carried out in a shear box.

## 5.1 Effects of Fibrous Reinforcement of Soil on Plough Performance

After investigating the effects of reinforcement in sand through the use of direct shear box tests, it can be seen that reinforcement could have a significant effect on plough performance. Therefore, five tests were carried out, each at a different fibre volume ratios, in order to analyse the effect of fibrous soil on an offshore pipeline plough in 1/25$^{th}$ scale tests. As explained in the methodology chapter the plough initially passed through an un-reinforced zone so that the plough can reach its steady state before reaching the fibrous zone. The fibre volume ratios used were 0.5 %, 1 %, 1.5 %, 2 % and 4 % with each fibrous zone being 1.5 m in length. As mentioned previously, each percentage of reinforcement used in testing is the amount of sand in the sample that has been replaced by reinforcement. Each of the tests was carried out at a speed of approximately 44 m/hr. The following results are from the 4 % tests.

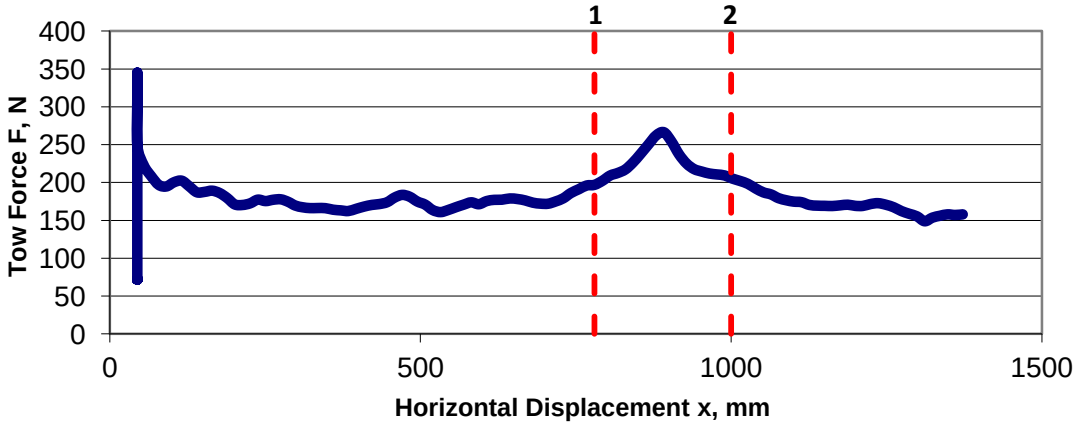


**Figure 52: 4 % Fibre Volume Ratio Test – Tow Force - 1/25$^{th}$ Scale**

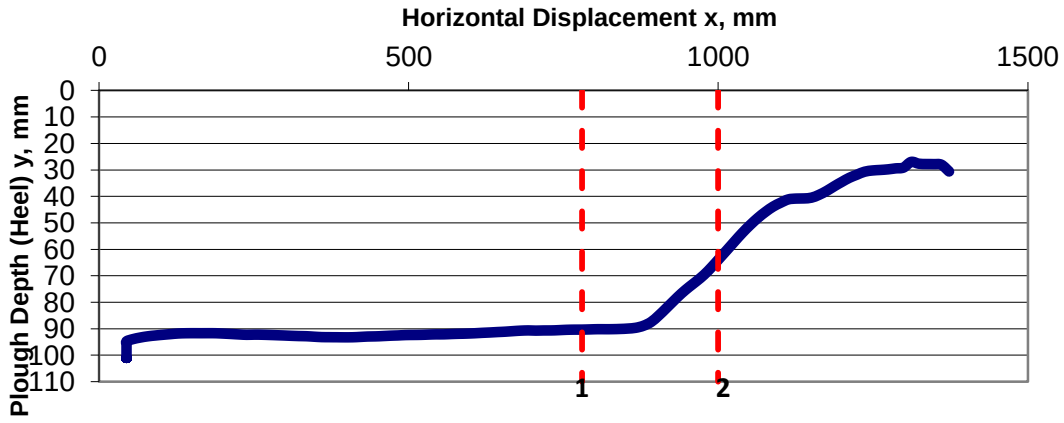


**Figure 53: 4 % Fibre Volume Ratio Test – Plough Depth - 1/25th Scale)**

The two vertical lines that can be seen in Figure 52 and Figure 53, marked 1 and 2 indicate the share of the ploughs position in the fibrous zone. Line 1 indicates that the front of the share is entering the fibrous zone and line 2 shows that the share has completely entered the fibrous zone. When analysing the effect of fibre on the tow force needed to pull the plough through the fibre in Figure 52 it can be seen that the force begins to increase just before the plough share enters the fibre zone. A reason for this could be that the plough picks up changes in the soil conditions before it actually reaches them. After the share tip has entered the fibrous zone the tow force begins to increase dramatically, reaching peak, at approx 266 N which has scaled value of 415. 6 t (4156.25 kN) after half of the plough share has entered the fibre zone. After the peak in tow force, the force begins to reduce until it reaches a magnitude similar to the steady state force seen in the un-reinforced zone at the start of the test. At the point where the tow force peaks at approximately 100 N more than the force needed to pull the plough in its steady state, which is an increase of 33 %. At the point of peak tow force, it can be seen in Figure 53 that the plough begins to ride out of the soil and reduces in depth dramatically. There is a reduction of nearly 70% in plough depth after the plough passes into the fibrous zone from the un-reinforced area, reducing from 90 mm (2.25 m) to approximately 30 mm (0.75 m). The significant reduction in depth could explain why the tow force reduces to a force similar to steady state in the unreinforced zone. This could be due to the long beam principle (Lauder *et al*, 2008) which has been discussed in the literature review. This is where the plough is always attempting to find an equilibrium of forces acting on the top and bottom of the share. The plough will alter its depth until it finds a position where it is most comfortable in a specific soil

condition and the forces are in equilibrium around the share. This would explain why the plough starts to ride out when the tow force peaks as it attempts to find a comfortable position in these conditions where there is an equilibrium of forces acting around the share. It must be noted that in Figure 52 it can be seen that there is a spike in the data at the beginning of the test. This data spike is due to the sudden acceleration of the plough from its stationary position. This will not happen in the field when testing due to the length and flexibility of the tow line.

The following test results are from the 2 % sample bed. The test was carried out at 44 m/hr and the plough was pre-embedded to depth of approximately 90 mm.

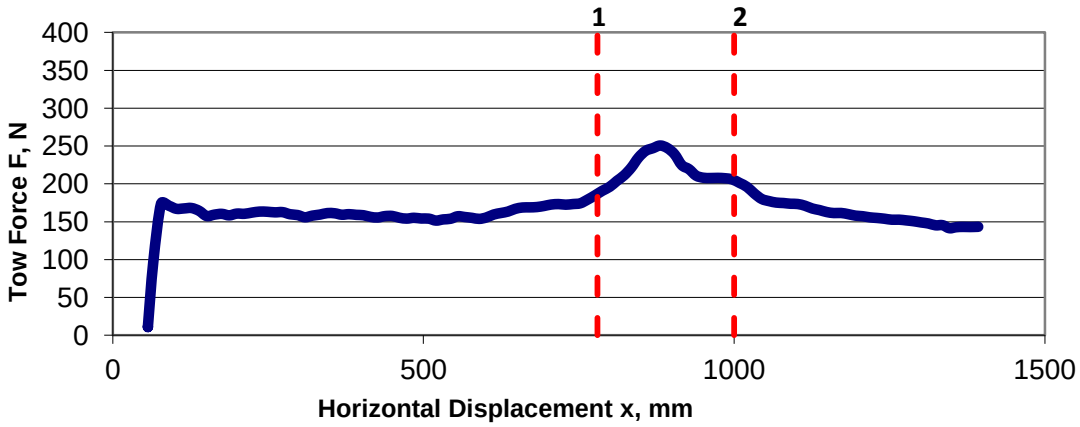


**Figure 54: 2 % Fibre Volume Ratio Test – Tow Force - 1/25th Scale**

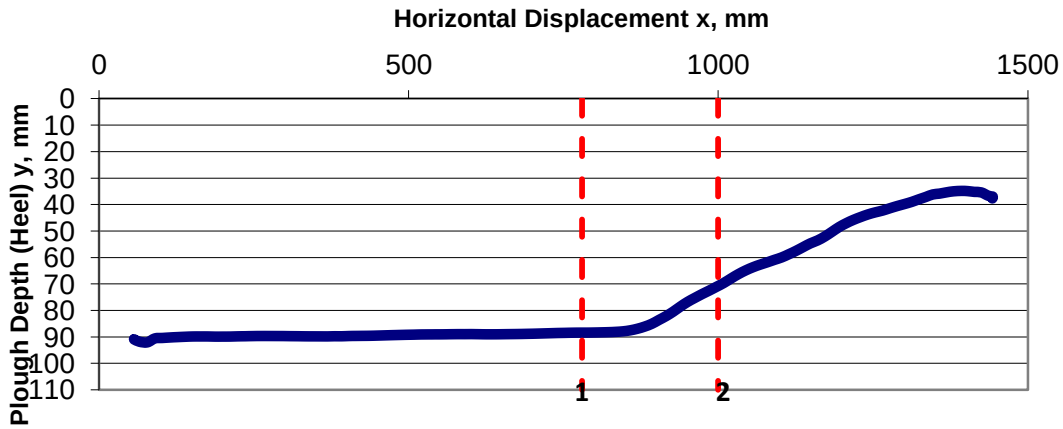


**Figure 55: 2 % Fibre Volume Ratio Test – Plough Depth - 1/25th Scale**

When inspecting Figure 54 it can be seen that the force begins to increase before the tip of the share reaches the fibrous. There is an increase in tow force of nearly 100 N when the plough enters the fibrous soil compared to the ploughs steady state peaking at approximately 250 N (390.6 t), once again this is an increase of approximately 33 %. Figure 55 shows that the plough starts to ride out from its steady state depth, when the tow force peaks in Figure 54, once approximately half the plough share has entered the fibrous zone with a plough depth of approximately 60 %, reducing from 90 mm (2.25 m) to approximately 35 mm (0.875 m). The behaviour of the plough in the 1 and 1.5 % sample beds are similar to that seen in Figure 52 and Figure 54 and will be shown in summarised in a figure later in the section.

The following results are taken from the 0.5 % sample bed. The test was carried out at 44 m/hr and the plough was pre-embedded to a depth of 90 mm.

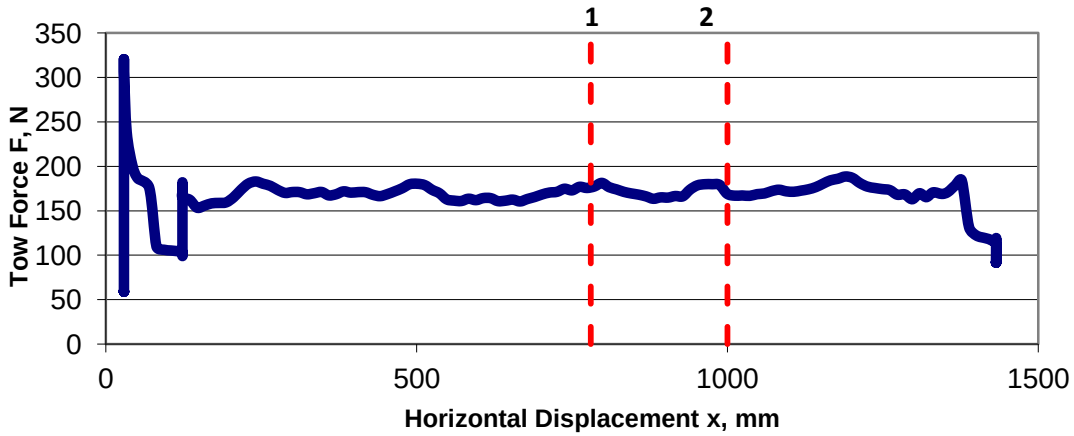


**Figure 56: 0.5 % Fibre Volume Ratio Test – Tow Force - 1/25th Scale**

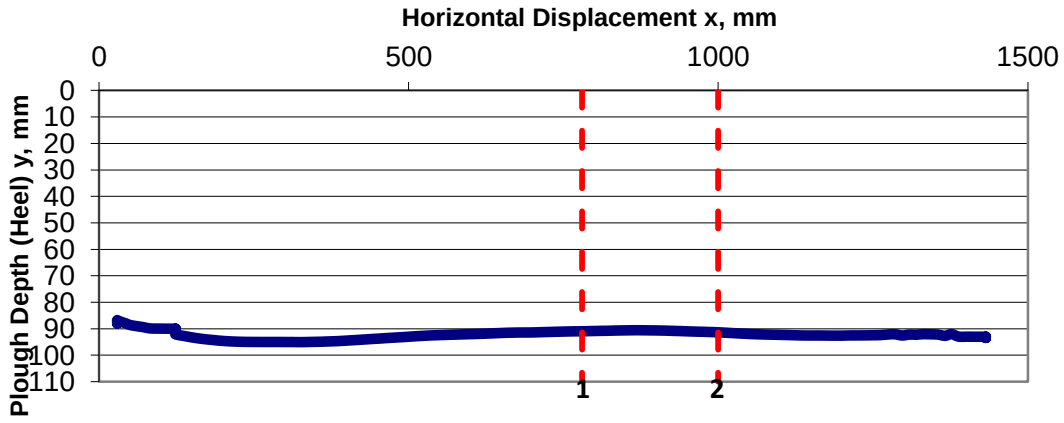


**Figure 57: 0.5 % Fibre Volume Ratio Test – Plough Test - 1/25th Scale)**

When analysing the data in Figure 56 and Figure 57 it can be seen that the 0.5 % fibrous zone has absolutely no effect on both tow force and plough depth. This suggests that there are not enough fibres within the sample to produce a significant build up around the share, allowing the plough to be in its steady state equilibrium throughout the test.

The following graphs show a summary of tow force and plough depths in each different sample bed tests in the 1/25th scale tank.

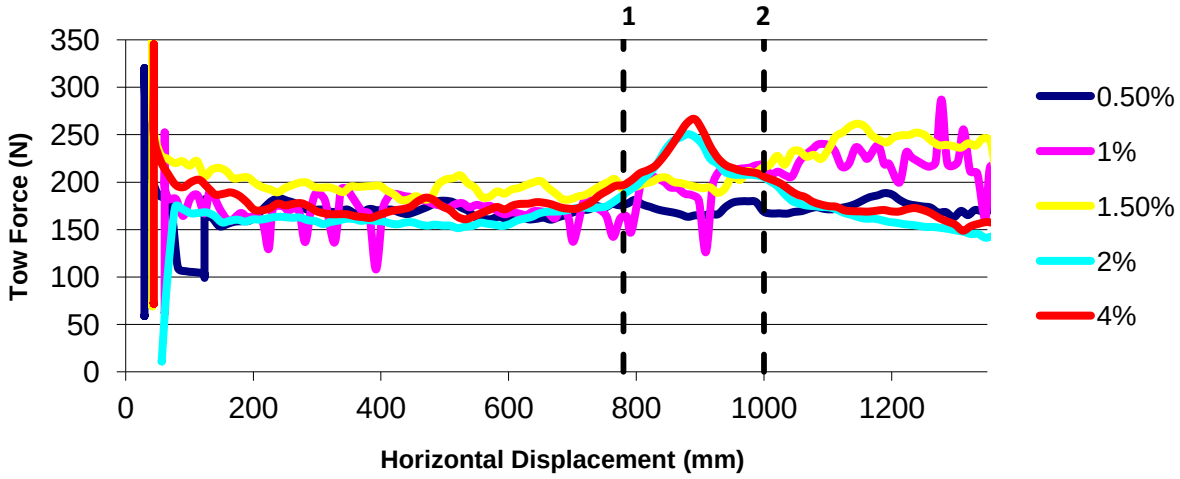


**Figure 58: 1/25th Scale Test Summary - Tow Force**

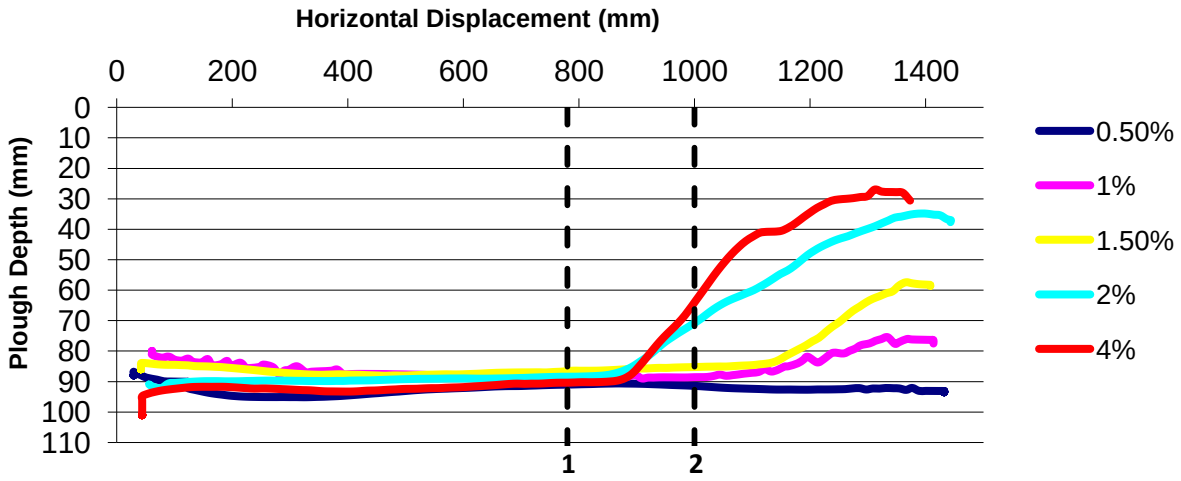


**Figure 59: 1/25th Scale Test Summary - Plough Depth (Heel)**

Figure 58 and Figure 59 show the trends mentioned when discussing the results of each test previously. Figure 58 clearly shows the difference between the 2 and 4 % tests, where the tow force peaks rapidly as the share passes into the fibrous zone, compared to the 1 and 1.5 % tests, where the tow force increases steadily once the whole share has entered the fibrous zone. The effects on plough depth in each test can be seen in Figure 59. It can be seen in Figure 59 that the rate of plough ride out depends on fibre ratio as what would be expected, with 4 % having the greatest rate of depth reduction and 1 % having the smallest rate. It can also be seen in Figure 59 that the point where the plough begins to pull out corresponds to where the tow force peaks for each test in Figure 58. The plough reaching its equilibrium can be seen clearly when inspecting the 2 and 4 % tests in Figure 58 and Figure 59. Once the tow force peaks in the 2 and 4 % tests in Figure 58 it begins to decrease back down towards a force similar to the steady state tow force seen in the un-reinforced zone. At the same time as the tow force is decreasing towards steady state in Figure 58, the plough depth is significantly reducing in Figure 59 until it reaches a depth where the plough is in equilibrium once again. This trend cannot be seen in the 1 and 1.5 % tests due to the finite length in the 1/25$^{th}$ tank. As it takes longer for the fibre to build up around the share and cause the tow force to peak, there is not enough space for the plough to keep moving to find its equilibrium again. It must be noted that tests could have be repeated multiple times to check the accuracy of the results found from tests in the 1/25$^{th}$ scale tank. However, it could be argued that due to the random distribution of fibres in each sample, it would be difficult to accurately duplicate a test.

## 5.2 Effects of Fibre and Rate Effects

Three tests were carried out in the 1/50$^{th}$ scale tank to analyse the effect, if any, of fibres on rate effects experienced by the plough when testing. Each of these three tests were carried out in a bed with 2 % fibre volume ratio at the three different speeds of 47, 75, 133 m/hr. The plough was pre-embedded to depth of approximately 40 mm at the beginning of each test. These speeds were chosen so that they could be compared to the equivalent in an un-reinforced bed at similar speeds carried out by Lauder (2011) using the same 1/50$^{th}$ scale model arrangement. However, these tests were not pre-embedded.

The following results are from the 47 m/hr rate effect test in a 2% sample bed, the plough was pre-embedded to a depth of approximately 40 mm. This test is compared to an un-reinforced test carried out at a speed of 36 m/hr.

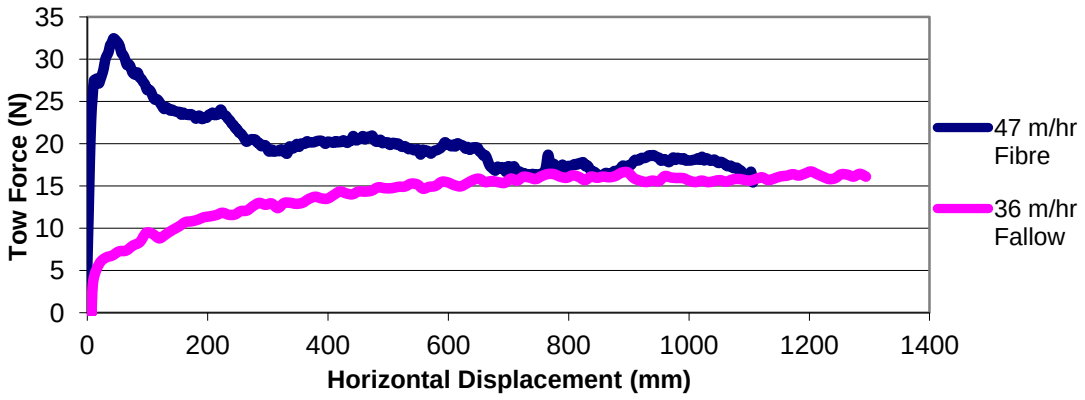


**Figure 60: 0/2 % Fibre Volume Ratio Test – Tow Force - 36 - 47 m/hr**

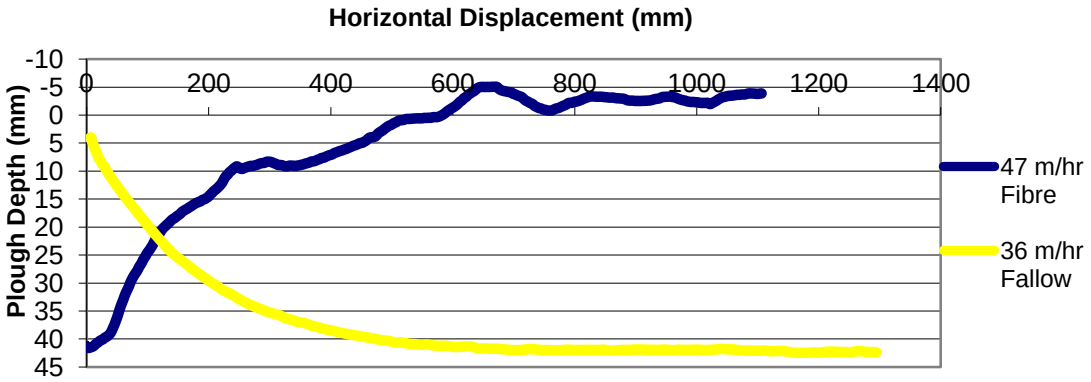


**Figure 61: 0/2 % Fibre Volume Ratio Test – Plough Depth - 36 - 47 m/hr**

When analysing Figure 60 it can be seen that tow force of the 47 m/hr test in the 2 % sample bed peaks at 32 N (400 t) within the first 100 mm of the test. The force then reduces by approximately 44 % to a tow force similar to that of the ploughs steady state in un-reinforced sand. It can be seen in Figure 61 that at the point where the tow force in the reinforced sample bed is approximately the same as that of steady state tow force in un-reinforced sand, the heel of the share has breached the sample bed surface. The heel of the share is above the sample bed surface by approximately 5 mm (0.25 m) for the remainder of the test. It can also be seen in Figure 61 that plough depth reduces rapidly from the beginning of the test to the plough finds it steady state in the fibrous soil. Similarly to the effects seen in the 1/25$^{th}$ scale tests, the tow force and plough depth in the 2 % sample bed find its steady state at roughly the same point in the test. Once again, this suggests that the plough is always trying to find equilibrium between tow force and plough depth. In this test, the ploughs equilibrium occurs when the plough is virtually skimming the surface of the sample bed. Figure 60 also shows the relationship between steady state tow forces, plough equilibrium, in the reinforced and un-reinforced sample beds at a similar speed. This suggests that a specific plough has an ideal tow force which is universal no matter what soil condition it is working in, meaning that the plough will change its depth in order to reach this ideal tow force which is the same in any type of soil condition. This preferred tow force could be dictated by the long beam principle, where the equilibrium of forces is controlled by the size and geometry of a specific plough.

The following test results are from the 75 m/hr rate effect tests in a 2 % sample bed, the plough was pre-embedded to a depth of approximately of 40 mm. This test is compared to an un-

reinforced test carried out at 83 m/hr. After the plough digging out significantly in Figure 61 it was decided that a second LVDT would be added so that the pitch of the plough could be calculated. By knowing the pitch, it is possible to calculate the position of the tip of the share in relation to the heel throughout the test.

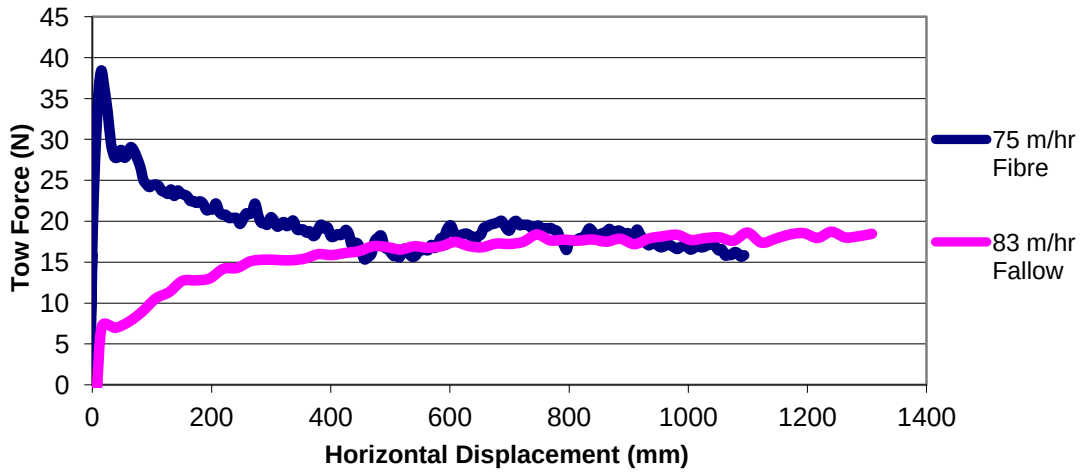


**Figure 62: 0/2 % Fibre Volume Ratio Test – Tow Force - 75 - 83 m/hr**

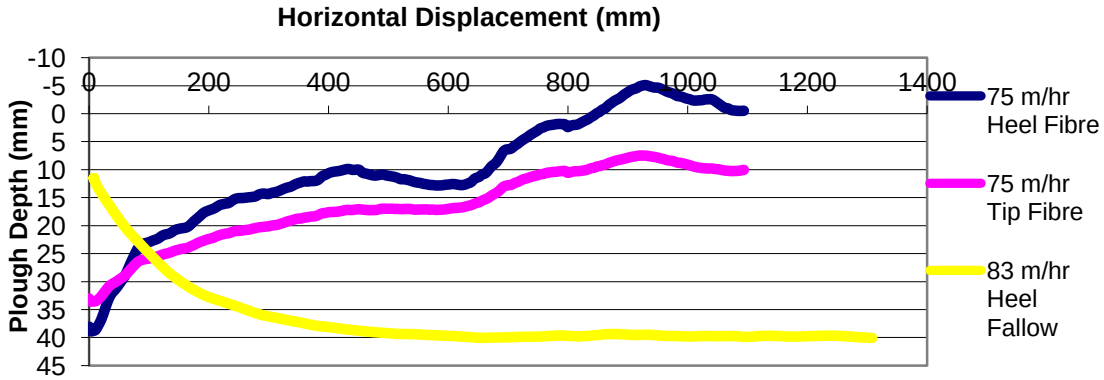


**Figure 63: 0/2 % Fibre Volume Ratio Test – Plough Depth - 75 – 83 m/hr**

It can be seen in Figure 62 that the tow force immediately peaks at 38 N (475 t) then begins to reduce rapidly. The tow force reduces much quicker, at a rate of 0.047 N/mm in the 75 m/hr rate test than the force measured in the 47 m/hr test, which reduces at a rate of 0.023 N/mm. Once again, the tow force reduces until it is approximately level with the ploughs steady state

behaviour in un-reinforced soil at a similar speed. Figure 63 shows the position of share heel and tip throughout the test. When analysing the position of the tip of the share throughout the test it can be seen that its depth begins to level out in correspondence to the levelling out of tow force in Figure 62. This suggests that the plough has found its equilibrium at a depth of approximately 10 mm (0.5 m) and a tow force of 18 N (225 t). In order for the plough to achieve its preferred steady state tow force of 18 N, it has to reduce plough depth by 75 %. When comparing the effects on the depth of the heel and tip of the share in Figure 63, it can be seen that the heel breaches the sample bed surface meaning that the tip of the share is having minimal effect on final trench depth as it is effectively skimming along the surface of the sample.

The following test results are from the 133 m/hr rate effects test in a 2 % sample bed, the plough was pre-embedded to a depth of approximately 40 mm. This test is compared to an un-reinforced test carried out in the same tank at 130 m/hr.

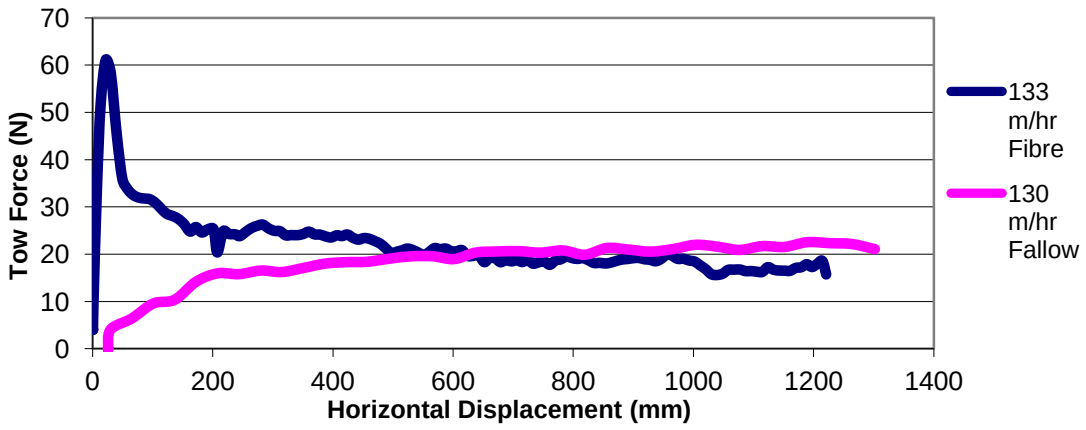


**Figure 64: 0/2 % Fibre Volume Ratio Test – Tow Force - 130 - 133 m/hr**

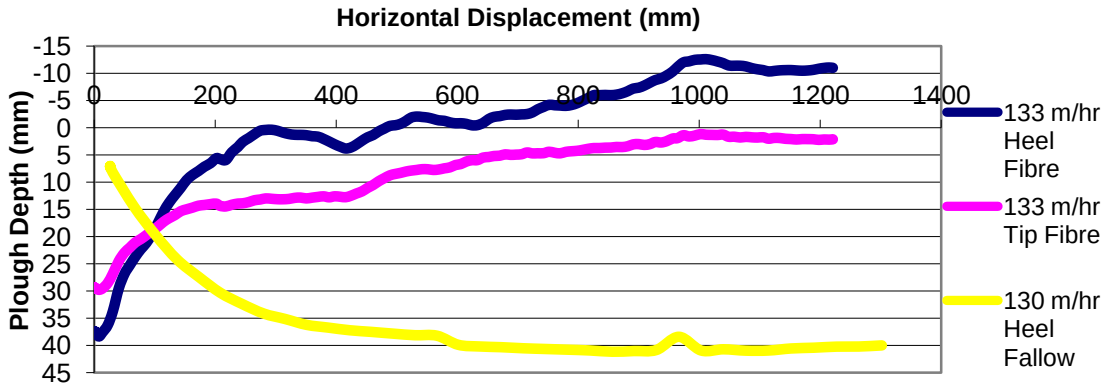


**Figure 65: 0/2 % Fibre Volume Ratio Test – Plough Depth - 130 - 133 m/hr**

Figure 64 once again shows that the tow force peaks at approximately 61 N (762.5 t) at the beginning of the 133 m/hr test then begins to drop rapidly until it approximately reaches the same steady state tow force at a similar speed in the un-reinforced sample bed, this steady state tow force seems to be universal for this plough at a set speed. It would have been interesting to compare the measured two forces between a sample with 0.5 % reinforcement and an unreinforced sample to investigate if there is any difference in plough behaviour and measured tow force. This could be compared to the results in the previous section where it was found that there was minimal difference between tow forces in the unreinforced and 0.5 % reinforced zones. However, in Figure 65 it can be seen as discussed previously that the ploughs depth steady state is not universal, as this is the only variable that the plough can change in order to reach its steady state tow force by reducing or increasing its depth. Figure 65 shows that the heel of the plough breaches the surface once the plough reaches its steady state tow force reducing its depth by approximately 95 %. Due to this massive reduction the heel of the plough breaches the sample bed surface within 500 mm of testing, with the tip of the share on the brink of breaching the surface of the sample bed at a minimal depth of approximately 2 mm (0.1 m). It could be argued that it would not be worthwhile ploughing at this speed in these conditions as the plough is unable to produce any type of trench. The extent of the plough ride out can be seen in the following figure, which was taken after the test seen in Figure 65 had been drained of water, where the heel of the share can be seen breaching the surface at the end of the test is shown.

**Figure 66: Picture of 1/50th Scale Plough Breaching Sample Bed Surface (: 0/2 % Test - 130 - 133 m/hr)**

The following figure is a combination of data produced from the three different speeds in the 2 % sample bed so that the rate effect on the plough in fibrous soils can be analysed.

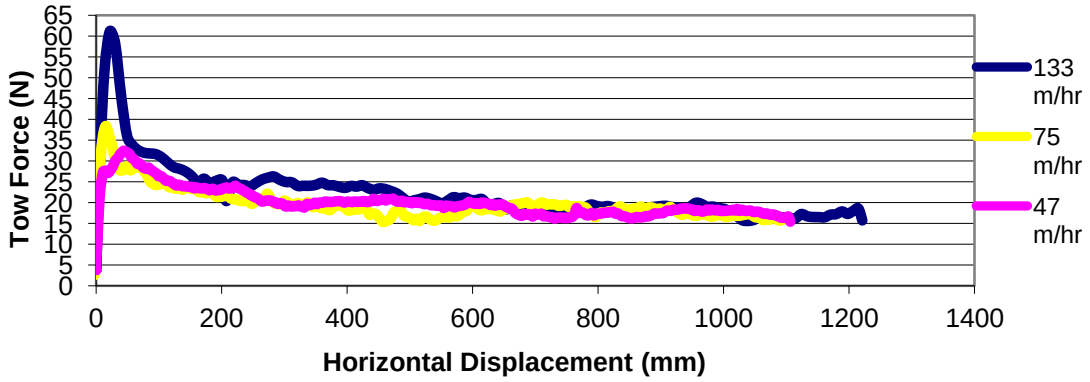


**Figure 67: Summary of Rate Effects in Fibrous Soil - Tow Force - 1/50th Scale**

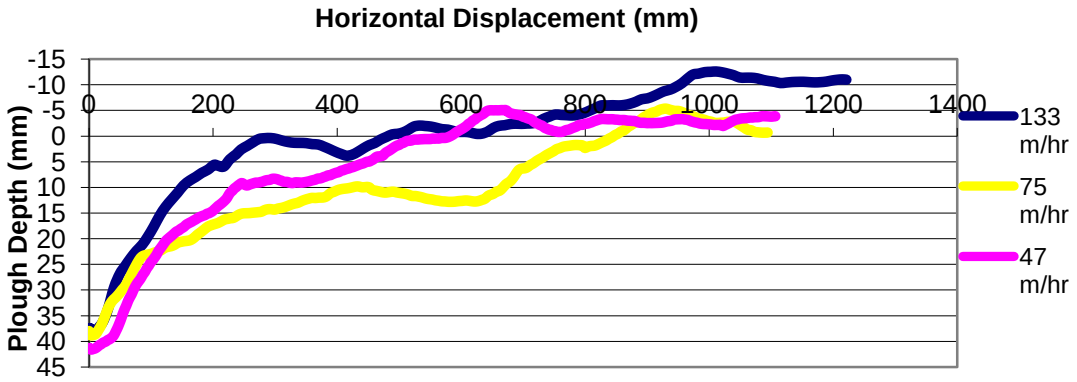


**Figure 68: Summary of Rate Effects in Fibrous Soil - Plough Depth (Heel) - 1/50$^{th}$ Scale**

When analysing the data in Figure 67 it can be seen that each test peaks at a different force, with the highest peak occurring at the beginning of the 133 m/hr test and lowest peak appearing in the slowest test of 47 m/hr. The reason for this is that at the beginning of the test the plough needs to accelerate from stationary to its set speed with a high acceleration and speed being resisted by a high force, explaining the increasing value of peak tow forces in each of the increasing speeds. However, after the tow forces peaking at different values depending on the ploughs speed, it can be seen that the tow force in each test is nearly identical meaning that there seems to be a minimal rate effect on the plough when working in fibrous soil. A reason for this is that there will be a preferential drainage path along the length of fibres due to the increase in voids ratio in the sample compared to that in an un-reinforced sample. In Figure 68 it can be seen that the initial rate of plough depth reduction is proportional to plough speed, with the highest speed having the highest initial rate of depth reduction and the slowest speed having the smallest. After these different rates of depth reduction, the plough depth seems to follow the same trend for the remainder of the test with minimal difference in plough depth between the three tests. Once again, this indicates that there is a minimal rate effect on the plough when testing in fibrous soils.

## 5.3 Comparison of Plough Depth and Trench Depth

In previous figures in this chapter, only the depth of the plough has been displayed throughout a test. However, it is important to measure the depth of the trench that is produced by the plough as it sometimes differs from the measured plough depth. In the following section a

comparison of plough and trench depth will be analysed for selected tests. Figure 69 show the difference between plough and measured trench depth for the 0.5, 2 and 4 % fibre volume ratio tests in the 1/25$^{th}$ scale tank.

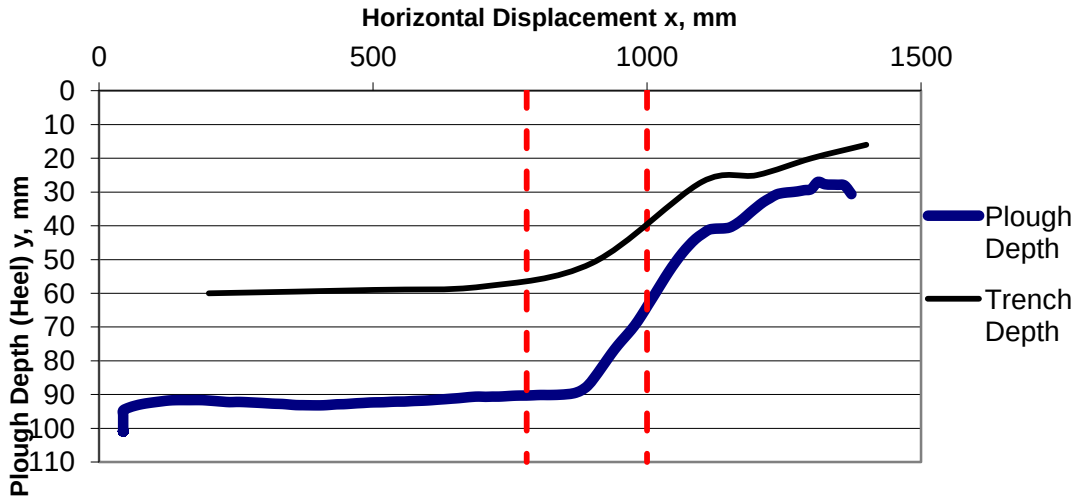


**Figure 69: Measured Trench Depth Profile (4 % Test - 1/25$^{th}$ Scale)**

Figure 69 shows that there is a significant difference between plough and trench depth throughout the test. When the plough is in its steady state there is a difference between plough and trench depth of approximately 35 %. As discussed previously, when the plough enters the fibrous zone the plough depth reduces dramatically, with the difference between measured trench depth and plough depth at the end of the test being approximately 33 %. The reason for the difference in depths is due to some of the sand that is displaced by the plough share falling back into the trench, reducing its depth. This 'fall back' effect is significant and needs taken into consideration when in the design stage as it could result in the trench not achieving the desired depth for pipeline installation which could prove costly as another passing of the plough may be needed to achieve the required trench depth.

Figure 70 show the comparison of plough and trench depth for the 2 % volume ratio test in the 1/25$^{th}$ scale tank.

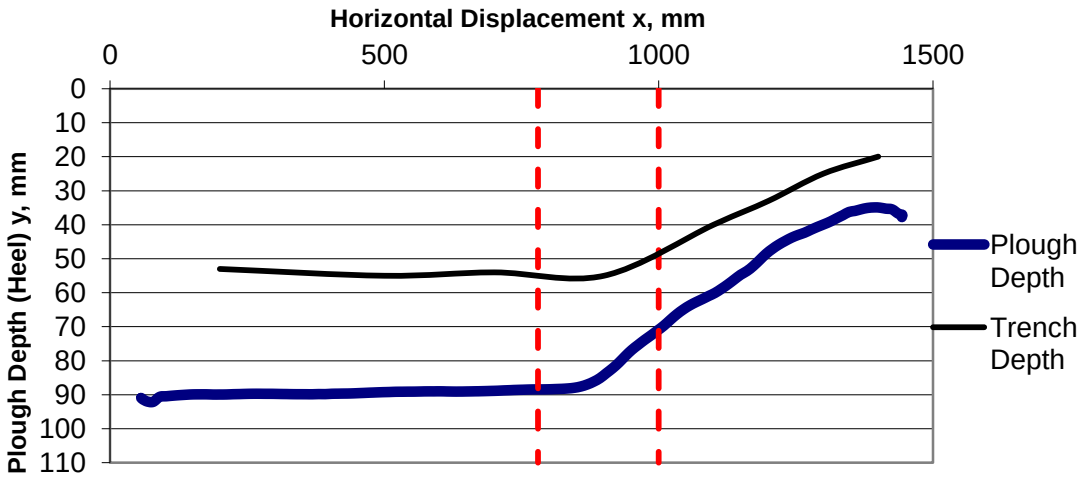


**Figure 70: Measured Trench Depth Profile (2 % Test - 1/25$^{th}$ Scale)**

The difference between plough and trench depth seen in Figure 70 when the plough is in its steady state in the fallow zone is approximately 39 %. The difference between plough and trench depth at the end of the test is approximately 42 %. When comparing the difference in plough and trench depth in the 2 and 4 % test while the plough is in its steady state in the fallow zone, it can be seen that there is a difference of 4 % indicating that the fall back of fallow sand is relatively constant. The difference in sand fall back at the end of both the 2 and 4 % tests is slightly higher, with a value of approximately 9 %. This indicates the fall back of sand into the trench is harder to predict due to the inclusion of fibres within the soil. A reason for this could be due to the fact that that the fibres are taking up more space within the soil heaps resulting in the excess sand being displaced into the trench. It is also important to analyse the change in trench shape when ploughing in the unreinforced and reinforced zone. A comparison of the shape of the trench can be seen in Figure 71 and Figure 72. Two points along the length of the trench have been compared, one point in the unreinforced zone (700 mm) and one in the reinforced zone (1300 mm).

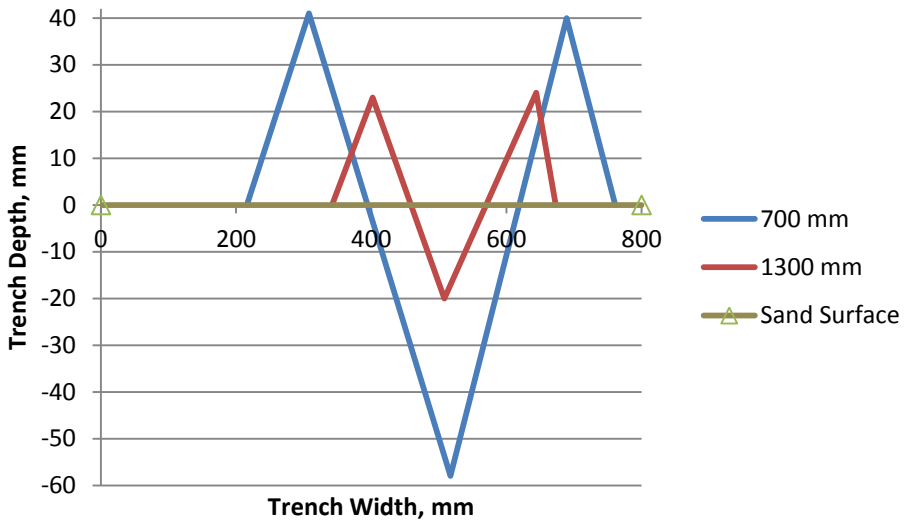


**Figure 71: Trench Shape - 4 % Test - 1/25th Scale**

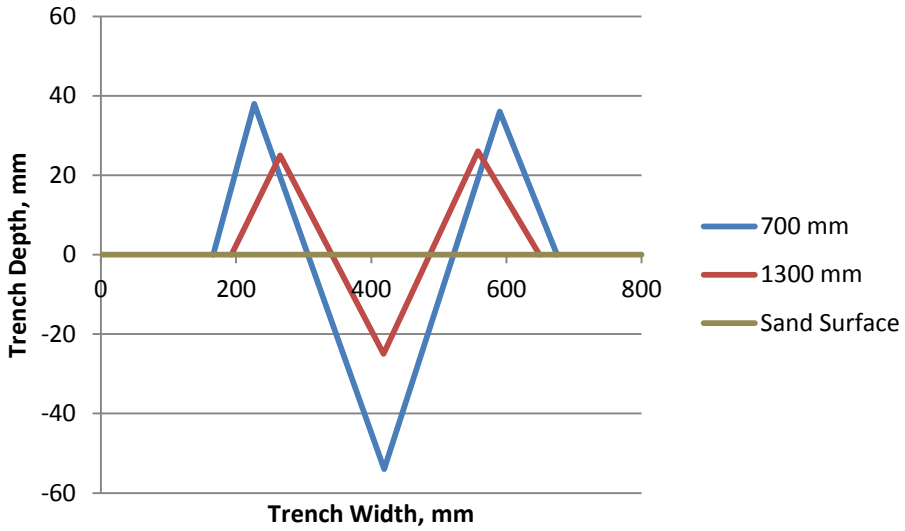


**Figure 72: Trench Shape - 2 % Test - 1/25th Scale**

As mentioned in the Methodology chapter, the points seen in Figure 71 and Figure 72 are found by measuring from predetermined reference points which are the top of the tank for vertical measurements and the left side of the tank for horizontal measurements. The vertical measurements seen in Figure 71 and Figure 72 have been zeroed to clearly display trench depth. The value used to zero trench depth in both tests is 460 mm. This is because the sand surface for every test in the 1/25th scale tank was set to 460 mm from the reference point at the top of the tank. It can be seen in both Figure 71 and Figure 72 that the shape of the trench

changes dramatically once the plough has entered the reinforced zone both in trench depth and width. However, this is to be expected as at this point, the plough has significantly ridden out of the sample reducing the size of spoil heaps produced has less soil is being displaced by the share.

The trench depths of tests carried out in the 1/50th scale tank were also measured. These measurements can be seen in Figure 73, Figure 74 and Figure 75.

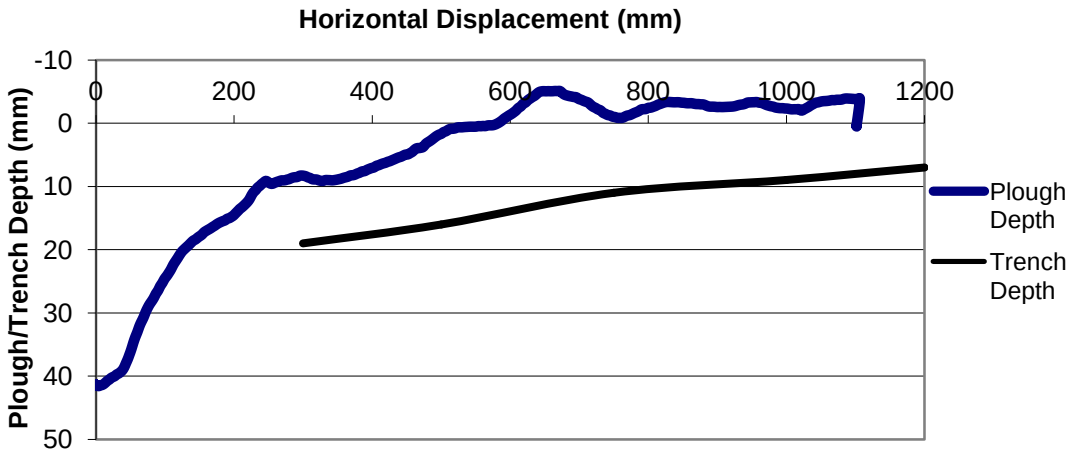


**Figure 73: Measured Trench Depth – 47 m/hr - 1/50th Scale**

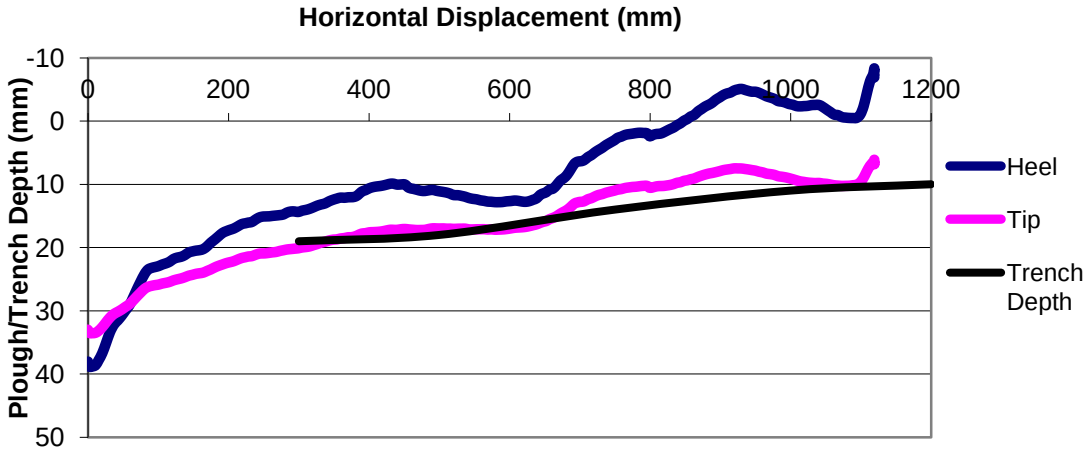


**Figure 74: Measured Trench Depth - 75 m/hr - 1/50th Scale**

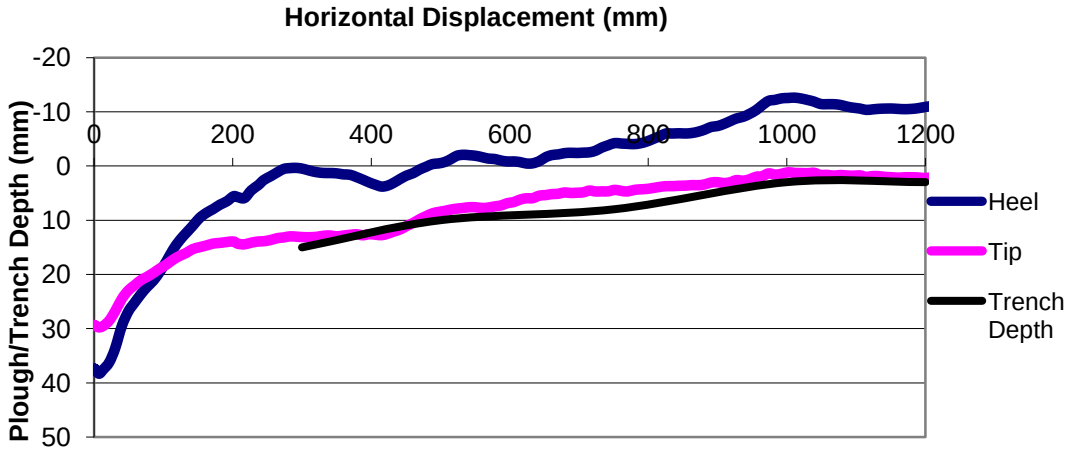


**Figure 75: Measured Trench Depth - 133 m/hr - 1/50th Scale**

When looking at Figure 73, it can be seen that there is a significant difference between plough depth and measured trench depth. However, the reason for this is that depth of the share tip was not measured in this test. When analysing the Figure 74 and Figure 75, it can be seen there is little to no difference between the depth of the share tip throughout the test and the measured trench depth indicating that there is no significant fall back of sand into the trench.

## 5.4 Plough Share Sensitivity

Each different fibre volume ratio has a different effect on the behaviour of the plough. It is thought that the plough can sense changes in soil type and density before it reaches the new zone. The reason for this could be due to the wedge of soil ahead of the plough being pushed by the share. This wedge of soil would experience the change in soil type and density before the plough reaches it, which, in theory will increase the tow force needed to pull the plough as it is harder for the share to push this new soil type. Once in a fibrous zone, the plough also experiences massive increases in tow force until it peaks. One of the reasons for this, apart from the obvious increase in resistance provided by reinforced soil, could be due to fibre build up in and around the share, effectively clogging the space up with fibre making it harder to plough through, in turn increasing the tow force. Both of these effects will be discussed in detail in the following section.

### 5.4.1 Position of the Plough in Relation to the Increase in Tow Force

In order to investigate the wedge of soil produced in front of the plough when testing and its effect on tow force when entering a new soil type, it was only possible to analyse this effect using tow force data from the 2 and 4 % tests as these are the only tests that tow force begins to increase before entering the fibrous zone.

The following test data seen in Figure 76 is from the 4 % test in the 1/25$^{th}$ scale tank.

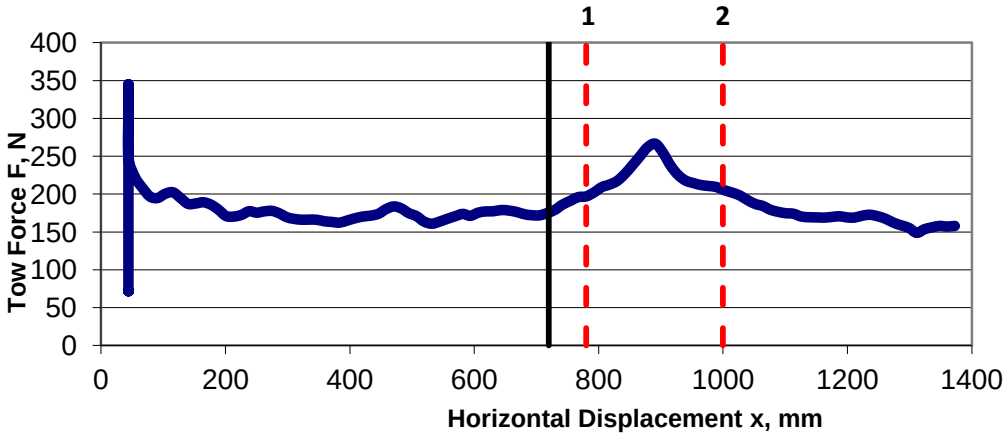


**Figure 76: Plough Sensitivity – Wedge Effect – 4 % Test - 1/25$^{th}$ Scale**

As seen in previous sections, lines 1 and 2 seen in Figure 76 indicate the share tip and heel entering the fibrous zone respectively. The black vertical line shows the initial increase in tow force before the plough enters the fibrous zone. Figure 76 shows the tow force begins to increase at a horizontal displacement of 720 mm, which is 60 mm away from the fibrous zone. This tow force increase occurs at a plough depth of 90 mm. These dimensions produce a wedge of soil ahead of the share with an angle of 56.3 degrees relative to the base of the plough share. This can be seen in Figure 77.

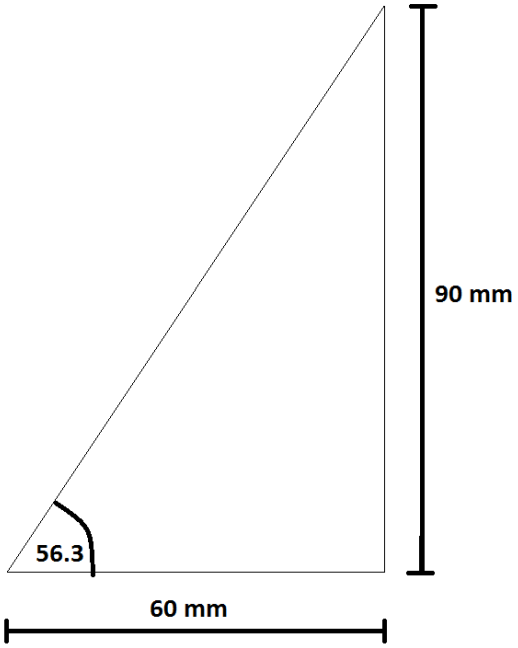


**Figure 77: Dimensions of Soil Wedge (4 % - 1/25th Scale)**

As the plough gets closer to the fibrous soil, the wedge being pushed by the share will need to progressively push more fibrous soil which will gradually increase the force needed to pull the plough. This explains why the tow force begins to increase before the share of the plough enters the fibrous zone.

The following data seen in Figure 78 is from the 2 % test in the 1/25th scale tank.

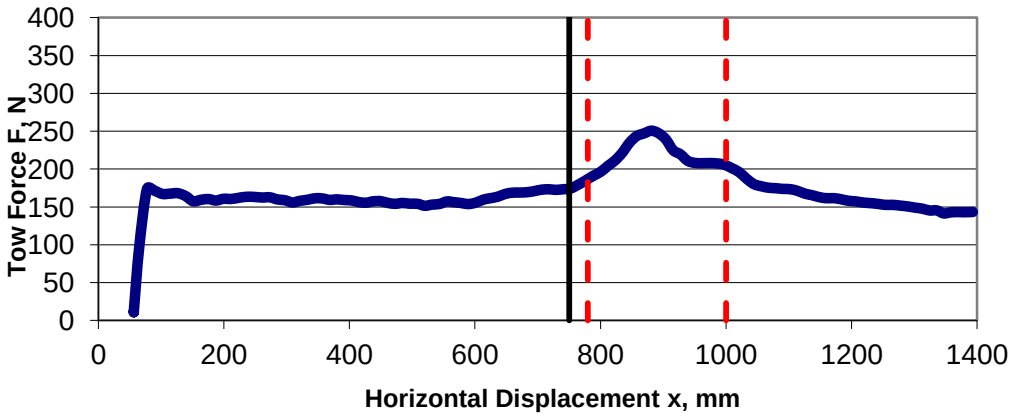


**Figure 78: Plough Sensitivity – Wedge Effect – 2 % Test - 1/25th Scale**

Figure 78 shows that the position of tow force increase before reaching the fibrous zone occurs later than seen Figure 76. The tow force increase occurs at a horizontal displacement of 750 mm, which is 30 mm away from the beginning of the fibre zone at a plough depth of 90 mm. These dimensions produce a wedge angle of the plough share of 71.6 degrees. These dimensions can be seen in Figure 79.

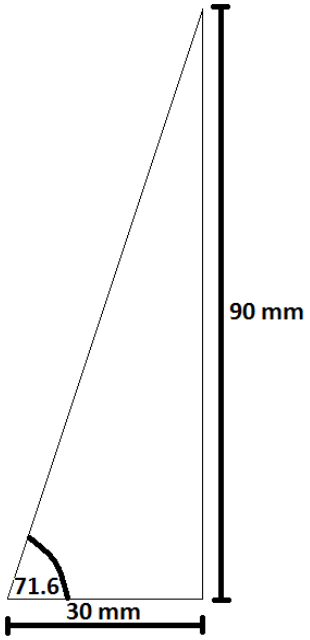


**Figure 79: Dimensions of Soil Wedge (2 % - 1/25$^{th}$ Scale)**

When comparing the two positions where the tow force begins to increase before entering the fibrous zone seen in Figure 76 and Figure 78 it can be seen that the data suggests that two different wedges are produced. However, this doesn't seem logical as the plough is in the same steady state, both in depth and tow force, in un-reinforced soil in both tests. In theory, the wedge produced by the plough in each test should be the same, however, the effect of the 4 % fibre zone should affect the plough earlier compared to that of the 2 % fibre zone as there is more resistance in the more fibrous zone. This trend can be seen in Figure 76 and Figure 78 as the tow force begins to increase 30 mm earlier in the 4 % sample bed than the 2 % sample bed.

### 5.4.2 Fibre Build Up on Share

Another effect that must be taken into consideration when analysing the increase in tow force when in a fibrous zone is the resistance provided by the reinforced soil and the related effect of

the space between the beam of the plough and the share being clogged up by fibres. This effect could be seen in every test carried out in both the 1/25$^{th}$ and 1/50$^{th}$ scale tanks but was best seen in Figure 67 and Figure 68 when testing in the 1/50$^{th}$ tank. As the plough is pre-embedded in each test, the tow force peaks (Figure 67) almost immediately in the 2 % test as it has to accelerate to each of the set speeds while the plough share is completely submerged in fibres from the beginning. This means that the fibre build up on the share clogs the space up almost immediately. The plough then has to reduce its depth, in each case the heel of the plough breached the sample bed surface, in order for the plough to reach its equilibrium between force and depth, which can be seen in Figure 68. Once each test was completed, the head of water was drained down to the sample bed surface in order for the plough to be excavated from the bed. After carefully removing the plough from the bed the extent of fibre build up around the share could be seen. This build up prior to and after excavation can be seen in Figure 80 and Figure 81.

**Figure 80: Picture of 1/50$^{th}$ Scale Plough Fibre Build Up Pre-Excavation**

**Figure 81: Picture of 1/50$^{th}$ Scale Fibre Build Up Post-Excavation**

The extent of fibre build up can be clearly seen in both Figure 80 and Figure 81. When looking at Figure 80, it can be seen that a large amount of fibres are trapped between the beam of the plough and the share when looking at the plough from above. A significant amount of fibres can also be seen being dragged along the side of the share. It is obvious that the fibres that are built up around the share will have a detrimental effect on desired tow force. The increase in tow force due to the build up of fibres could be due to the plough having trouble displacing soil around the share due to the increase in resistance provided by the movement of soil. The picture of the fibre build up around the share after being excavated, seen in Figure 81, shows the effect more clearly. The significance of the build up is significant in scale compared to the size of the share on the 1/50$^{th}$ scale plough. A reason for this could be as the same fibres were used in both test scales, the fibres in the 1/50$^{th}$ scale tank are effectively double the size of the fibres in the 1/25$^{th}$ scale tank.

## 5.5 Comparison with Cathie and Wintgens (2001)

It was possible to compare the results from the 1/25$^{th}$ scale tank to tow forces generated by the Cathie and Wintgens (2001) model which can be seen in Equation 10.

$$F = C_w W' + C_s \gamma' D^3 + C_d v D^2$$

**(10)**

Model data was created using this equation by using set depths ranging from 0 to 100 mm and using values for $C_w$, $C_S$ and $C_d$ which were given in Cathie and Wintgens (2001). This method creates a curved line which can be compared to data obtained from the 1/25$^{th}$ scale ploughing tests. The test results seen in Figure 82 are the comparison of the 4 % sample bed data (Figure 52) being compared and matched to the Cathie and Wintgens (2001) model. The test was carried out at 44 m/hr and the saturated unit weight of the soil was 6.88 kN/m$^3$.

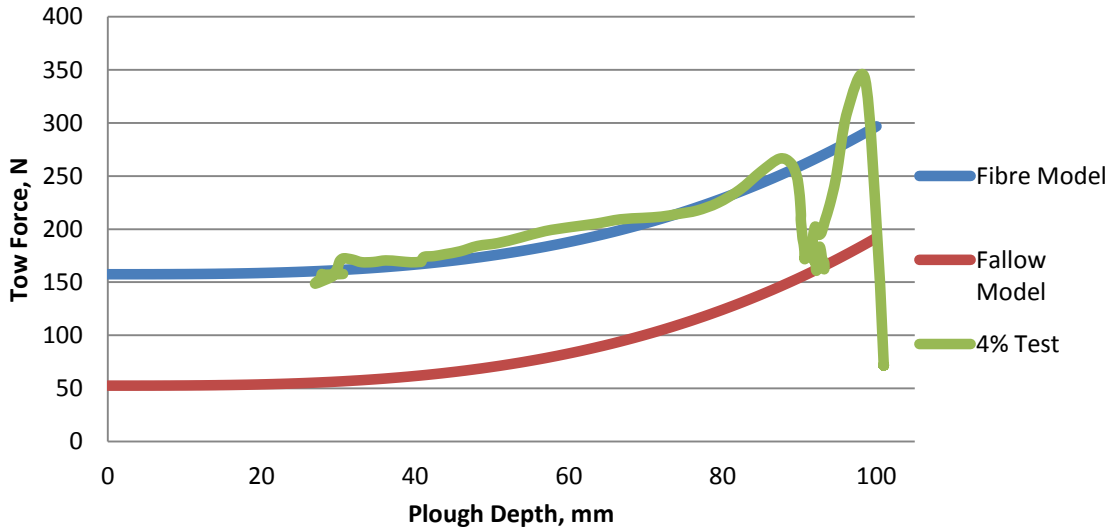


**Figure 82 - Cathie and Wintgens (2001) Model (4 % Test - 1/25 Scale)**

The blue line seen in Figure 82 is a line created to match the data measured when the plough is in the fibrous zone and the red line is created to match the data measured when ploughing in the unreinforced zone. The cluster of data from the 4 % test that is touching the fallow model line indicates where the plough was in its steady state. The parameters used to match the model line to the actual data can be seen in Table 22.

| | | |
|---|---|---|
| $C_w$ | 0.4 | |
| $W'$ | 131.23 | N |
| $C_s$ | 20 | |
| $\gamma'$ | 6.88 | kN/m$^3$ |
| $C_d$ | 0.4 | |
| $v$ | 44 | m/hr |

**Table 22: Table of Parameters - Cathie and Wintgens (2001) Fallow Model - 4 %**

In order for the fibre model line to match up with the test data when ploughing in the fibrous zone, the $C_w$ term, the friction coefficient, had to be increased by 300 % to 1.2 to match the increase in force when the plough enters the fibrous zone. The other parameters used to match the fibrous model line to the test data were exactly the same as what was used in the fallow model. This could be due to the fact that $C_w$ is the frictional term in the Cathie and Wintgens (2001) model, which dictates how much force is needed to begin to move the plough. As there is far more resistance when pulling the plough in the fibrous zone compared to the fallow zone, a greater force is needed to pull the plough, which why only $C_w$ increases as there is more friction acting on the plough. This could also be hiding an additional strength term that needs to be taken into consideration when analysing the effect reinforced soil on ploughing.

Figure 83 shows the 2 % sample bed data (Figure 54) being compared and matched to the Cathie and Wintgens (2001) model in both fallow and fibrous zones. The test was carried out at 44 m/hr and the saturated unit weight of the soil was 6.88 kN/m$^3$.

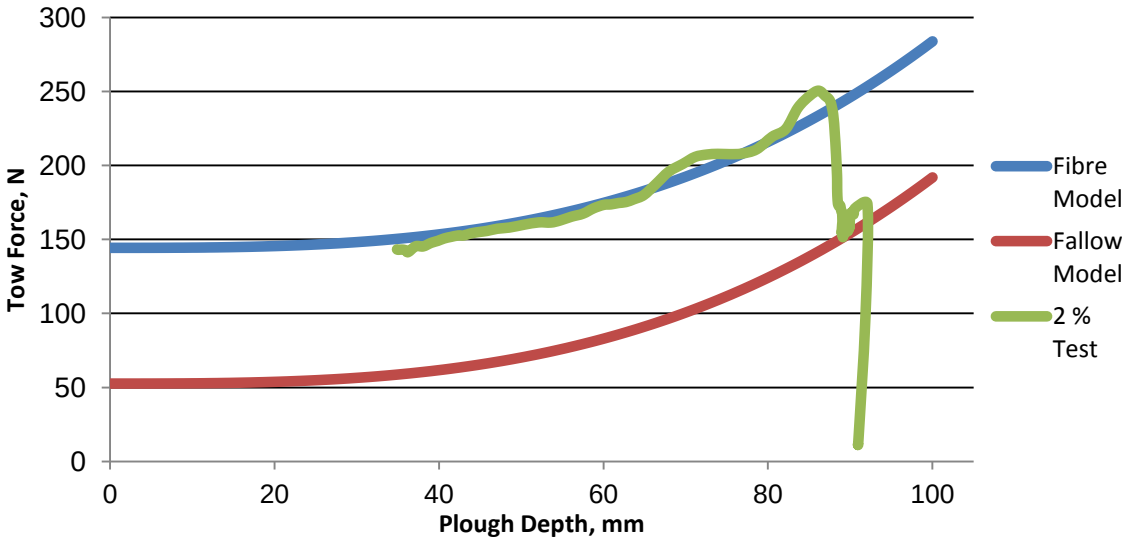


**Figure 83: Cathie and Wintgens (2001) Model (2 % Test - 1/25 Scale)**

The parameters used to match the fallow model line with the 2 % test during the ploughs steady state were the same as what was used in Table 22. In order for the fibrous model line to match up with the 2 % test data line, $C_w$ had to be increased to 1.1, which once again is nearly a 300 % increase.

Figure 84 shows the data of the 1.5 % test being compared to the Cathie and Wintgens (2001) model in both fallow and fibrous zones of the sample. The test was carried out at 44 m/hr and the saturated unit weight of the soil was 6.88 kN/m$^3$.

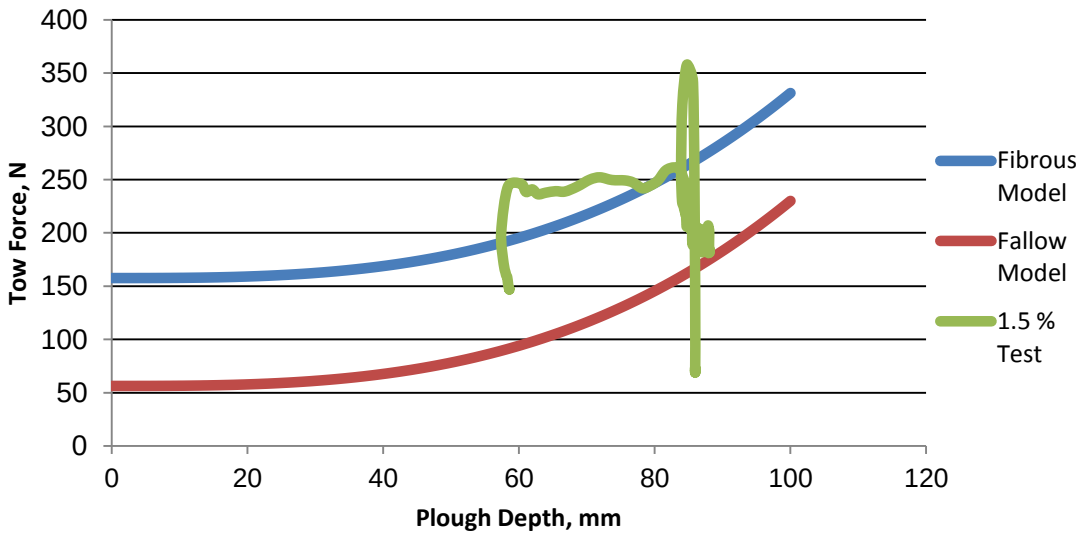


**Figure 84: Cathie and Wintgens (2001) Model (1.5 % Test - 1/25 Scale)**

The parameters used to match the fallow model with the 1.5 % test data line during the ploughs steady state and the can be seen in Table 23.

| | | |
|---|---|---|
| $C_w$ | 0.43 | |
| $W'$ | 131.2313 | N |
| $C_s$ | 25 | |
| $\gamma'$ | 6.88 | kN/m$^3$ |
| $C_d$ | 0.4 | |
| $v$ | 44 | m/hr |

**Table 23: Cathie and Wintgens (2001) Fallow Model – 1.5 %**

The parameters used to match the fibrous model with the peak data in the 1.5 % test data line were the same as what was used in Table 23 apart from $C_w$ which had to be increased to 1.2 which is approximately an increase of 300 %.

Figure 84 shows the fibrous model line only matches the 1.5 % test data when the tow force peaks once the plough enters the fibrous soil. Unlike what was seen in Figure 82 and Figure 83 where the test data in each case follows the fibrous model line while the plough is digging out due to the plough trying to find an equilibrium of forces acting on the top and bottom of the share, the 1.5 % test data's force reduces only slightly for the remainder of the test after

peaking, even though the plough depth reduces by approximately 20 mm after entering the fibre zone. This could be due to the difference in forces acting on the top and bottom of the share being much smaller than the 2 and 4 % tests, meaning that the equilibrium of forces around the share is reached quicker, resulting in a smaller reduction in depth from steady state. In order for the fibrous model to match the 1.5 % test data, the friction coefficient, $C_w$ needs to be increased to 1.7 and the passive pressure coefficient, $C_S$ needs significantly reduced to 7. In order to fully understand this effect, more tests would need to be carried out at the same fibre volume ratio to verify the results seen in Figure 84.

Figure 85 shows the data from the 1 % test being compared to a fallow and fibrous data model using the Cathie and Wintgens (2001) model. The test was carried out at 44 m/hr and the saturated unit weight of the soil was 6.88 kN/m$^2$.

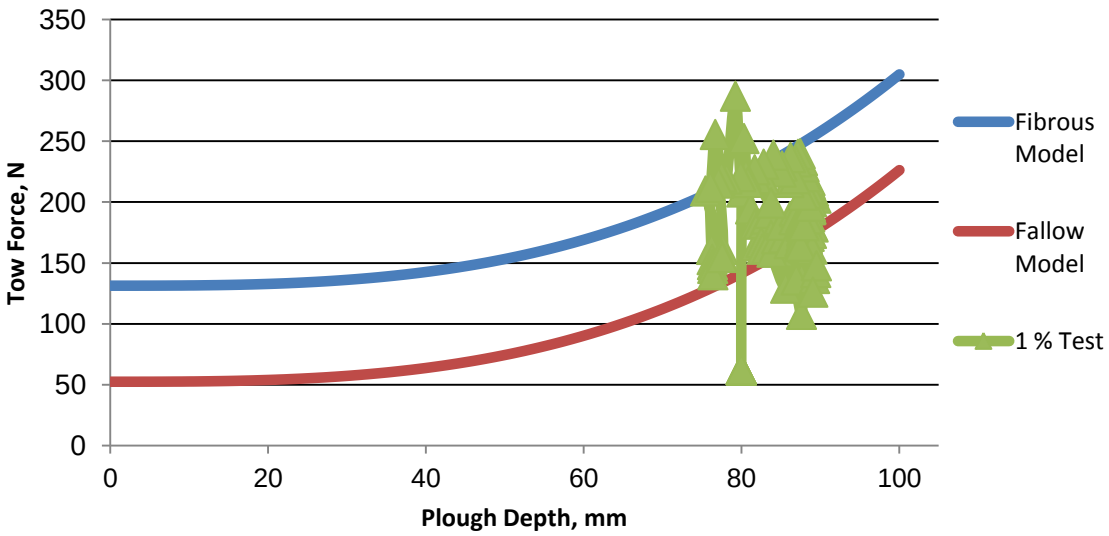


**Figure 85 : Cathie and Wintgens (2001) Model (1 % Test - 1/25 Scale)**

As mentioned in a previous section, the test data seen in Figure 85 is noisy as two of the runners which are connected to the I-beams used to move the plough would get caught on the track causing the load cell to shake during the test. This makes it hard to compare the test data to the Cathie and Wintgens (2001) model lines seen in Figure 85. Table 24 shows the parameters used to match the fallow models to the test data.

| | | |
|---|---|---|
| $C_w$ | 0.4 | |
| $W'$ | 131.23 | N |
| $C_s$ | 25 | |
| $\gamma'$ | 6.88 | kN/m$^3$ |
| $C_d$ | 0.4 | |
| $v$ | 44 | m/hr |

**Table 24: Cathie and Wintgens (2001) Fallow Model – 1 %**

Once again $C_w$ is the only parameter that changes when comparing the fibrous model to the test data, increasing by two and a half times to 1 compared to when the plough is in its steady state in the fallow zone. It must also be noted that the plough seems to be effected by the fibres much later in the test, meaning that there is less data to compare to the fibrous model line as the majority of the data is located on the fallow model line. Once the tow force peaks while the plough is in the fibrous zone, the tow force and plough depth only slightly reduces. This suggests that the plough reaches its force equilibrium quickly while being pulled through the sand reinforced with a 1 % fibre volume ratio, meaning that this amount of reinforcement has little effect on the performance of the plough.

Figure 86 shows the 0.5 % sample bed data being compared and matched to the Cathie and Wintgens (2001) model in both fallow and fibrous zones. The test was carried out at 44 m/hr and the saturated unit weight of the soil was 6.88 kN/m$^2$.

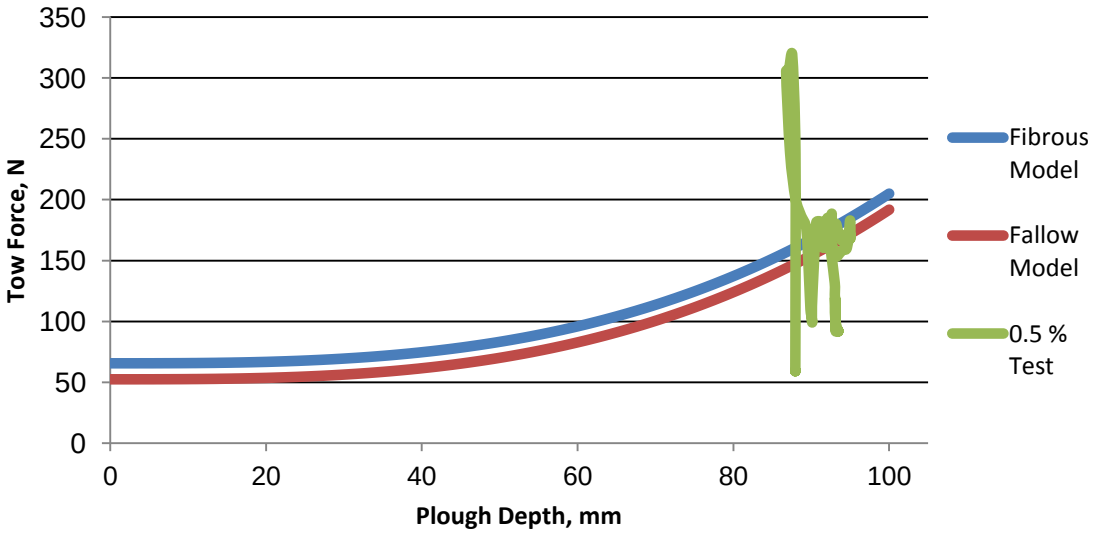


**Figure 86: Cathie and Wintgens (2001) Model (0.5 % Test - 1/25 Scale)**

It can be seen in both Figure 56 and Figure 86 that the 0.5 % fibre volume ratio has little to no effect on the tow force and depth of the plough. It can be seen in Figure 86 that is extremely difficult to separate the test data in the fallow zone from the fibrous zone, therefore, it is assumed that the parameters used in the Cathie and Wintgens (2001) model do no change for the duration of the test. These can be seen in Table 25.

| | | |
|---|---|---|
| $C_w$ | 0.4 | |
| $W'$ | 131.2313 | N |
| $C_s$ | 20 | |
| $\gamma'$ | 6.88 | kN/m$^3$ |
| $C_d$ | 0.4 | |
| $v$ | 44 | m/hr |

**Table 25: Cathie and Wintgens (2001) Fallow and Fibrous Model - 0.5 %**

In all cases but the 0.5 % the friction coefficient, $C_w$ increases by approximately 300 % when being pulled in the fibrous zone compared to the fallow zone. Whereas, the passive pressure coefficient, $C_S$ and the rate effect coefficient, $C_d$ remain constant regardless of which zone the plough is being pulled through. A reason for this could be that $C_w$ is hiding another coefficient within the Cathie and Wintgens (2001) model that needs to be taken into consideration when the plough is in reinforced soils. Different methods of achieving this will be investigated in the following sections.

## 5.6 Other Force Prediction Models

It may be possible to use other force prediction models or combine two different ones to investigate if this can be used to predict the behaviour of a plough during testing. As discussed in the literature review chapter Ivanovic *et al* (2011) created an equation which can calculate the drag force of an object, similar to a plough, being pulled through a soil. This drag force equation is similar to the passive pressure element which is included in the Cathie and Wintgens (2001) model. Cathie and Wintgens (2001) can calculate this using Equation 11 (the rate effect coefficient has been removed of comparative purposes).

$$F - C_w W = C_s \gamma D^3 \quad \textbf{(11)}$$

This can be compared to the following equation which was found by Ivanovic *et al* (2011).

$$F = W' \tan \delta + 0.5 K_p \gamma' D^2 L$$

**(12)**

| Front face angle, β (degrees) | $K_p$ |
|---|---|
| 60 | 10 |
| 90 | 12 |
| 105 | 20 |
| 120 | 30 |
| 150 | 40 |

**Table 26: Passive coefficient, Kp values for different front face angles, β (Ivanovic et al, 2011)**

As the share has an average angle of 41 degrees a Kp value of 8 has been interpolated from Table 26. As the width of the share is difficult to determine due to its complex shape, Equation 12 will be slightly altered to suit the plough. The modified formula can be seen in Equation 13.

$$F = W' \tan \delta + 0.5 K_p \gamma' D^3$$

**(13)**

Where, the only difference between Equation 12 and Equation 13 is that the frontal width of the object, L has been replaced with another depth term. The rationale behind this modification is that if the multiplication of the frontal width of the object, L and the depth term in Equation 12 resulted in a volume. If the drag force equation created by Ivanovic *et al* (2011) can replace its corresponding section of the Cathie and Wintgens (2001) model, Equation 14 must be satisfied.

$$F - C_w W = 0.5 K_P \gamma D^3$$

Or,

$$F - W \tan \delta = 0.5 K_P \gamma D^3$$

**(14)**

Where,

- $C_w W = W \tan \delta$ (Lauder, 2011)

The following results were calculated using Equation 14 with the use of set parameters.

| Depth, m | F, N | F-$C_w W$, N | $C_s \gamma D^3$, N | F-$W \tan \delta$,N | $0.5 K_P \gamma D^3$ |
|---|---|---|---|---|---|
| 0.01 | 60.546 | 0.334 | 0.334 | 1.839 | 0.334 |
| 0.02 | 62.882 | 2.670 | 2.670 | 4.176 | 0.534 |
| 0.03 | 69.225 | 9.013 | 9.013 | 10.518 | 1.803 |
| 0.04 | 81.575 | 21.363 | 21.363 | 22.869 | 4.273 |
| 0.05 | 101.937 | 41.725 | 41.725 | 43.230 | 8.345 |
| 0.06 | 132.313 | 72.101 | 72.101 | 73.606 | 14.420 |
| 0.07 | 174.705 | 114.493 | 114.493 | 115.999 | 22.899 |

**Table 27: Comparison of Cathie and Wintgens (2001) Model to Ivanovic et al (2011) Drag Force Model Results Summary**

Where,

| | |
|---|---|
| Interface Friction Angle, $\delta$ | 24 |
| W | 150.530 |
| Wtan $\delta$ | 58.707 |
| Kp | 8 |
| $C_w$ | 0.4 |
| $C_w$W | 60.212 |
| γ' | 16.69 |
| $C_S$ | 20 |

**Table 28: Parameters Used When Calculating Drag Force Model Results**

It must be noted that the force seen in Table 27 is calculated using the following equation using the relative parameters seen in Table 28.

$$F = C_w W + C_S \gamma D^3 \quad \textbf{(15)}$$

Table 27 shows that when comparing drag force models $F - C_w$ is equal to $C_s \gamma D^3$ for all depths where as $F - C_w$ or $F - \tan \delta$ does not equal and is significantly different than $0.5 K_P \gamma D^3$. This is most likely due to the modification that was made and described in Equation 13. Another reason for the difference in results is that an interpolated value for Kp of 8 was used when calculating the results seen in Table 27 in which there is a high possibility that this assumption is inaccurate. The reason for this is that Ivanovc et al (2011) states that in order to achieve the best results, the value of Kp was adjusted for each test while keeping the rest of the

parameters constant. If this is the case in terms of the plough Kp needs to increased by a magnitude of 5 to 40 in order to satisfy Equation 14

## 5.7 Investigating the Effect of the Inclusion of Soil Reinforcement on Cathie and Wintgens (2001) Model

There is a possibility that there could be another term that could be added to the Cathie and Wintgens (2001) to predict the effect of fibrous soil on tow force increase. It could be possible to predict a force that is determined by fibre ratio by analysing the shear plane created by the plough when testing and finding a corresponding cohesion value in order to generate a force. However, the shape of the shear plane created by a plough is still unknown so, in order to find out more about the plane, a photograph of a plough during testing in plan view which was obtained from Lauder (2011) was used to simulate a shear plane. As the exact dimensions of the plough used in the picture and its plough depth are known, it was possible to scale the shear plane accurately to generate a 3 dimensional model. The picture that was used to scale the shear plane can be seen in Figure 87. The shear plane has been outlined in black.

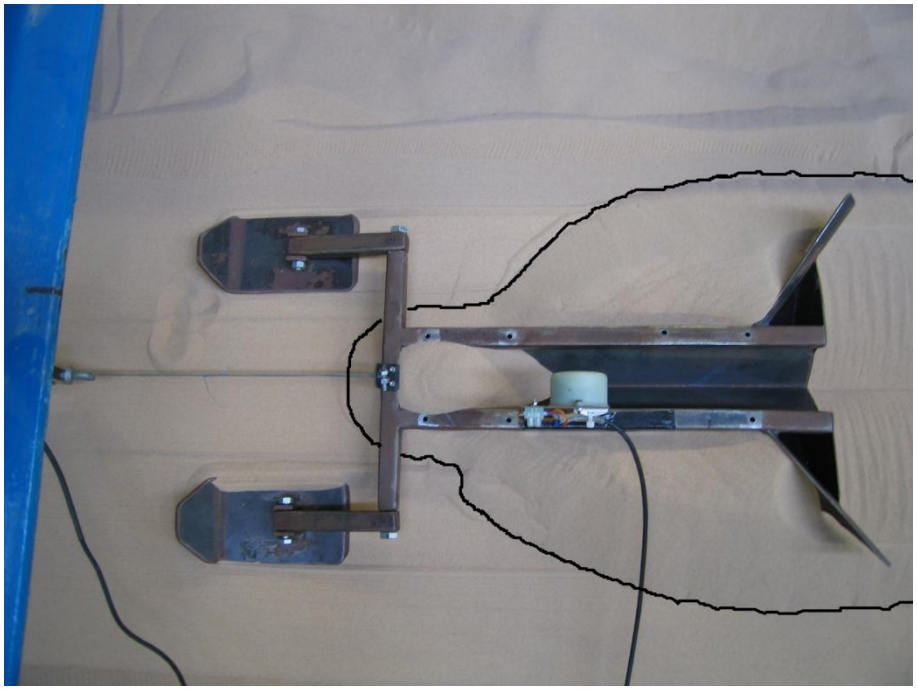

**Figure 87 - Plan of Ploughing Shear Plane**

In order to scale the shear plane, measurements were taking along the highlighted line, this process can be seen in the following figure.

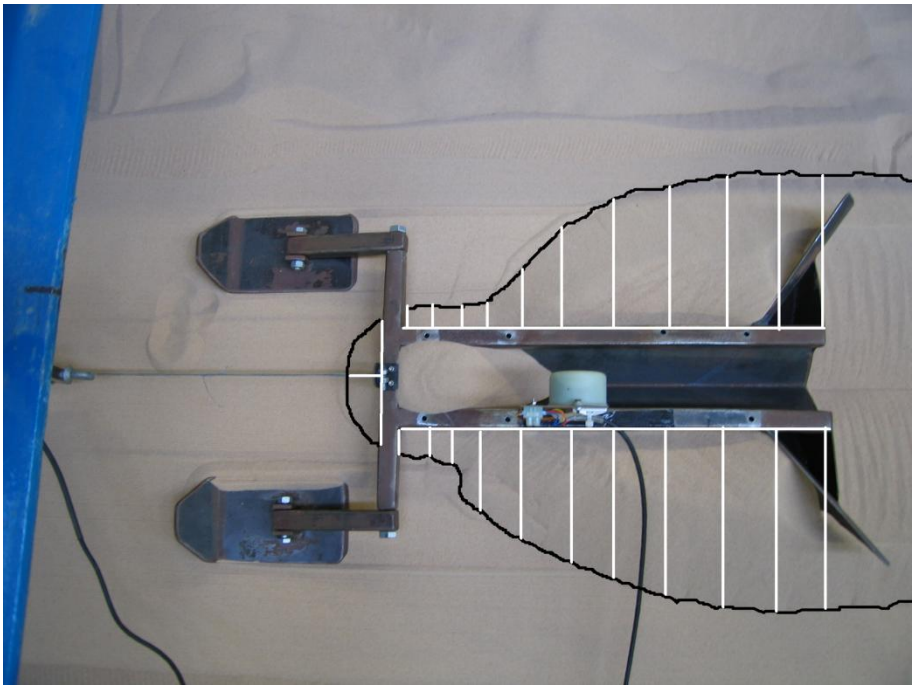

**Figure 88 - Scaling Plan of Ploughing Shear Plane**

After scaling the shear plane, the coordinates were entered into Google SketchUp which is a 3D modelling package which can give the user the area of a three dimensional shape. The plough depth of the test seen in Figure 88 is 81 mm and the bed was unreinforced. Figure 89 is the isometric view of the shear plane produced by the test seen in Figure 88.

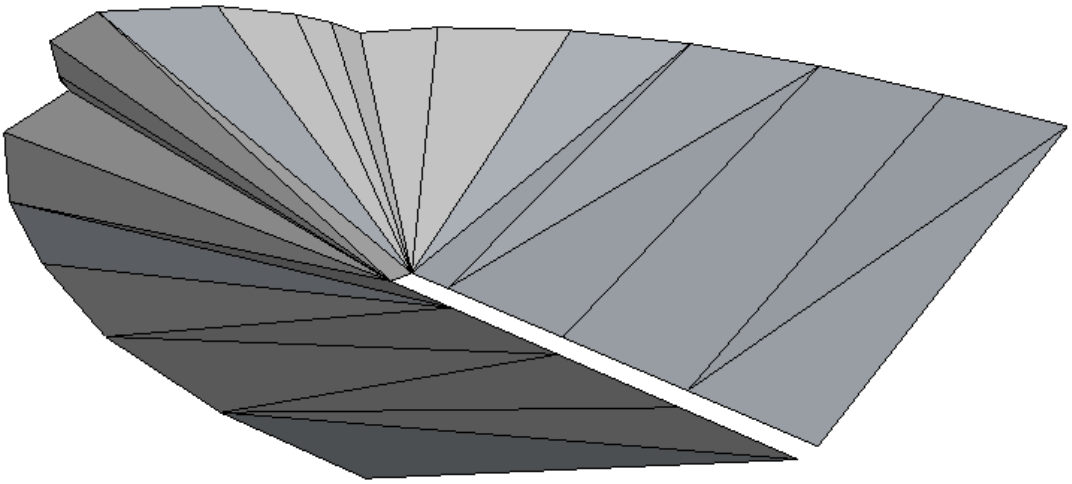

**Figure 89 - 3D Model of Shear Plane**

The surface area of the failure plane calculated for this test was 0.147m$^2$ which was calculated by creating a 3D model for each test carried out in the 1/25$^{th}$ scale tank. It was decided that each 3D model would be constructed at the point where the plough reaches its peak tow force as this is the point where the plough depth begins to reduce. It is thought that the majority of resistance to the plough, along the shear plane, occurred ahead of the share with the resistance along the side of the plough having minimal effect. A reason for this is because the majority of the resistance against the plough is going be created by the wedge of soil ahead of the plough that it is trying to push out of the way. The soil at either side of the plough which has been displaced is sliding along the surface of the share in the opposite direction providing only a small fraction of frictional resistance against the share. This allowed the complex shape of the shear plane, seen in Figure 87, to be simplified to the shape of half a pyramid. The newly created shear plane shape can be seen in Figure 90.

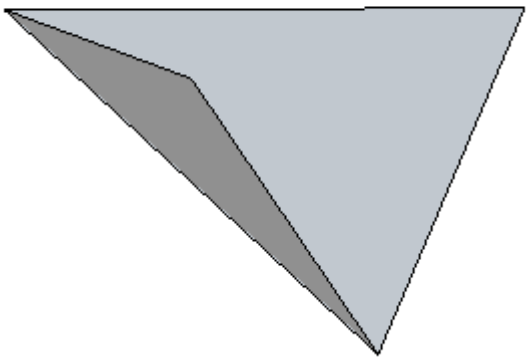

**Figure 90 - Simplified Shear Plane**

By using a simplified shape for the shear plane, it was now possible to easily calculate the surface area of the shape by using a formula.

$$A = Base\ Area + \frac{1}{2} Perimeter \times Slant\ Length \quad \textbf{(16)}$$

The dimensions of a simple pyramid can be seen in Figure 91.

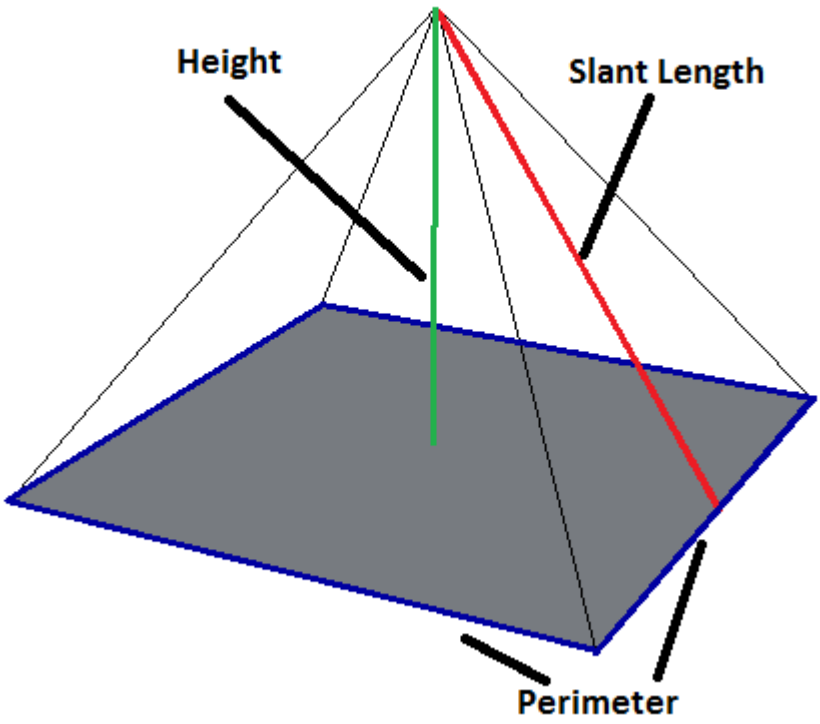


**Figure 91- Basic Pyramid Dimensions**

The grey area seen in Figure 91 is the base area of the pyramid. However, in the case of the shear plane which can be seen in Figure 90, the base area is not present and the pyramid is halved. This allows for Equation 16 to be simplified, to represent the shear plane seen in Figure 90. The simplified equation to calculate the lateral surface area of the shear plane can be seen in Equation 17.

$$A = \frac{1}{2} Perimeter \times Slant\ Length \tag{17}$$

As shear planes are soil type dependant, the formula used to calculate surface area of the shear plane, seen in Equation 17, had to be rearranged in terms of depth, friction angle and dilation angle in order for it to relate to a specific test. This was done by splitting the simplified shear plane, seen in Figure 90, into three sections, perimeter, height of the pyramid or length of the shear plane ahead of the share and slant length. The perimeter section can be seen in Figure 92.

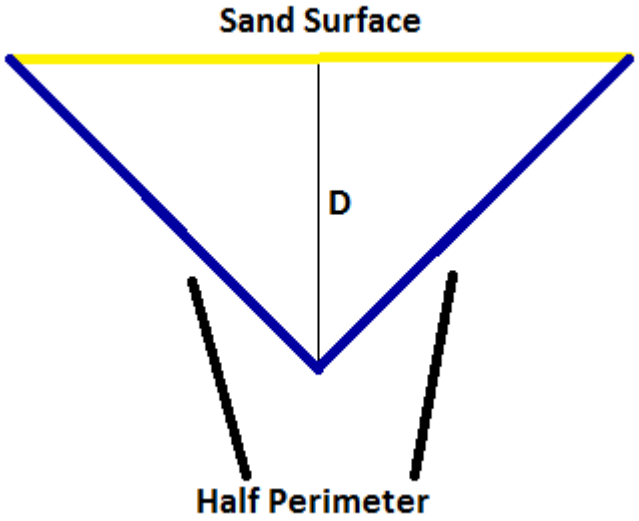


**Figure 92 - Pyramid - Perimeter Section Dimensions**

Where D is plough depth at a specific point. The position of the plough share in Figure 92 is where plough depth line, marked by D, meets the perimeter line.

The length of the shear plane ahead of the share section can be seen in Figure 93.

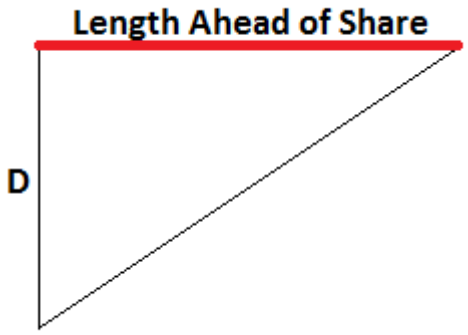


**Figure 93 - Pyramid - Length Ahead of Share Section Dimensions**

Where D is plough depth at a specific point. The position of the share tip in Figure 93 is at the base of the plough depth line.

The slant length section can be seen in Figure 94.

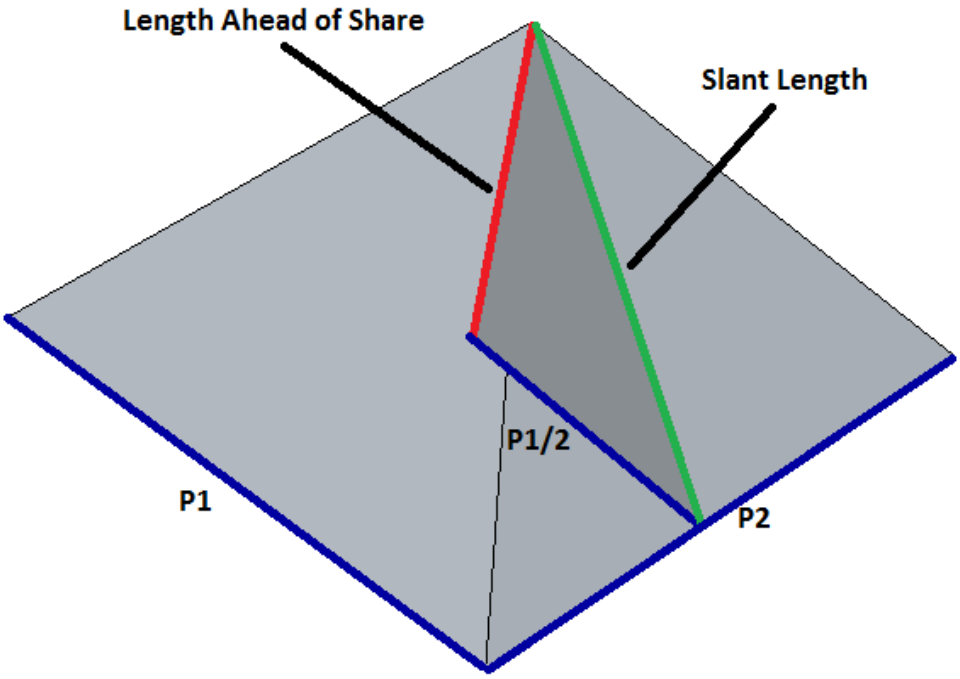


**Figure 94 - Pyramid - Slant Length Dimensions**

As seen in Figure 94, the perimeter has been split into faces with one face being P1 and the other being P2. The reason for this is to allow the slant length to be calculated using Pythagoras' Theorem. P1 is halved as the line marked by P1/2 goes to the centre of the pyramid from the midpoint of line P2. The slant length can then be calculated using Equation 18.

$$Slant\ Length = \sqrt{P1/2^2 + L^2} \quad \textbf{(18)}$$

Where, L is the length of the shear plane ahead of the share.

In order to relate the formula to calculate shear plane surface area to actual test data, soil parameters had to be incorporated into the equation to make it work. The soil parameters that were known for each test and could be used in the surface area calculations were the friction and dilation angle of the soil. With the friction angle controlling the steepness of the trench wall perpendicular to the plough share and both the friction and dilation angle are controlling the gradient of the shear plane, or soil wedge, being pushed ahead of the plough by the share. Figure 95 shows the incorporation of the friction angle into the diagram. By using the friction

angle it allows the perimeter to be calculated through the use of trigonometry as the depth of the plough, at this specific point, is known.

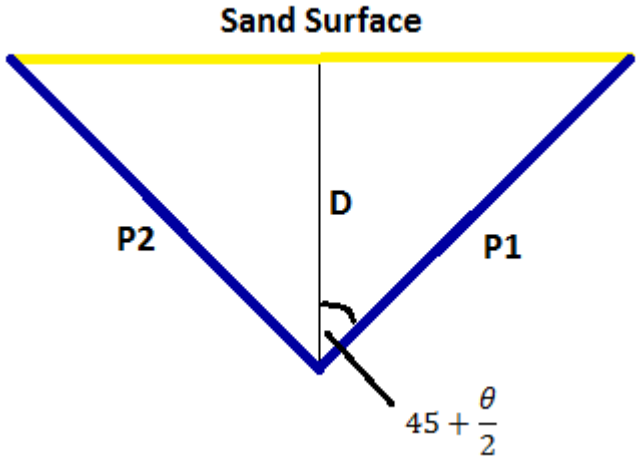


**Figure 95 - Pyramid - Perimeter Section Dimensions with Friction Angle**

The formula to calculate the length of the perimeter seen in Figure 95 is shown in Equation 19.

$$P1 = \frac{D}{\cos(45+\frac{\theta}{2})} \tag{19}$$

As this equation is derived from the lateral surface area of a whole pyramid, the perimeter is divided up into individual sides, P1 and P2 which can be seen in Figure 95. Therefore, the perimeter of a whole pyramid using this method would be 4(P1) as it is a square base. However, as the shape of the shear plane is effectively half of this, see Figure 92, the full perimeter of the plane can be used as 2(P1).

Using a similar technique to this, it is possible to calculate the length of the shear plane ahead of the plough share through the use of trigonometry by using the friction and dilation angle of the soil. This can be seen in Figure 96.

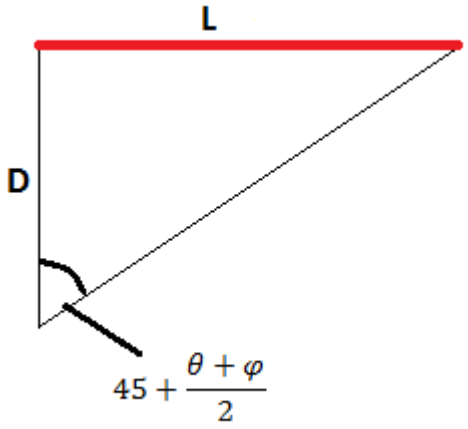


**Figure 96 - Pyramid - Length Ahead of Share Section Dimensions with Friction and Dilation Angle**

The formula to calculate the length of the shear plane ahead of the share, derived from Figure 96, can be seen in Equation 20.

$$L = \tan\left(45 + \frac{\theta + \varphi}{2}\right) \times D$$

**(20)**

In order for this approach to work, the slant length, which can be seen in Figure 94, of the shear plane had to be calculated. By using Equation 18 to calculate the slant length, it can be seen that both equations for the perimeter, Equation 19, and the length of the shear plane ahead of the plough, Equation 20 had to be incorporated in the formula used to calculate slant length. This can be seen in Equation 21.

$$Slant\ Length = \sqrt{\frac{1}{2}P1^2 + L^2}$$

$$Slant\ Length = \sqrt{\left(\frac{1}{2} \times \frac{D}{\cos\left(45 + \frac{\theta}{2}\right)}\right)^2 + \left(\tan\left(45 + \frac{\theta + \varphi}{2}\right) \times D\right)^2}$$

**(21)**

It was now possible to create a formula that calculates the surface area of the shear plane by combining the three previous equations. This can be seen in Equation 22.

$$A = \frac{1}{2} Perimeter \times Slant\ Length$$

$$A = \frac{1}{2} P1 \times \sqrt{\frac{1}{2} P1^2 + L^2}$$

$$A = \frac{D}{\cos(45 + \frac{\theta}{2})} \times \sqrt{\left(\frac{1}{2} \times \frac{D}{\cos\left(45 + \frac{\theta}{2}\right)}\right)^2 + \left(\tan\left(45 + \frac{\theta + \varphi}{2}\right) \times D\right)^2}$$

**(22)**

It was now possible to use this equation to calculate the surface area of the shear plane at a specific point in the test and compare it to the surface area generated by the 3D modelling program at the exact same point in the test. This process was carried out for each test and tabulated in Table 29.

| | Normal Effective Stress, kPa | Peak Friction Angle, | Depth, m | Dilation Angle | Sketchup Area, $m^2$ | Calculated Area, $m^2$ | Difference, $m^2$ |
|---|---|---|---|---|---|---|---|
| 0% | 17 | 43.94 | 0.081 | 9.81 | 0.145 | 0.111 | -0.034 |
| 1% | 17 | 47.29 | 0.087 | 13.71 | 0.147 | 0.172 | 0.025 |
| 2% | 17 | 49.81 | 0.086 | 12.88 | 0.147 | 0.189 | 0.042 |

**Table 29: Summary of Shear Plane Surface Area Calculations**

When comparing the calculated area results using Equation 22, which can be seen in Table 29, to the area obtained from SketchUp it can be seen that there is a slight difference for each test indicating that the model used to calculate the area may be slightly inaccurate. This suggests that a more accurate measurement of the shear plane produced by the plough during testing is needed to determine the accuracy of the Equation 22. It must also be noted that when calculating the area of the shear plane, it is assumed that the shear plane along either side of the plough has minimal effect. This could be a reason for the difference in calculated area to the area of the shear plane using SketchUp seen in Table 29 as the combined effect of resistance created by the shear plane along each side of the plough could be having a significant effect on tow force required to pull the plough through the soil. In future testing a better understanding could be achieved by attaching a video camera directly above the plough

during testing so that the shear plane appearing on the surface of the sand can be recorded for the entire test, giving an accurate understanding of how it changes when it encounters fibres.

As discussed in the previous chapter, the possibility of incorporating the limiting bond force equation of the reinforcement (Jewell and Wroth (1987)) which was designed to predict the increase in force due to the inclusion of reinforcement in a direct shear test.

$$P_{RL} = \sigma_\theta \times A_r \times \tan\delta$$

**(23)**

Where,

- $A_r$, will be the area of the shear plane when comparing to ploughing results.
- $\delta$, will be the interface friction angle between sand and fibre.
- $\sigma_\theta$, is calculated using Equation 24 which has been slightly altered to suit plough tests.

$$\sigma_\theta = \gamma' D \frac{1 + \sin\emptyset_{ps} \sin(\emptyset_{ps} + 2\theta)}{\cos^2\emptyset_{ps}}$$

**(24)**

Where,

- $\gamma'$, is the saturated unit weight of the soil.
- $D$, is the depth of the plough at a specific point in the test.
- $\emptyset_{ps}$, is the friction angle of the soil.
- $\theta$, is the angle of the plough share

It must be noted that the main difference between Equation 24 and Equation 9 is that $\gamma' D = \sigma_{yy}$. This is because effective stress will change with depth throughout the test.

The accuracy of this method was investigated by calculating the limiting bond force, $P_{RL}$ for each test carried out with 1/25$^{th}$ scale plough when the tow force peaks. This will show if the peak tow force exceeds the limit force calculated in Equation 23 for each test. As Equation 23 calculates the increase in force from unreinforced to a reinforced sample, the difference between steady state and the tow force measured when the plough is in the reinforced zone of the test had to be calculated. This was achieved by averaging the tow force of the plough when

it was in the unreinforced zone to give the ploughs steady state tow force and subtracting this value from the entire test. This means that only the increase in the tow force due to reinforcement will be shown on the graph (which can be seen in Figure 97) allowing the results to be compared to the calculated limiting bond force, $P_{RL}$. Four tests, the 1, 1.5, 2 and 4 % fibre volume ratio tests in the 1/25$^{th}$ scale tank, will be used to analyse its effectiveness.

Figure 97 compares the 1 % fibre volume ratio test carried out in the 1/25$^{th}$ scale tank to Jewell and Wroth's (1987) limiting bond force predicting model seen in Equation 23.

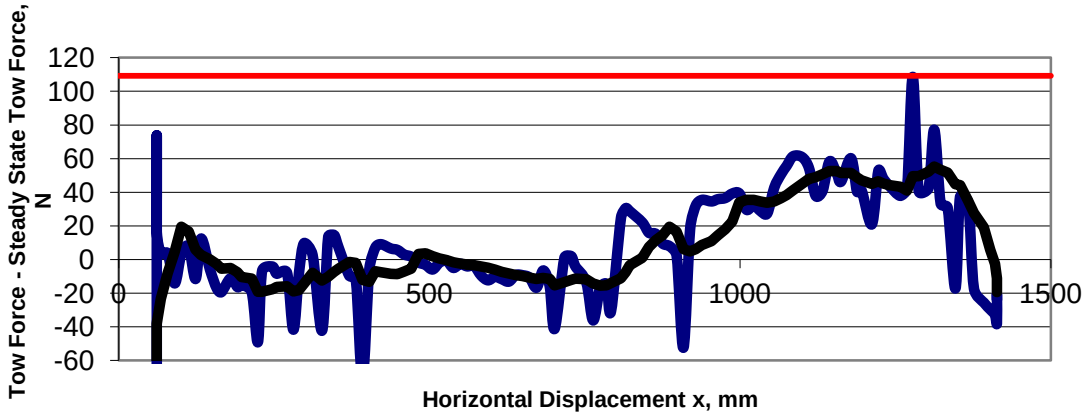


**Figure 97: The Comparison of Plough Test to the Limiting Bond Force Equation (Jewell and Wroth (1987)) - 1 % Test - 1/25th Scale**

The red line seen in Figure 97 is the limiting bond force for this specific test which has been calculated using Equation 23. The force displayed in the graph is calculated by subtracting the average steady state force from the measure tow force throughout the test, which can be seen on the y-axis.

| | | |
|---|---|---|
| Saturated Unit Weight | 6.69 | $kN/m^2$ |
| Share Angle (To Vertical) | 49 | degrees |
| Interface Friction Angle | 19 | degrees |
| Peak Friction Angle | 48 | degrees |
| Area | 0.172 | $m^2$ |
| Plough Depth | 0.087 | m |
| Normal Effective Stress | 0.582 | $kN/m^2$ |
| Inclined Normal Effective Stress | 1.840 | $kN/m^2$ |
| Prl | 0.109 | kN |
| Prl | 109.183 | N |

**Table 30: Summary of Values and Results of Limiting Bond Equation - 1 % Test - 1/25th Scale Test**

As mentioned previously, there was a problem with the apparatus during the 1 % test which can be seen in Figure 97 causing the data line to be noisy. Therefore, an average trend line has been added to show the tow force measured throughout the test. The area which can be seen in Table 30 was calculated using Equation 22. The peak friction angle used was obtained through direct shear test which has been discussed in the previous chapter. The share angle (to vertical) was obtained by averaging the angle of the tip of the share and actual share. An example of the difference between the two can be seen in Figure 98. The blue line indicates the average angle of the entire scale. Please note that diagram is not to scale.

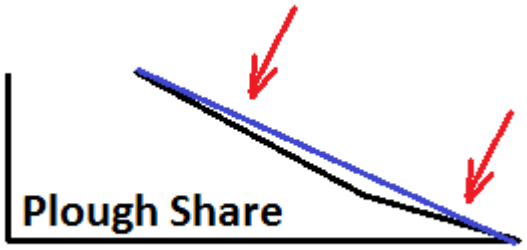


**Figure 98: Diagram of Share Angle Geometry (Not to Scale)**

It can be seen in Figure 97 the peak tow force reached by the plough when advancing through the 1 % fibre volume ratio zone is approximately 50 N less than the limiting bond force predicted using Equation 23. This indicates that the plough is unable to reach the predicted peak force during the test as the long beam principle prevents the force increasing to this value due to the force equilibrium around the share. As the tow force begins to peak, the tow force acting on the top of the share is significantly increasing. To counteract this increase in force the plough reduces is depth until the forces acting on the plough are in equilibrium again. This

indicates that the plough is working to prevent itself reaching its worst case scenario during the test.

Figure 99 shows the comparison of the 1/25$^{th}$ scale 1.5 % plough test to the limiting bond equation.

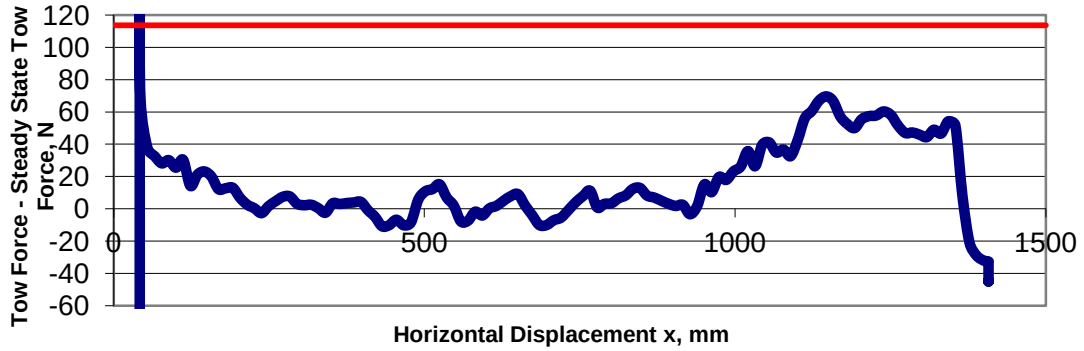


**Figure 99: The Comparison of Plough Test to the Limiting Bond Force Equation - 1.5 % Test - 1/25th Scale**

| | | |
|---|---|---|
| Saturated Unit Weight | 6.69 | kN/m$^2$ |
| Share Angle (To Vertical) | 49 | degrees |
| Interface Friction Angle | 19 | degrees |
| Peak Friction Angle | 50 | degrees |
| Area | 0.173 | m$^2$ |
| Plough Depth | 0.084 | m |
| Normal Effective Stress | 0.562 | kN/m$^2$ |
| Inclined Normal Effective Stress | 1.912 | kN/m$^2$ |
| Prl | 0.114 | kN |
| Prl | 113.593 | N |

**Table 31: Summary of Values and Results of Limiting Bond Equation - 1.5 % Test - 1/25th Scale Test**

It must be noted that as a 1.5 % sample was not tested in the direct shear apparatus there was no peak friction angle calculated. For the purpose of this analysis a peak friction angle for the 1.5 % test was calculated by taking the average between the 1 and 2 % peak friction angles obtained from direct shear tests. Once again it can be seen that there is a difference between peak tow force and the calculated limiting bond force at the point of peak tow force of approximately 45 N. This indicates that the plough prevents itself from reach the tow force limit

in a 1.5 % sand sample by slightly reducing its depth to regain the force equilibrium around the share.

Figure 100 shows the comparison of the 1/25$^{th}$ scale 2 % plough test to the limiting bond equation.

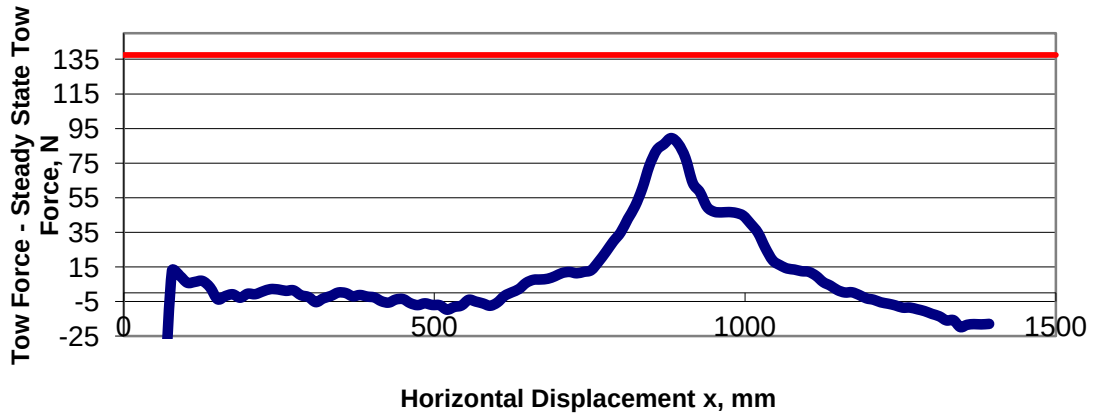


**Figure 100: The Comparison of Plough Test to the Limiting Bond Force - 2 % Test - 1/25th Scale**

| | | |
|---|---|---|
| Saturated Unit Weight | 6.69 | kN/m$^2$ |
| Share Angle (To Vertical) | 49 | degrees |
| Interface Friction Angle | 19 | degrees |
| Peak Friction Angle | 52 | degrees |
| Area | 0.189 | m$^2$ |
| Plough Depth | 0.086 | m |
| Normal Effective Stress | 0.575 | kN/m$^2$ |
| Inclined Normal Effective Stress | 2.116 | kN/m$^2$ |
| Prl | 0.137 | kN |
| Prl | 137.467 | N |

**Table 32: Summary of Values and Results of Limiting Bond Equation - 2 % Test - 1/25th Scale Test**

Figure 100 shows a difference between peak tow force in the 2 % fibre volume zone and the limiting bond force at the point of peak tow force of approximately 45 N. Once again the plough does not reach its limit tow force for the test due to the plough reducing its depth (Figure 55) in order to achieve equilibrium of tow force around the share.

Figure 101 shows the comparison of the 1/25$^{th}$ scale 2 % plough test to the limiting bond equation.

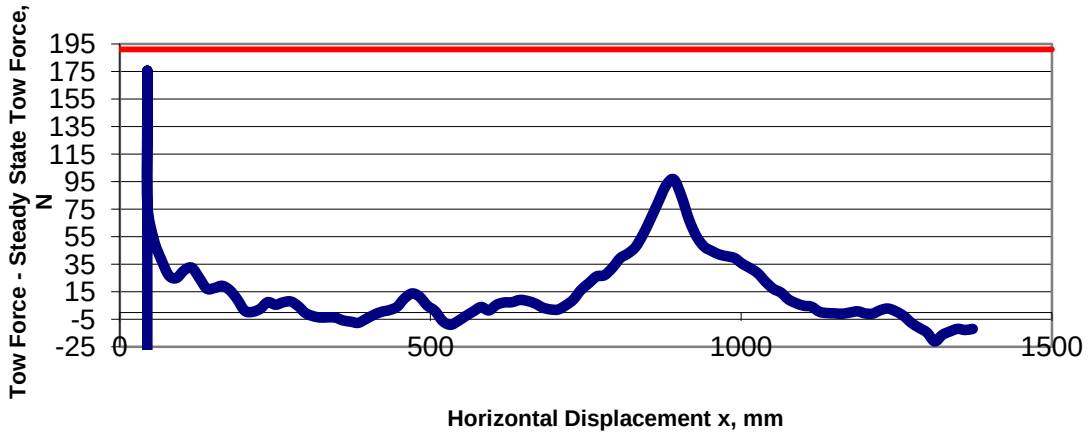


**Figure 101: The Comparison of Plough Test to the Limiting Bond Force Equation - 4 % Test - 1/25th Scale**

| | | |
|---|---|---|
| Saturated Unit Weight | 6.69 | kN/m$^2$ |
| Share Angle (To Vertical) | 49 | degrees |
| Interface Friction Angle | 19 | degrees |
| Peak Friction Angle | 55.50 | degrees |
| Area | 0.224 | m$^2$ |
| Plough Depth | 0.087 | m |
| Normal Effective Stress | 0.582 | kN/m$^2$ |
| Inclined Normal Effective Stress | 2.481 | kN/m$^2$ |
| Prl | 0.191 | kN |
| Prl | 191.185 | N |

**Table 33: Summary of Values and Results of Limiting Bond Equation - 4 % Test - 1/25th Scale Test**

As a 4 % sample was not tested in the direct shear apparatus, a peak friction angle of 55.5 degrees was used for the purpose of this analysis. This was calculated by taking the average of the difference between 0 and 1 % and 1 and 2 % peak friction angles.

A difference of approximately 95 N between peak tow force and the limiting bond force at the point of peak tow force can be seen in Figure 101. This difference is significantly higher than what was observed in Figure 97, Figure 99 and Figure 100. A reason for this bigger difference between peak tow force and the limiting bond force calculated using Equation 23 could be due to this specific plough having its own limit tow force due to its geometry. When comparing

Figure 100 and Figure 101 it can be seen that even though there is double the amount of fibres present in the 4 % sample bed compared to the 2 %, there is only a difference of approximately 7 N when comparing peak tow forces. However, one major difference between the 2 and 4 % sample beds is that the plough reduces its depth in the 4 % sample bed significantly more than the reduction in depth in the 2% sample bed. If this theory on a plough having its own limit tow force due to its geometry is correct, this explains why there is a larger difference in the 4 % sample bed between peak tow force and the limiting bond force equation at the point of peak tow force compared to the other three tests.

Due to the difference in peak tow force and the limiting bond force at the point of peak tow force in each of the test results, it is possible to introduce a fibrous soil coefficient, Cf that reduces this difference and gives an accurate prediction of force increase due to the inclusion of fibres within a sample. For analytical purposes, a fibrous soil coefficient, Cf of 0.7 was used and produced the following results.

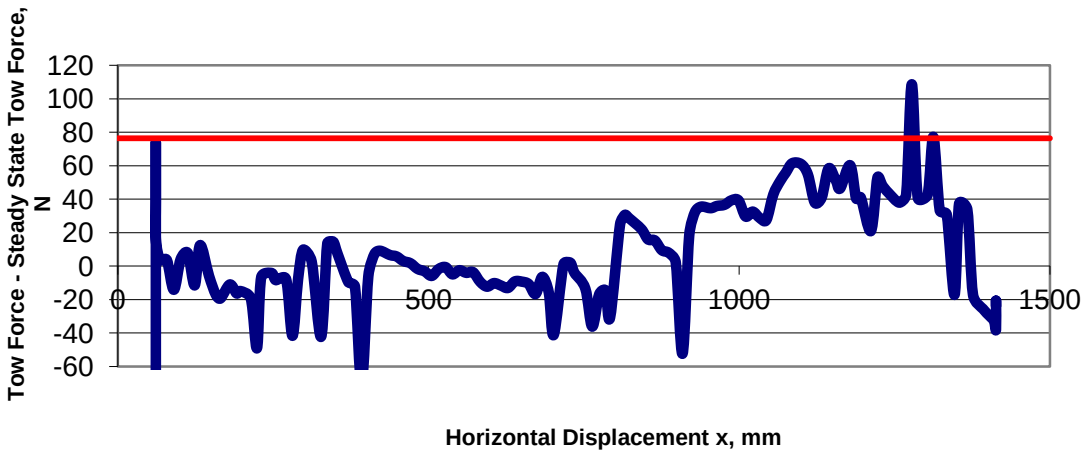


**Figure 102: The Comparison of Plough Test to the Limiting Bond Force Equation with Fibrous Soil Coefficient, Cf = 0.7 - 1 % Test - 1/25th Scale**

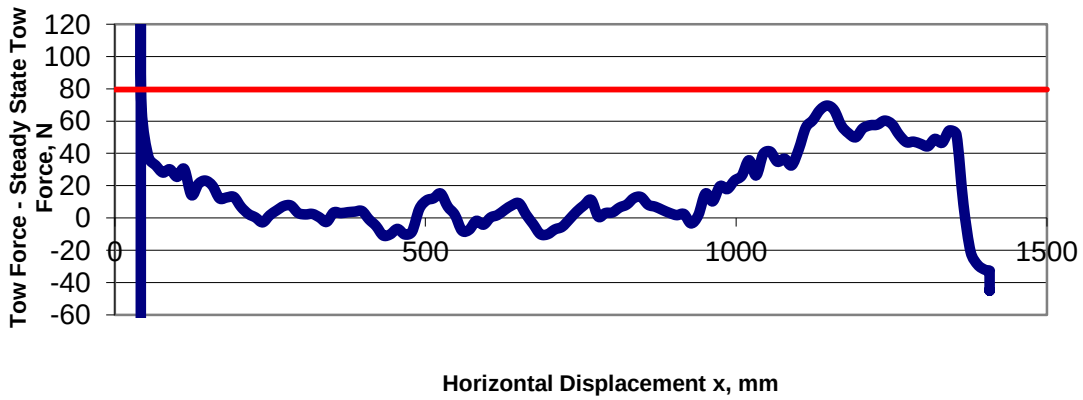


**Figure 103: The Comparison of Plough Test to the Limiting Bond Force Equation) with Fibrous Soil Coefficient, Cf = 0.7 - 1.5 % Test - 1/25th Scale**

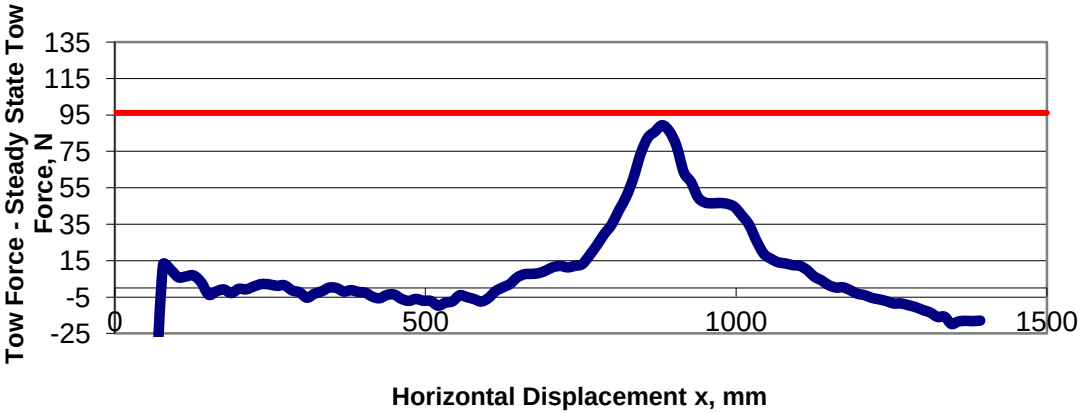


**Figure 104: The Comparison of Plough Test to the Limiting Bond Force Equation) with Fibrous Soil Coefficient, Cf = 0.7 - 2 % Test - 1/25th Scale**

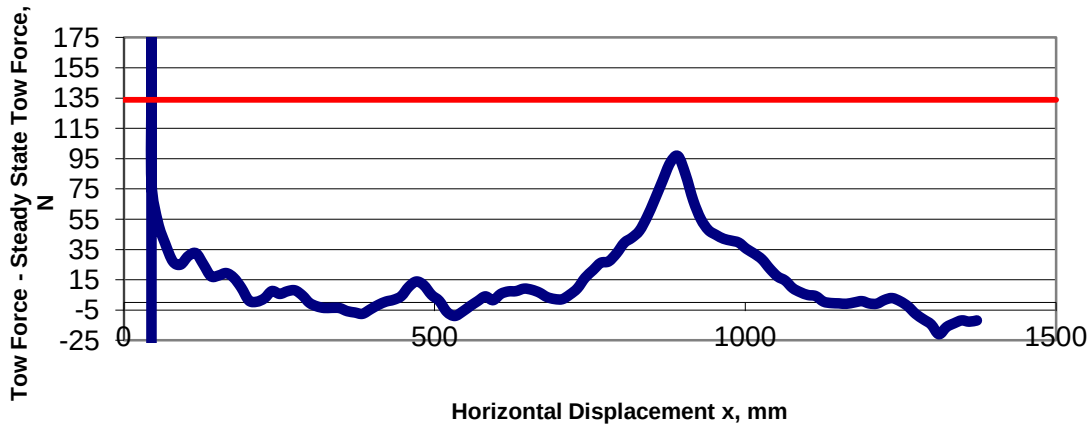


**Figure 105: The Comparison of Plough Test to the Limiting Bond Force Equation with Fibrous Soil Coefficient, Cf = 0.7 - 4 % Test - 1/25th Scale**

It can be seen in Figure 102, Figure 103, Figure 104 and Figure 105 that with the inclusion of the new fibrous soil coefficient, Cf, a more accurate prediction of limiting bond force is achieved which could possibly be used in the field. It is now possible include the limiting bond force equation with the inclusion of the fibrous soil coefficient into the Cathie and Wintgens (2001) to predict the increase in force when working in a reinforced soil. This can be seen in Equation 25.

$$F = C_w W' + C_s \gamma' D^3 + C_f \gamma' D \frac{1 + \sin \emptyset_{ps} \sin(\emptyset_{ps} + 2\theta)}{\cos^2 \emptyset_{ps}} A \tan \delta + C_d v D^2$$

Or,

$$F = C_w W' + C_s \gamma' D^3 + C_f \sigma_\theta A \tan \delta + C_d v D^2$$

**(25)**

In order to test the accuracy of this tow force prediction model when working in fibrous soils, which can be seen in Equation 25, more tests will need to be carried out and compared. At the moment, more testing is needed to determine the area of the shear plane being needed to calculate the increase in tow force due to the inclusion of fibres in a soil. Further work needs to be carried out investigating how the shear plane behaves throughout a test. As mentioned previously, this could be achieved by simply fixing a camera above the plough so that the shear plane that is being formed on the surface of the soil can be recorded for the entire test. More

testing is also needed to analyse the actual value of Cf when using Equation 25. It could be possible that this coefficient varies with fibre volume ratio instead of being kept a constant as was mentioned previously. Another possible way of understanding how the shear plane is produced by the plough would be to analyse it in a finite element analysis computer package meaning exact parameters would need to be known for this method to be effective. However, this would be difficult to carry out as it is unknown how a finite element analysis package would be able to calculate the effect of the inclusion of fibres within the soil. The interface friction angle that is used in Equation 25 also needs further investigation. For analysis purposes, the interface friction angle between sand and fibre, which was obtained from Gray and Ohashi (1983), was used when calculating the limiting bond force. The interface friction between the share (steel) and fibre need to be investigated further as well as other possible combinations that may be having an effect. However, this method is a credible possibility which would benefit from further testing.

# Chapter 6. Conclusion

Offshore pipeline ploughs often encounter some sort of reinforced soil while ploughing on the sea bed but this effect is not fully understood. Testing carried out in this project has laid a foundation of understanding how the plough reacts to being pulled through reinforced soil through a series of controlled laboratory tests, however, this effect will need to be investigated further to fully understand how the plough behaves in these circumstances. The following chapter will discuss conclusions drawn from the testing carried out and also discuss the implications of reinforced soil on industrial practice.

## 6.1 Effects of Reinforced or Fibrous Soils on Offshore Pipeline Ploughs

The following section will discuss conclusions drawn from testing carried out in the 1/25$^{th}$ and 1/50$^{th}$ scale. The following conclusions were made through the implementation of a testing schedule.

- The tow force needed to pull the plough through reinforced sand increases dramatically when compared to the ploughs steady state force. Through testing it can be seen that once the tow force peaks, it initiates a reduction of plough depth. The plough begins to reduce its depth at this point as the forces acting on the share need to be in equilibrium for it to plough steadily due to the long beam principle (Palmer *et al*, 1979). The depth of the plough needs to reduce significantly due to the resistance provided by the reinforcement.

- When comparing the results of pulling a plough through reinforced sand (post peak) to unreinforced sand it can be seen that the steady state tow force is independent from reinforcement. This indicates that there is no significant rate effect produced by the reinforcement. However, to gain the steady state tow force in a reinforced sample, the depth reduces greatly, to a point where the heel of the plough share has breached the surface of the trench. Once again, this is due to the long beam principle as plough depth reduces until there is equilibrium of forces acting around the share.

- From testing it can be seen that the dimensions of the shear plane produced by the plough when cutting through sand is directly affected by the inclusion of

reinforcement. It was also found that the tow force begin to increase before entering the reinforced soil when the fibre volume ratio of reinforcement was above 2 %. This could be due to the shear plane coming into contact with the reinforcement earlier than the plough, increasing the tow force required to pull the plough due to the extra resistance produced.

- Through analysis, it was found that the inclusion of new fibrous soil coefficient, $C_f$, is plausible by incorporating the Jewell and Wroth (1987) Limiting Bond Force Equation into the Cathie and Wintgens (2001) model to predict the increase in tow force when ploughing in a reinforced soil.

- It was also found that the build up of reinforcement around the plough share could produce a secondary problem as this could increase the force required to pull the plough through the soil due to the resistance being produced by the clogging of area around the share.

## 6.2 Possible Implications for Industrial Practice

The implications of not understanding the full effects of how an offshore pipeline plough will behave when being pulled through reinforced soil could prove to be enormously costly for a contractor carrying out a project due to the following facts.

- As it was found in testing that the plough significantly reduces its depth to counteract the massive increase in force due to reinforcement. This could result in numerous multi passes of the plough being required to reach the specified trench depth for minimum pipeline coverage. If the pipeline is not sufficiently buried a number of different potentially costly problems could occur such as:
    - The pipeline buckling due to not enough resistance being provided by the soil covering it.
    - The pipeline becoming damaged from fishing gear pulled along the sea bed or ship anchors.
    - No protection being provided by soil against corrosion.
- Damage could also be caused to the plough or boat pulling the plough if the effect of the reinforced soil the plough is going to encounter is not fully understood and planned

for. If too much force is required to pull the plough through the reinforcement, it could result in too much strain being put on the vessel pulling the plough, potentially resulting in catastrophic damage or cause damage to the plough itself. This could happen due to the following possibilities:

- Underestimating the effect of the reinforcement, resulting in a higher tow force need to pull the plough the anticipated in the design stage of the project.
- Pulling the plough too fast in a reinforced soil.
- The plough becoming damaged if larger pieces of reinforcement are encountered such as tree trunks on the sea bed.

From the discussed possible implications of reinforced soil on industrial practice, it is clear that it is imperative to carry out an accurate and thorough site investigation of a proposed pipeline route. If significant soil reinforcement is going to be encountered on a proposed route, it would be worthwhile to investigate alternative routes as if the reinforcement is not fully understood and prepared for, it could prove extremely costly for the project.

## 6.3 Recommendations for Future Research

As the research carried out in this dissertation is one of the first of its kind, new problems which were not initially considered were being encountered on a regular basis. The following section presents recommendations for future research to further develop what was concluded in this research project.

- It is suggested that more tests are carried out using different types of reinforcement. This would develop an understanding of how the plough behaves when encountering different materials and give a broader view of the effect of soil reinforcement on offshore pipeline ploughing.

- It would also be worthwhile to investigate the behaviour of the shear plane produced by the plough when being pulled through both reinforced and unreinforced soil. Further understanding of the shear plane could be achieved by attaching a camera, which only observes the area of soil ahead of the plough, to the trolley system used to pull the plough so any change could be recorded. It would also be interesting to investigate how the shear plane behaves using finite element analysis as it would be

possible to generate computer models of the shear plane in different types of soils. However, this may be difficult due to all the variable factors encountered during ploughing.

- It is also suggested that a series of tests are carried out which would investigate the rate effect created by the inclusion of reinforcement. This could be achieved by changing the speed of the plough while in a reinforced sample. This would allow the change in force and plough depth to be recorded and compared to the same type of test in an unreinforced sample.

- It is also recommended that the Proposed Tow Force Prediction Model when working in reinforced soils is developed further. The possibility of adapting it to be dependent on the fibre volume ratio of the soil would be beneficial as this could possibly be used in industrial practice to accurately predict the increase in tow force encountered when ploughing in reinforced or fibrous soils.

- Another series of tests that are suggested in order to develop the understanding of ploughing in reinforced soils is to have a sample which allowed the plough to enter then leave a section of reinforced soil. For example, if at the beginning of the test, the plough was in an unreinforced zone. It could then enter a reinforced zone of soil for a set distance before exiting the reinforced zone back into an unreinforced zone. By doing this, it would give the plough the opportunity to reach its specified trench depth. Even though it would be expected that the plough reach the force and plough depth it was at before entering the reinforced zone, it would be interesting to investigate.

- It is also suggested that a Cone Penetration Test is carried out in the reinforced sample bed to investigate if the reinforcement is picked up at all. If the CPT does detect the reinforcement, it would be interesting to investigate how accurate it is.

# Chapter 7. References


Bolton, M.D. (1986). "The strength and dilatancy of sands" *Geotechnique* **36**(1), 65-78

Bransby, M.F., Yun, G., Morrow, D.R. & Brunning, P. (2005). "The performance of pipeline ploughs in layered soils." *Frontiers in Offshore Geotechnics*, pp. 597-606 Gourvenec & Cassidy (Eds).

Brown, M.J**.,** Bransby, M.F. & Simon-Soberon, F., 2006. "The influence of soil properties on ploughing speed for offshore pipeline installation." *6th Int. Conf. On Physical Modelling in Geotechnics ICPMG'06, Hong Kong, 4-6th August 2006. 709-714.*

Brown,M.J., Bransby, M.F., Tovey, S. & Lauder, K., 2010. "Experimental Investigation of Pipeline Plough Performance in Reinforced Soils." Industry Report.

Cathie, D.N. & Wintgens, J.F. (2001). "Pipeline Trenching Using Plows: Performance and Geotechnical Hazards" *Proceedings of the Thirty-third Annual Offshore Technology Conference, Houston April/May 2001, pp. 1-14 (13145)*

Finch, M. & Machin, J.B. (2001) "Meeting the challenges of deepwater cable and pipeline burial" *Proceedings Thirty-third Annual Offshore Technology Conference, Houston (13141) April/May 2001, pp 1-14*

Finch, M., Fisher, R., Palmer, A. & Viggiani, G. (2000). "An integrated approach to pipeline burial in the 21st Centuary" *Deep Offshore Technology 2000*

Finch, M., Fisher, R., Palmer, A. & Viggiani, G. (2000). "An integrated approach to pipeline burial in the 21st Centuary" *Deep Offshore Technology 2000*

Geotechnical Section, School of Architecture, Landscape and Civil Engineering. University College Dublin, 2008. "Report on laboratory tests carried out on fibrous sand and organic clay from Adriatic Sea LNG"

Gray[1], D. H, Asce, A. M. & Ohashi[2], H., 1983. "Mechanics of Fiber Reinforcement in Sand"

Ivanovic, A., Neilson, R.D, Giuliani, G. & Bransby, M.F., 2011. "Influence of object geometry on penetration into the seabed." *Frontiers in Offshore Geotechnics II – Gourvenec & White (eds)*

Jewell, R. A. & C. P. Wroth, C. P., 1987. “Direct shear tests on reinforced soils”

Lauder, K.D., 2011. “The performance of pipeline ploughs.”

Lauder, K.D., Bransby, M.F. &Brown, M.J. (2008) “Experimental testing of the performance of pipeline ploughs” *Proceedings of the Eighteenth International Offshore and Polar Engineering Conference, July 2008, Vancouver, Canada*

Palmer, A.C. (1999). “Speed effects in cutting and ploughing” *Geotechnique* **49**(3), 285-294

Palmer, A.C., Kenny, J.P., Perera, M.R. & Reece A.R. (1979). “Design and operation of an underwater pipeline trenching plough” *Geotechnique* **29**(3), 305-322

Reece, A.R. & Grinsted, T.W. (1986). “Soil Mechanics of Submarine Ploughs” *Proceedings of the Eighteenth Annual Offshore Technology Conference,* Houston (5341) May 1986*, pp.* 453-461

Tovey, S., 2009. “The performance of offshore pipeline ploughs in fine sands.”

Yetimoglu*, T & Salbas, O., 2002. “A study on shear strength of sands reinforced with randomly distributed fibers.” *Geotextiles and Geomembranes **21** (2003) 103-110*